IMRT and Rotational IMRT (mARC) Using Flat and Unflat Photon Beams

Dissertation

zur Erlangung des akademischen Grades

Dr. rer. med

an der Medizinischen Fakultät

der Universität Leipzig

eingereicht von

MSc. med. physik

Amal Nabil Atef Sheta

geboren am 10.04.1979 in Al Mansoura, Ägypten

angefertigt am

KLinik und Poliklinik Für Strahlentherapie und Radioonkologie

Betreuer:

Prof. Dr. Ulrich Wolf

Prof. Dr. med. Thomas Kuhnt

Universität Leipzig AöR

KLinik und Poliklinik Für Strahlentherapie und Radioonkologie

Beschluss über die Verleihung des Doktorgrades vom: 21.06.2016

IMRT and Rotational IMRT (mARC) Using Flat and Unflat Photon Beams

Dissertation

for the academic degree of

Dr. rer. med

Faculty of Medicine

University of Leipzig

submitted by

MSc. med. physics

Amal Nabil Atef Sheta

Born on 10.04.1979 in Al Mansoura, Egypt

Completed at

The Department of Radiation Therapy

Supervisors:

Prof. Dr. Ulrich Wolf

Prof. Dr. med. Thomas Kuhnt

Clinic of Leipzig University

Department of Radiation Therapy

Date: 21.06.2016

Contents

ABSTRACT

Amal Nabil Atef Sheta

IMRT and Rotational IMRT (mARC) Using Flat and Unflat Photon Beam

University of Leipzig

110 **Pages**, 87 **References**, 47 **Abbreviations**, 10 **Tables**, 28 **Figures**

For more than 50 years flattening filters have been inserted into the beam path of linacs to produce a uniform energy fluence distribution of the photon beam and make it suitable for clinical use. Recently, linacs without flattening filter (Flattening Filter Free - FFF) are increasingly used in radiotherapy because of its benefits, e.g. high dose rate ($\simeq$ 2000 MU/min), reduced scattered and leakage radiation. Hypofractionated radiotherapy is interested in the high dose rate of FFF beams to shorten the treatment delivery time (TDT) especially the FFF beams have acceptable flatness at small field sizes. Radiotherapy techniques that deliver intensity-modulated beams (IMBs), e.g. Tomotherapy, intensity modulated radiation therapy (IMRT) and volumetric modulated arc therapy (VMAT), deal with the non-uniformity of the FFF beam profile and produce homogeneous dose to the target as FF beams do. Siemens modified the Artiste linac in order to enable photon beam delivery with and without a flattening filter. The VMAT version developed by Siemens for Artiste linacs as a novel radiation technique is a modulated arc therapy (mARC). mARC technique is available with single, double and multiple complete or partial arcs.

The aims of the current study were the determination of the main characteristics of 7 MV and 11 MV FFF photon beams in comparison with their corresponding 6 MV and 10 MV FF photon beams from Artiste digital linacs. Furthermore, IMRT planning comparisons using FF and FFF photon beams were performed using an Oncentra planning system. The performance of various mARC techniques were estimated and compared with Step and Shoot (S&S) IMRT by using a RayStation planning system. The mARC plans created by FF and FFF beams were evaluated to know which

technique is the best. All the treatment plans were created for simple and complex-shaped target volumes. The treatment plans are compared using two parameters - plan quality and treatment efficiency. In addition to the planning study, the plan quality assurance of IMRT and mARC plans were performed using two different volumetric quality assurance devices, Delta^4 and Octavius 4D.

Removal of the flattening filter causes changes in the dosimetric features of photon beams. IMRT plans with and without flattening filter were clinically acceptable where both plans have similar quality. In comparison with IMRT-FF, IMRT-FFF plans require more MUs and for some clinical cases require longer TDT. mARC technique can deliver dose distributions that are comparable to S&S-IMRT and could be an alternative with a potential to improve the efficiency of the IMRT treatment delivery.

Abbreviation list

3DCRT three dimentional conformal radiation therapy.

AMAT aperture-modulated arc therapy.

CN conformity number.

CP control points.

CT computed tomography.

$\mathbf{D}_2$ maximum dose.

$\mathbf{D}_{98}$ minimum dose.

$\mathbf{d}_{max}$ depth of dose maximum.

$\mathbf{D}_{mean}$ average dose.

DA dual arc.

DAO direct aperture optimization.

DD dose difference.

DICOM Digital Imaging and Communications in Medicine Standard.

DMLC dynamic multi leaf collimator.

DSS direct step and shoot.

DTA distance to agreement.

DVH dose volume histogram.

F.G.S final gantry spacing.

F.S field size.

Abbreviation list

FF flattening filter.

FFF flattening filter free.

HI homogeneity index.

IMAT intensity modulated arc therapy.

IMBs intensity modulated beams.

IMRT intensity modulated radiation therapy.

mARC modulated arc therapy.

MLC multi leaf collimator.

MU monitor units.

MU/Fx number of MU per fraction.

MU/min monitor units per minute.

MU/seg number of MU per segment.

OARs organ at risks.

OP optimization point.

PDD percentage depth dose.

PMMA polymethylmethacrylate.

PTV planning target volume.

QA quality assurance.

SA single arc.

SBRT streotactic body radiotherapy.

SMLC static multi leaf collimator.

Abbreviation list

SRT stereotactic radiation therapy.

SSD source surface distance.

SWAT sweeping window arc therapy.

TDT treatment delivery time.

TPS treatment planning system.

VMAT volumetric modulated arc therapy.

Chapter 1

Introduction

Cancer is a generic term for a large group of diseases that can affect any part of the body. Other terms used are malignant tumours and neoplasms. One defining feature of cancer is the rapid creation of abnormal cells that grow beyond their usual boundaries, and which can then invade adjoining parts of the body and spread to other organs, the latter process is referred to as metastasizing. Metastases are the major cause of death from cancer. According to the world cancer report of the World Health Organization, cancers figure among the leading causes of morbidity and mortality worldwide, with approximately 14 million new cases and 8.2 million cancer related deaths in 2012. The number of new cases is expected to rise by about 70 % over the next 2 decades [11].

Many treatment options for cancer exist, with the primary ones including surgery, chemotherapy, radiation therapy, hormonal therapy, targeted therapy and palliative care.

Radiation therapy involves the use of ionizing radiation in an attempt to either cure or improve the symptoms of cancer. It works by damaging the DNA of cancerous tissue leading to cellular death.

Radiotherapy is, after surgery, the most successfully and most frequently used treatment modality for cancer. It is applied in more than 50 % of all cancer patients. It is typically used in addition to surgery and/or chemotherapy but for certain types of cancer, such as early head and neck cancer, it may be used alone. Radiation can be from either internal sources as socalled brachytherapy or external radiation sources (teletherapy), which is the most common form of radiotherapy. During the past few decades medical linear accelerators (linacs) have become the predominant machine in treatment of cancer with ionizing radiation using external radiation source [66].

Clinical photon beams are produced in linacs with a target/flattening filter combination. The intensity of the x-ray beam produced in the target is mainly forward

peaked (Bremsstrahlung x-rays) and a flattening filter is used to flatten the beam (FF beam) and make it useful for clinical applications [66].

Flattening filters have been used for more than 50 years. They cause reduction of dose rate and undesirable issues like photon scatter, electron contamination and leakage radiation. Although removal of flattening filter produces non-uniform beams, modern radiotherapy treatment techniques have interest in using flattening filter free (FFF) photon beams because of their benefits, e.g. high dose rate, reduced scattered radiation. In the beginning stereotactic radiotherapy (SRT), which treat very small tumors using a larger number of small treatment fields (about 3 cm) and large dose per fraction, was interested in the high dose rate of FFF beams to shorten the treatment delivery time (TDT). Also, it was found that FFF beams have acceptable flatness at small field sizes and are suitable, as well as flattening filter (FF) beams, for stereotactic radiation therapy (SRT) technique [18]. After that the other modern radiotherapy treatment techniques, Tomotherapy, IMRT and VMAT are based on the modulation of beam fluence applied FFF beams. These techniques use multi leaf collimator (MLC) to modify the actual fluence distributions producing varying fluence patterns across the beam to achieve extremely conformal dose distributions and thus flattening filters become unnecessary.

Medical linacs are compact machines mounted isocentrically so as to allow practical radiation treatment aiming the beam toward the patient from various directions [66]. To spare normal tissues and OARs, which radiation must pass through to treat the tumour, shaped radiation beams are aimed from several angles of exposure to intersect at the tumour, providing a much larger absorbed dose there than in the surrounding healthy tissue. This is the motivation of developing new radiation therapy techniques.

There are many teletherapy techniques for cancer treatment such as three dimentional conformal radiation therapy (3DCRT), SRT, IMRT, Tomotherapy and VMAT.

IMRT technique has been used since 1994. It is a radiation treatment technique with multiple beams incident from different directions in which at least some of the beams are intensity-modulated so that each beam intentionally delivers a non-uniform dose to the target. The desired dose distribution in the target is achieved after superimposing such beams. The additional degrees of freedom to adjust intensities of individual rays are utilized to achieve a better target dose conformity and/or sparing of critical

structures [23].

IMRT delivery has become clinically widespread after the MLC was commercially available. MLC act as automatic field shapers and are programmed to deliver IMRT in two different ways, step and shoot (S&S) IMRT and dynamic IMRT (DIMRT).

Arc therapy as a rotational IMRT was described for the first time by Yu in 1995 [86] as intensity modulated arc therapy (IMAT) through the use of conventional linac as an alternative way of tomotherapy, that can treat large tumor volumes in a single pass, or very few passes of the gantry. Arc therapy allows the tumor to be treated from all angles with continuous movement of the gantry and variable dose rate.

Now many arc therapy techniques, known as VMAT, are available for clinical use and all of them are modified forms of IMAT. In this work, we focus on S&S-IMRT and the Siemens version of VMAT, called mARC.

mARC is the VMAT version developed by Siemens for Artiste linacs. In contradiction to other VMAT techniques, mARC is delivered by alternating beam-on, beam-off periods, with fixed apertures during beam on periods and modified apertures during beam-off periods; treatments can be resumed at any time on the spot [7].

Modern radiotherapy treatment techniques such as Tomotherapy, IMRT and VMAT, which use MLC as modifying device to produce varying fluence patterns across the beam and SRT for the treatment of very small tumors using a larger number of treatment fields and large doses per fractions, are interested in using FFF photon beams because of its benefits such as high dose rate, reduced scattered radiation. The first study interested in FFF beams was by O'Brien et al. in 1991 who studied their use on a linac [61].

Complex treatment plans of IMRT and arc therapy techniques need pretreatment dosimetric verification to ensure accurate and safe delivery of precalculated doses. The application of the treatment plan to a phantom followed by comparing the calculated and the measured doses has become a widespread method for the dosimetric verification of the plans created by these modern radiotherapy techniques. Quality assurance (QA) devices like Delta^4 diode array phantom (ScandiDos, Uppsala, Sweden) and Octavius 4D (PTW, Freiburg, Germany) based on ion chamber array have established to be suitable for arc plan verification as well as IMRT .

Three methods are used for the comparison between two dose distributions (mea-

sured dose and planned dose) - dose difference (DD), distance to agreement (DTA) and gamma evaluation. In this work gamma evaluation is used because it combines pass-fail criteria of both DD and DTA providing an index as a numerical value representing the acceptance criteria between them.

Aims of The Work

The changes in the physical characteristics of the photon beam due to the removal of the flattening filter may cause changes of IMRT and mARC treatment plans and their delivery.

The way of mARC plan optimization and the flexibility of its planned dose delivery lead to the possibility of shortening the delivery time so mARC technique should combine the speed of arc therapy with step and shoot modulation and it would be reasonable to assume an improvement in treatment efficiency and a comparable plan quality.

This work is divided into three parts:

1. Determination of the main dosimetric characteristics (depth dose curves, profiles, dose rate, surface dose) of 7 MV and 11 MV FFF beams of Artiste digital linacs and comparison with those of 6 MV and 10 MV flat beams.

2. Comparison of S&S-IMRT treatment plans of simple and complex-shaped target volumes using photon beams with and without flattening filter to:

   (i) determine whether the treatment plans using FFF beams are clinically acceptable or not

   (ii) assess the effect of removing the FF on the quality and efficiency of the treatment plan delivery

3. A treatment planning comparison of mArc and S&S-IMRT to estimate the performance of various mARC techniques (single arc (SA) and dual arc (DA)) for tumor sites of different complexity and volumes and compare their performance with S&S-IMRT with static beams. The study also explains the effect of final gantry spacing (F.G.S) on the quality and delivery efficiency of the mARC treatment plan. Furthermore, the mARC plans created by FF and FFF beams were evaluated.

In the present work, plan quality and treatment efficiency are the comparison parameters between the treatment plans. In addition to the planning study, the plan quality assurance of IMRT and mARC plans was performed by two different volumetric quality assurance (QA) devices, Delta^4 with two perpendicular diode detectors

arrays and Octavius 4D as an electronic array of ion chambers. This dosimetric verification aimed at evaluating the accuracy of mARC delivery as a new technique in the clinic, the possibility of the plan verification and the efficiency of both phantoms to verify IMRT and mARC plans.

Chapter 2

Theory

2.1 Linac head configuration

The linac is the most common device to treat cancer with external beam radiation. It uses high radio-frequency (RF) electromagnetic waves to accelerate charged particles - electrons - to high energies in a linear path, inside the wave guide then to the accelerator head. Fig.2.1 illustrates a schematic of a medical linear accelerator.

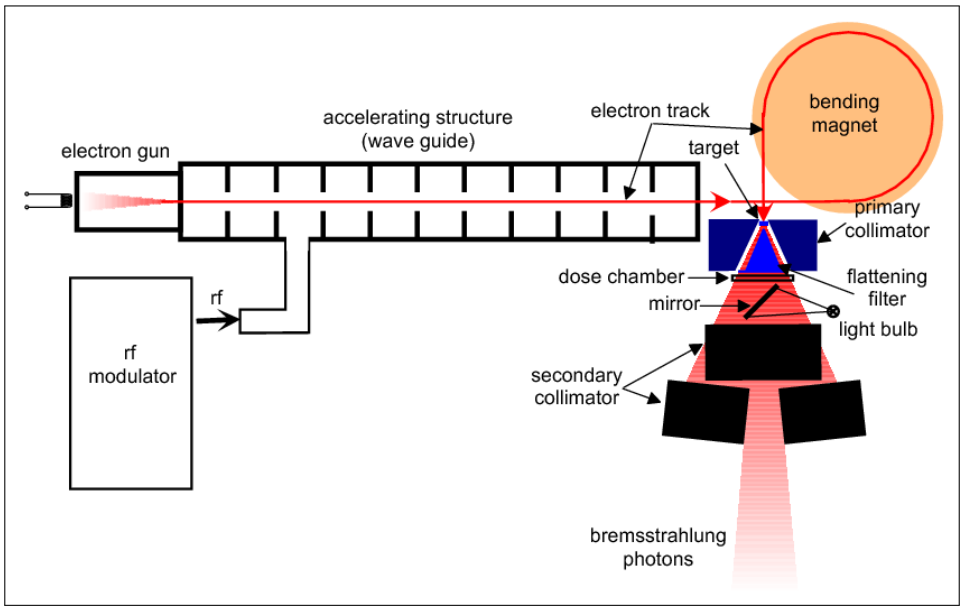

Figure 2.1: A schematic of a medical linear accelerator

The major parts of the linac treatment head are the target (often called the X-ray target), primary collimator, flattening filter, ion chamber and secondary collimators.

Accelerated electrons collide with the target to generate an X-ray beam. For a given energy of electrons, more X-rays can be produced if a target material with a higher atomic number (Z number) is used. Therefore, tungsten and gold are commonly used as target materials.

The production of X-rays is based on a process called Bremsstrahlung production

(meaning "braking radiation"), which is the result of radiative collisions between a fast-moving electron and an atomic nucleus. When the electron passes near a nucleus, it can be deflected from its path by Coulomb forces of attraction and lose its energy as bremsstrahlung radiation (i.e., an X-ray). X-rays are produced in all directions, but high-energy X-rays are produced in the forward direction. Therefore, in a linear accelerator, higher photon intensity is observed in the area close to the central line (i.e., the extended line following the direction of the incident electron) below the X-ray target.

The X-ray beam is first collimated by the primary collimator, which has a circular aperture through which a photon beam can pass to make a radiation field. The primary collimator is typically made of tungsten.

For patient treatment a radiation beam with uniform intensity across the field is desirable and to create a uniform photon beam a conical filter called flattening filter is used. The central area of the flattening filter is thicker to attenuate more photons in the central area. Fig.2.2 shows the resulting photon beam with and without flattening filter.

The amount of radiation produced by the linear accelerator is monitored by an ionization chamber, often called a monitor chamber. The monitor chamber not only controls the amount of radiation delivered to the patient, but it also checks the uniformity of the delivered radiation beam [50].

After passing through the monitor chamber, the beam can be further collimated by continuously movable X-ray collimators, consisting of two pairs of tungsten jaws, which provide rectangular field sizes ranging from zero to 40×40 cm^2 at a distance of 100 cm. The field size is visualized by a light localizer and mirror units.

Different manufacturers modified the collimating systems of modern linac and incorporated MLC into their collimation designs. The MLC system consist of two banks of independently moving tungsten alloy leaves that can be used to generate almost any field shape. The leaf settings for each field are computer controlled. Modern treatment planning system (TPS) are able to configure MLC shaped fields and the patient's MLC configuration files are sent via a local area network to the linac's control console [45, 43].

2.2 Flattening filter disadvantages

As mentioned above flattening filters are inserted into the beam path of the linacs to produce a uniform fluence and make it suitable for clinical use but it produces many undesirable issues. Flattening filter absorbs a large fraction of primary photons and hence removes an amount of beam intensity leading to significant decrease of output dose rate. The flattening filter is a major source of photon scatter and electron contamination acting as a secondary source of radiation, which is difficult to model and calculate by the TPS. Furthermore, it increases leakage radiation which increases the whole body doses of the patient and so a large amount of shielding around the linac head is required to reduce that leakage.

Inserting the flattening filter in the beam path causes an off-axis softening effect, which leads to a pronounced variation in profile shape with depth. This variation is overshoot or horns at the depth of dose maximum and undershoot pronounced shoulders at large depth, resulting in the off-axis dose being substantially lower than that at the central axis. At low energies and shallow depths, beam horns can be up to 8 %. In contrast, for unflattened beams the shape of the profile does not change by more than a few percent with depth [40].

2.3 Flattening filter free beams

Although the flattening filter causes unfavourable effects, the rational was to use it for obtaining uniform dose distributions for more than 50 years where a non-uniform fluence was considered not suitable for routine clinical applications. With the development of modern radiation therapy, the use of the filter declined. SRT which treats very small tumors using a larger number of treatment fields and large doses per fraction does not need to use flattening filter because there are no significant differences in beam fluence profile across the field between flattened and unflattened beams for small field sizes. Furthermore, the flattening filter is no longer a necessary component for modern techniques based on the modulation of inhomogeneous beam fluence such as Tomotherapy, IMRT and VMAT. In those techniques MLC as modifying device is used to modify the actual fluence distributions producing varying fluence patterns

across the beam to achieve extremely conformal dose distributions.

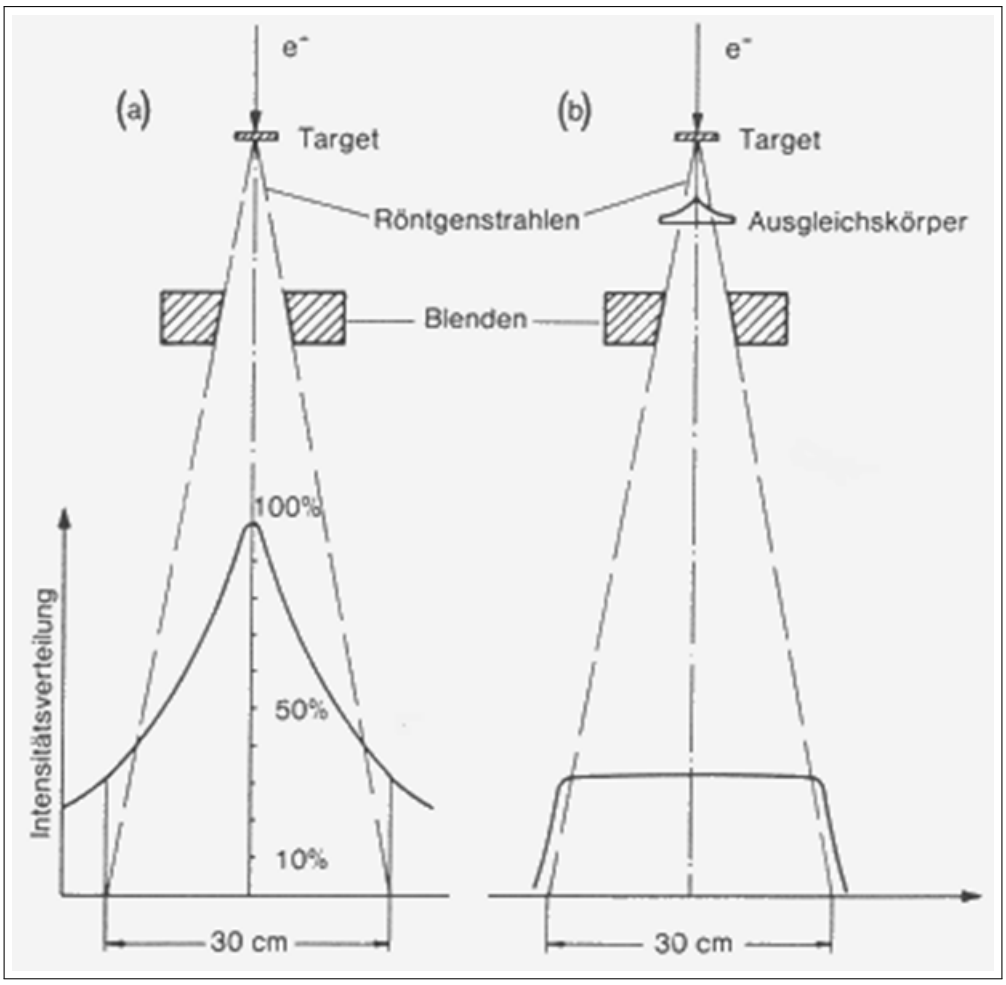

Figure 2.2: Schematic diagram illustrates the effect of the flattening filter removal on the photon beam profile [54].

Because all of the modern techniques have interest in using FFF photon beams, many investigators studied the influence of FFF beams on radiation treatments. The first study focused on FFF beams was in 1991 by O'Brien et al. [61] who investigated the small beams for radiosurgery treatment by a linac without flattening filter. They studied the characteristics of the beams from an AECL Therac-6 linear accelerator after removing the flattening filter and they found that the flatness is acceptable for field sizes used for stereotactic radiosurgery techniques and the dose rate increased by a factor of 2.75.

Cyberknife as a linac dedicated to radiosurgery was introduced by John Adler [17] in the early 1990s. Cyberknife is a recent machine producing photon beams of 6 MV, runs at a dose rate of 10 Gy/min without flattening filter [17, 32, 55]. It can be fitted

with a set of collimators providing a small circular beam with a diameter ranging from 5 to 60 mm [21, 23]. Tomotherapy was described by Mackie et al. in 1993 [59] and the helical tomotherapy system was introduced by Jeraj et al. in 2004 [47], both techniques have no flattening filter too. Tomotherapy is a dedicated IMRT system, which does not need flat dose profile because a binary multileaf collimator is used to modulate the treatment field to produce conformal dose distributions.

FFF beams have advantages approved by many studies for different techniques like high dose rate and reduced scattered radiation. The Monte Carlo study of radiation characteristics of helical Tomotherapy by Jeraj et al. [46] registered low spectral variation across the field, an extremely low leakage radiation and an increase in the dose output in the center of the field by approximately two fold compared to the beam edge of the field. This leads to an increased average dose rate and consequently reduced treatment times for patients. For linacs, the studies prove that the flattening filter removal results in an increase in dose rate, non-uniform beam profiles, softening of the x-ray spectra and reduction in head scattered radiation [28, 52, 72]. The reduction in head scatter and head leakage result in decreased peripheral dose which may be useful for sparing organs at risk at the field edges [53]. The reported dose rate of FFF beams is about 2.3 and 5.5 times higher than that of the FF beams [28, 81]. Increasing the dose rate reduces the beam-on time and may reduce the TDT, especially for hypofractionated SRT [61]. Also Brendan et al. [67] concluded that the use of FFF linac for streotactic body radiotherapy (SBRT) of liver and lung malignancies is associated with substantial improvement in TDT.

2.4 Intensity modulated radiation therapy

The term IMRT refers to a radiation therapy technique in which non-uniform fluence is delivered to the patient from any given position of the treatment beam to optimize the composite dose distribution. The treatment criteria for plan optimization are specified by the planner and the optimal fluence profiles for a given set of beam directions are determined through inverse planning. The optimally modulated fluences are converted into MLC leaf sequence files, which are electronically transmitted to the linear accelerator, which is computer-controlled, that is, equipped with the required software and

hardware to deliver the intensity modulated beams (IMBs) as calculated [50].

To produce modulated fluence profiles, precalculated by a TPS, the accelerator must be equipped with a system that can change the given beam profile into a profile of arbitrary shape. For that purpose many classes of intensity-modulated systems have been devised. These include compensators, wedges, transmission blocks, dynamic jaws, moving bar, multileaf collimators, Tomotherapy collimators, and scanned elementary beams of variable intensity. Nowadays, the computer controlled MLC is the most commonly used device for delivering IMBs [50].

The clinical implementation of IMRT requires at least two systems: (1) a treatment planning computer system that can calculate non-uniform fluence maps for multiple beams directed from different directions to maximize dose to the target volume while minimizing dose to the critical normal structures, and (2) a system of delivering the non-uniform fluence as planned. Each of these systems must be appropriately tested and commissioned before actual clinical use.

2.5 Multi leaf collimator

MLCs initially were designed as a field shaper to replace shielding blocks. Because each leaf of the MLC can be independently moved, a field pattern with stepped edges can be created. Because of scatter and electron transport these sharp steps become blurred with depth in tissue. So MLCs permit the quick and flexible adjustment of the irradiation fields to the tumor shape and avoid the organs at risk. The MLC was patented in 1959 by Gscheidlen, first commercially developed by Scanditronix in the mid-1980s and did not come into widespread clinical use until the early to mid-1990s. The modern MLCs as available from Elekta, Siemens and Varian have been re-engineered for IMRT [23].

Almost all modern linear accelerators are equipped with MLCs. For linear accelerators, the computer-controlled MLC seems to be the most practical device for delivering intensity-modulated beams. This is achieved in three different ways: (a) Multi-segmented Static Fields Delivery (MSF-MLC), which goes under the name step-and-shoot (S&S), (b) the dynamic delivery (sliding window) and (c) IMAT [84, 23, 25].

2.6 Step and shoot IMRT

The step-and-shoot technique of IMRT dose delivery was proposed by Bortfeld et al. in 1994 [24]. it is a straightforward extension of the conventional multiple-field irradiation technique. The patient is treated by multiple fields of different angles and each field is subdivided into a set of sub-fields (segments) irradiated with uniform beam intensity levels. The segments are created by the MLC. The dose is delivered by superimposing a number of fields and partially overlapping the segments. For each segment a well-defined number of monitor units monitor units (MU) is delivered. Then the beam is turned off while the leaves of the MLC move to the positions required for the next IMRT segment. After the verification and record system (V&R) has validated the new leaf positions, the beam is turned on again and the dose is delivered for this segment. This process is repeated for all segments per incident beam angle and all beam directions. The theory of creating sub-fields and leaf-setting sequence to generate the desired intensity modulation has been discussed by Bortfeld et al [24]. For a while most inverse treatment planning programs have a build-in leaf-sequencing algorithm. The total number of segments depends on the complexity of the fluence maps, the number of beams and other technical factors [50, 25].

Shepard et al. [71] presented another inverse planning technique for S&S - IMRT called direct aperture optimization (DAO). With this technique, all of the constraints imposed by the MLC are included in the optimization, thereby eliminating the need for a separate leaf-sequencing step. A key feature of this approach is that the user specifies the number of segments to be delivered as a constraint in the optimization. With DAO algorithm, the leaf positions and aperture weights are optimized simultaneously. Another key feature of DAO is that it does not rely on the use of a segmentation routine to select the initial leaf positions. Rather the leaf positions are initialized to match the beam's eye view of the target.

2.7 Dynamic delivery

The intensity modulation is achieved by an individual variation of the velocities of the moving leaves. The "dynamic" mode is an extension of the "sweep" mode of the static

dose delivery [25]. The leaves of a dynamic multi leaf collimator (DMLC) are motor driven and their motion is under the control of a computer, which also accurately monitors the leaf positions [50]. Stein et al. introduced an algorithm that computes leaf trajectories and they deduced a relationship between treatment time and maximum leaf speed. They found that the maximum leaf speed should be not less than 20 mm per second to achieve good performance [73]. The treatment time to deliver calculated leaf trajectories is approximately the time the leaves need to move from the leftmost side to the rightmost side plus the delivery time to irradiate the leaf sweep decomposition [25].

An often discussed question is which delivery technique is superior to the other. Both techniques have their advantages and disadvantages. From the technical point of view the "dynamic" approach is more complex than the S&S approach. For the "dynamic" process the leaves are moving while the beam is turned on and therefore a very accurate control of the leaf positions, leaf speed, and dose rate must be achieved at the same time. On the other hand, a shorter delivery time is the main advantage of this technique. The static approach allows an easier verification process and is considered as a natural extension of established conventional dose delivery techniques. Plan comparisons of static multi leaf collimator (SMLC) and DMLC optimized plans have shown that both techniques could achieve acceptable dose distribution for the target volume with differences less than a few percent [63, 25].

2.8 Intensity modulated arc therapy

In 1965 arcs involving dynamic field shaping using a MLC were first described by Takahashi. IMAT has been presented by Yu in 1995 through the use of conventional linac as an alternative way of Tomotherapy, that can treat large tumor volumes in an arc manner using a single or very few passes of the gantry [86].

Yu predicted that with the increase in the number of gantry angles, the number of intensity levels at each gantry angle can be reduced without degrading plan quality. He argued that the plan quality is a function of the total number of quanta defined as the product of the number of beam angles and the number of intensity levels. In other words, it is the total number of aperture shape variations that determines the

plan quality [56, 86, 30].

IMAT technique uses the dynamic way to shape the fields as well as rotate the gantry in the arc therapy mode. At the same time IMAT is a logical development of the S&S method in that each field (positioned along the arc) is subdivided into subfields of uniform intensity, which are superimposed to produce the desired intensity modulation. However, the MLC moves dynamically to shape each subfield while the gantry is rotating and the beam is on all the time. Multiple overlapping arcs are delivered with the leaves moving to new positions at a regular angular interval, for example 5 degrees. Each arc is programmed to deliver one subfield at each gantry angle. A new arc is started to deliver the next subfield and so on until all the planned arcs and their subfields have been delivered. The magnitude of the intensity step per arc and the number of arcs required depend on the complexity of the treatment. A typical treatment takes three to five arcs and the operational complexity is comparable to conventional arc therapy [50, 87].

The novelty of IMAT was somewhat held back initially due to the absence of a matching planning technique. That problem was solved in 2002 when Shepard and Earl et al. [71] developed their inverse planning tool DAO for S&S-IMRT delivery [71]. The efficiency advantage of DAO makes it ideal for planning IMAT. Following their successful development of DAO for S&S-IMRT delivery Earl et al. in 2003 applied this DAO approach to IMAT treatment planning. Ulrich et al. in 2007 developed an optimization technique for a single-arc delivery. That technique requires a variable dose rate delivery with gantry rotation. The scheme by Ulrich et al. and Earl et al. [38, 77] can take a long time for the optimization to converge. By assuming that the machine dose rate can vary as needed, Otto [62] in 2008 devised a coarse-to-fine DAO, he uses progressive beam angle sampling to optimize a large number (>100) of apertures using DAO. Otto referred to his single arc IMAT algorithm as VMAT [23, 30].

Not only the DAO was the trial for IMAT planning but other techniques and algorithms have been developed such as sliding window IMRT and arc delivery by MacKenzie and Robinson [58], aperture-modulated arc therapy (AMAT) by Crooks et al. [33] and sweeping window arc therapy (SWAT) technique by Cameron [27] to deliver an IMRT treatment in one arc rotation. In 2007, Tang et al. [75] showed that a multi-arc IMAT could be converted into a single arc by spreading the stacked

apertures to neighbouring angles with a minimal effect on the plan quality. Bzdusek et al. [26] and Bedford [19] introduced very similar approaches. First they optimized the intensity profiles on beams at static gantry angles evenly spaced over the range of one or more arcs. Initial aperture shapes are generated to approximate the optimized intensities. These apertures are then spaced evenly over the angular range to form a single arc, and their weights and shapes are further optimized using a direct aperture optimization algorithm, taking into account the allowed range of leaf motion of the MLC [30].

Until 2007 linac manufacturers did not have control systems capable of delivering IMAT and no TPS offered robust inverse planning tools for IMAT. The first linac provided with IMAT delivery technique became commercially available by Varian, after the adaptation of Otto's VMAT algorithm [62], under the trade name, RapidArc^{TM}. The linac control was also updated to allow dose rate variation during gantry rotation. Not long after Varian's announcement, Elekta started to market their IMAT solution under the trade name VMAT^{TM}. Bzdusek et al. [26] in 2009 have introduced a rotational IMRT solution, which is marketed by Philips Medical Systems, Inc. under the trade name, SmartArc^{TM} [30].

In 2010 Siemens presented a novel "burst mode" modulated arc delivery mARC approach by using Siemens Artiste digital linear accelerator without flattening filter supporting a very high dose rate of 2000 monitor units per minute (MU/min). Salter et al. [70] tested the modifications that allow the Artiste linac to perform mARC delivery. To support the creation of burst mode treatment plans that the linear accelerator can deliver a prototype version of a commercial TPS was also tested. Burst mode delivery differs from continuous mode delivery used by other volume modulated arc therapy techniques in that radiation is not delivered continuously across the arc but in small radiation bursts while the gantry is rotating.

2.9 Modulated arc therapy

mARC is the Siemens approach of volume modulated arc therapy as rotational IMRT. As mentioned before, mARC (Siemens), RapidArc^{TM} (Varian) and VMAT (Elekta), are different trade names of radiation therapy based rotational IMRT techniques. All

these arc therapy techniques are modified forms of IMAT, which was described for the first time by Yu [86, 29]. Yu implemented IMAT to deliver highly conformal dose distributions by combining gantry rotation and dynamic multileaf collimation. Instead of delivering intensity modulated beams with fixed gantry angles, IMAT delivers optimized dose distributions by rotating the radiation beam around the patient. During VMAT and RapidArc delivery the beam maintains ON and the field shape which is formed by a multileaf collimator (DMLC) changes continuously as determined by the treatment plan. Siemens has another philosophy of arc delivery in that dose is delivered in bursts over very short arc angles called arclets and only after an MLC segment shape has been completely formed and verified by the controller. By that way the delivered dose at each moment is precisely known and certainly there is no dose during MLC shaping [70].

Figure 2.3 represents a schematic diagram of the arclet. The arclet is the main component of the arc and it is a short angle defined by an optimization point (OP), which is situated at its middle and an arclet angle (α), which determines its span. Two control points (CP) define the beginning and end of each arclet. The OP is defined by the treatment plan, used to the plan optimization and the radiation will be delivered symmetrically about it. According to RayStation planning system the number of the OPs is controlled by the value of the F.G.S - the spacing between two OP - according to equation (2.1) :

$$\text{Number of OPs} = \text{No of arclets (segments)} = \lfloor \frac{\text{arc span}}{\text{F.G.S}} \rceil \tag{2.1}$$

It is recommended that the F.G.S is not smaller than 4° in order to keep overall delivery times small, and not more than 15° to get good optimizing plans [6]. The arclet angle (α) is never less than 1° and recommended to be between 2° and 4° because the actual dose distribution may differ substantially from the calculated one for arclet angles larger than 5° [7]. The specific characteristics of the mARC delivery are illustrated in Fig.2.4. As shown in the figure, each complete arc is delivered in one direction and does not need to span a full 360° The arc is divided into arclets. While the radiation is on (beam-on intervals), the leaf positions, jaw positions, collimator angles, gantry speed, dose-rate and table position remain fixed within the arclet and

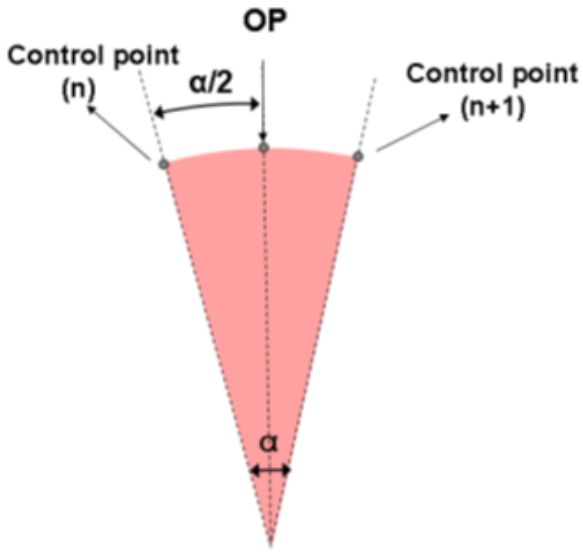

Figure 2.3: Schematic representation of an arclet [6].

the dose is delivered over the arclet [6].

At the end of the arclet the radiation is off (beam-off intervals) in the so-called silent periods, the arclet shapes, and collimator angles are adapted to the values of the next arclet provided by the treatment plan. During these intervals, the gantry speed is automatically modulated by the firmware included in the control console in order to allow for the necessary adaptations where it turns on the beam at the correct gantry positions, supervises the treatment through each α angle and handles various exceptions and error conditions as well as to minimize the treatment time of the mARC. Consequently, depending on the calculated MU for each arclet, the treatment delivery system will run at an appropriate dose rate to improve the linearity between the selected MU and the delivered dose. The treatment delivery system observes the arclet boundaries and trades off the gantry and MLC leaf speed in order to ensure an optimum performance of delivery (shortest time possible) without having to violate the maximum MLC leaf speed. Therefore, the prescribed arclet angle is interpreted by the Artiste as an upper boundary for the angle so during actual delivery the arclet may be smaller than prescribed but will never be larger, i.e. with more dose the gantry speed will be slowed down. Gantry speed and dose rate that are held constant during individual arclet may vary from one arclet to another but the position and the angle of the treatment table can be changed only from one arc to another.

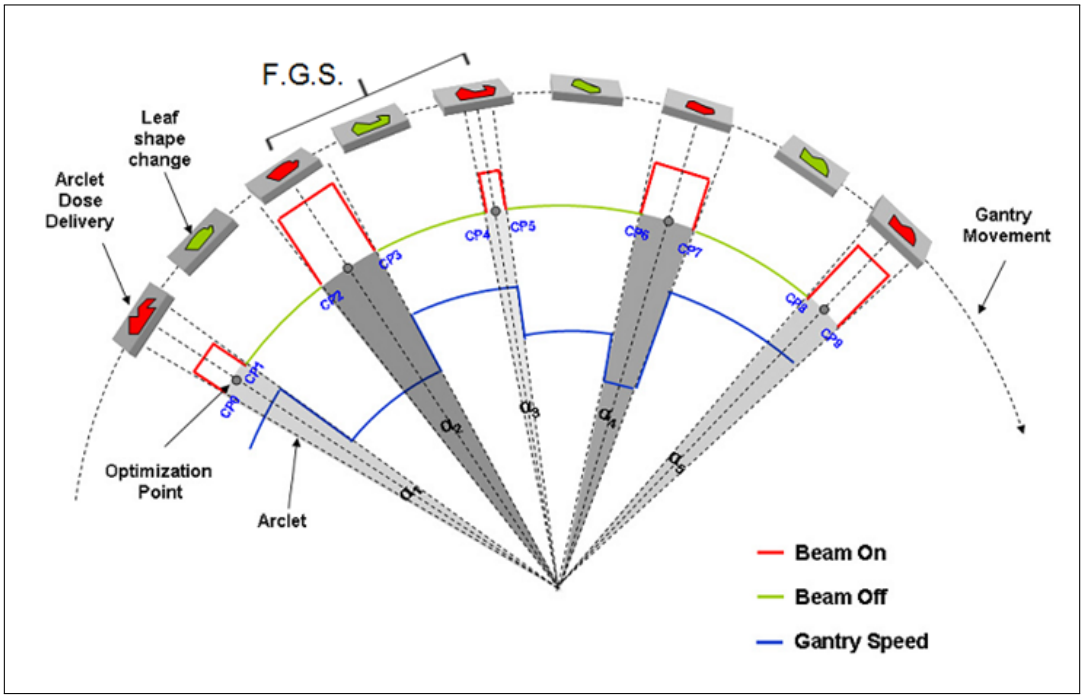

Figure 2.4: Schematic overview of mARC delivery in the clockwise direction. The arclets are colored in red, the silent periods in green and the gantry speed in blue. In this example, the arclets differ from each other and they have been denoted as a1, a2, etc [6].

For mARC, the planner determines the gantry start and stop angles of the arc, the direction of the rotation (clockwise or counterclockwise). Furthermore, the planner has to chose SA, DA or multiple arcs to create the optimal plan. If overlapping arcs are desired to achieve the optimal dose distribution, the second arc should have the opposite direction compared to the first arc in the interest of time [6, 70].

By the end of 2014, three TPS which support mARC plans were available in the market, Panther Prowess (PRoARC), Varian's Eclipse^{TM} and RayStation (Ray Arc). Panther PRoARC is Prowess' approach which used Prowess' DAO technology to optimize the delivery of radiation dose. Panther TPS-PRoARC supports multiple vendors' (Siemens, Varian, or Elekta) hardware and their rotational IMRT techniques [14]. In 2014 Varian Medical Systems and Siemens Healthcare showcased the new capabilities within Varian's Eclipse^{TM} treatment planning software to deliver mARC treatments using Siemens linacs (Artiste) [10]. In 2012 RaySearch Laboratories (RaySearch LaboratoriesAB, Stockholm, Sweden) released RayStation planning system version 2.5 supporting all rotational arc capable linacs from Elekta, Varian and Siemens [8]. RaySearch Laboratories announced that the first clinical mARC treatment, planned with

RayStation, has been delivered at Europe Hospitals in Brussels, Belgium on 30^{th} April 2014 [9].

mARC optimization by RayStation TPS

RayStation TPS allows for mARC plans to be created in a similar way to fixed beam plans. The beams are replaced by arcs, which are divided into arclets and the dose delivered over these arclets as illustrated above in Fig.2.4. Otherwise the optimization functions are the same, the interface is the same and the optimization process follows the same pattern as for SMLC optimization: a preliminary fluence optimization step, sequencing into machine parameters followed by direct optimization of machine parameters.

Optimizations steps

This section describes the steps performed during optimization of a single arc plan. With multiple arcs there are a few differences that are described in a later section.

Algorithmic details

1. Initial fluence maps are generated at the start and the stop angle and at 24 degree increments from the start angle. The fluence maps are initialized to the target projections.

2. The fluence maps are optimized resulting in one fluence profile per initial angle.

3. At the sequencing phase, the optimized fluence maps are converted into arc CPs distributed over the entire arc.

4. Before optimization starts, all CPs are processed to comply with the motion constraints of mARC: max leaf speed, valid dose rates, delivery time. This often means that leaves are shifted

5. Machine parameter optimization is performed on all CPs taking all applicable machine and user constraints into account.

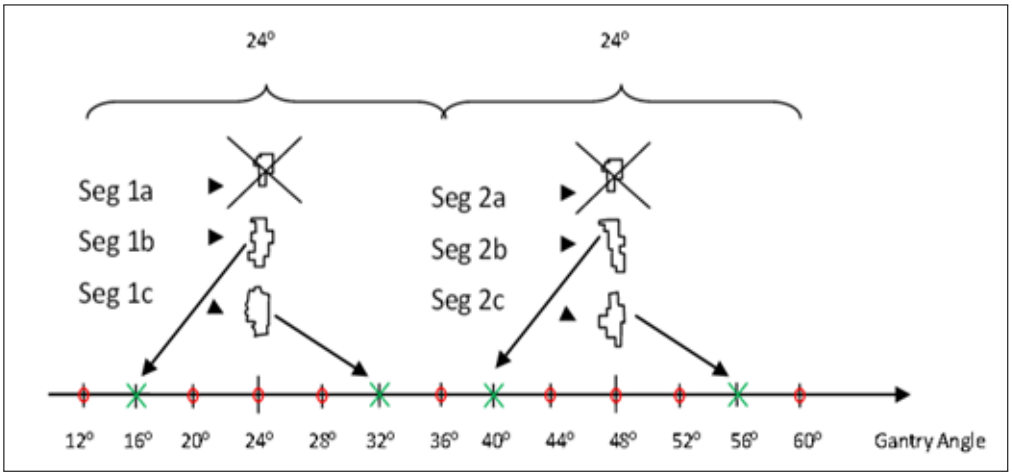

Figure 2.5: Illustration of the conversion phase before machine parameter optimization starts, including segment filtering and redistribution. In this example the optimized fluences at the initial directions 24° and 48° are converted into 3 control points respectively, where one control point is discarded and two are repositioned (green x). Additional control points created by cloning the control points resulting from the conversion are distributed to achieve the desired gantry spacing (red circles) [5].

6. Finally, jaws and passive leaves are positioned [5].

It is possible to optimize more than one arc simultaneously. This can be done in two different ways - either the properties of all arcs are user defined, or the DA feature is used.

Multiple Arcs

In RayStation, it is possible to define any number of arcs, the properties of which can be individually selected. Therefore, the arcs may cover different gantry angle intervals, rotate in the clockwise or counter-clockwise direction. All arcs are treated as individual arcs and optimized simultaneously. If two arcs cover the same gantry angles, it is likely that the fluence profiles of the two arcs at sequencing are very similar resulting in similar apertures around the arc, which is not an optimal starting point for the optimization. Therefore, this feature is primarily useful when multiple arcs with no or limited overlap are desired. For machines where jaw motion can be switched off, it is possible to create multiple arcs that cover different parts of the target (or different targets) by manually setting the jaws prior to starting the optimization [5].

Dual arcs (DA)

Another way to create a multiple arc plan is to use the DA feature, whereby a second arc will be created during the sequencing stage. The first arc rotates in the selected direction and the second in the opposite direction. In this manner the gantry does not need to be reset before delivery of the second arc. Only one set of fluence profiles are optimized for an arc selected to be optimized as a DA just as for the SA case [5].

2.10 Verification of IMRT and mARC treatment plans

IMRT and mARC increase the complexity of radiotherapy techniques requiring dosimetric verification before clinical delivery, which has become a standard procedure in clinical routine in order to ensure accurate and safe delivery of precalculated dose of patient treatment plans. Different volumetric QA devices are used to verify IMRT and mARC treatment plans [20, 42, 51]. In our clinic we use Delta^4 (ScandiDos, Uppsala, Sweden) as a diode detector array and Octavius 4D (PTW, Freiburg, Germany) as an electronic array of ion chambers.

Both devices act as treatment plan verification systems and have become commercially available, tested and evaluated by many users [69, 20, 31]. These novel QA systems offer useful features like dose verification in 3D and real time measurement [78] and overcome many of the limitations of the traditional methods - ion chambers and films.

Delta^4 software and Octavius 4D software (VeriSoft) are provided with three methods - DD and DTA in addition to gamma index - to compare the planned and measured doses. Gamma index has been represented by Daniel A. Low et al. [57] as a method for determining an acceptance criterion that simultaneously considers the DD and DTA. The determination of γ throughout the measured dose distribution provides a presentation that quantitatively indicates the calculation accuracy.

Chapter 3

Materials and Methods

3.1 Materials

3.1.1 Linear accelerator

Siemens (Oncology Care Systems, Concord, CA, USA) has released a fully digital Artiste linear accelerator that includes a 160-leaf MLC, which offers high tumor conformity by combining high leaf-motion speeds (4 cm s^{-1}), leaf accuracy of 0.5 mm, very low leaf transmission values of approximately 0.4 % and a leaf span of 20 cm [74]. Siemens modified the Artiste linac in order to enable photon beam delivery with and without a flattening filter. The Artiste offers FFF beams up to four nominal energies of 7, 11, 14, and 17 MV, plus one FF beam energy (6 MV, 10 MV, 15 MV or 18 MV) - which is called "Multiple-X treatment mode". Energy is selected according to the needs of each clinic [7].

In 2011 the radiotherapy clinic of Leipzig University was equipped with two digital Artiste linacs. Both linacs offer the possibility of Multiple-X treatment mode. The chosen energies were 7 MV, 11 MV FFF and 10 MV FF beams. 7 MV, 11 MV FFF beams support variable dose rates between 500 MU/min and 2000 MU/min and 10 MV FF beams are available with dose rate up to 500 MU/min. In 2012 Artiste linacs in our clinic were upgraded to apply mARC treatment.

The control console of the Artiste uses specific mechanisms to maintain the dose linearity for segments with low MU to be delivered with the high dose rates. The following mechanisms can be distinguished:

(a) Automatic switch to the low dose rate, applicable for non-mARC treatments. The concept of this mechanism is to maintain the dose linearity for segments with low MU to be delivered with the high dose rates, the control console will automatically switch from a dose rate higher than 500 MU/min to the low dose rate of 500 MU/min.

Figure 3.1: Artiste Linac

This automatic dose rate switch can be applied to any segment for which the dose/dose rate combination would result in reduced linearity. The minimum allowed dose is calculated based on the following formula:

$$\text{Minimum dose per segment} = \frac{0.3}{60} \times min \times \text{dose rate} \tag{3.1}$$

Thus, any segment with a dose < 10 MU will be delivered with 500 MU/min instead of 2000 MU/min.

(b) Automatic downscaling of the dose rate, applicable for mARC treatments. The mechanism for maintaining the dose linearity is different for mARC treatments. Instead of simply switching from the high dose rate to the low dose rate of 500 M/min, the Control Console scales the dose rate to a value that delivers the desired MU in 0.3 s. which is the estimated time the dosimetry system needs for stabilization.

For treatments that use high dose rates, the linear relation between the arclet MU and the dose delivered by the arclet may be compromised in the regime of low arclet MU. This reduced linearity is due to the beam formation time and the need of the dosimetry system to stabilize after the beam is turned on. The typical time required

for stabilization is in the order of a few hundred milliseconds.

To improve the linearity between the selected MU and the delivered dose, the dose rate is reduced for arclets below a certain MU, the so-called upper threshold MU. As an example, if the maximum dose rate of a treatment mode is 2000 MU/min, the upper threshold MU is 10 MU. For arclets above the upper threshold MU, the maximum dose rate of 2000 MU/min is used. For arclets below 2.5 MU, the lower threshold MU, the minimum dose rate of 500 MU/min is used. For arclets between 2.5 MU and 10 MU, the dose rate follows a linear relation varying between 500 MU/min and 2000 MU/min.

The dose rate may vary between arclets depending on the arclet MU but it does not vary within a single arclet. The reduction of the dose rate will improve the dose linearity with the minor drawback of increasing slightly the overall treatment time. The actual dose rate for arclets with MU between the lower and the upper threshold is calculated as follows:

$$\text{dose rate} = \frac{MU}{0.3\ \text{s}} \times \frac{60\ \text{s}}{min} \tag{3.2}$$

where 0.3 s is the estimated time the dosimetry system needs for stabilization and MU is the monitor units to be delivered.

The check and if necessary the adjustment of the dose linearity are part of the machine QA that needs to be performed on a regular base in order to ensure the required accuracy [7, 70].

3.1.2 Dosimetric tools

The dosimetric characterization of FF and FFF beams of Siemens Artiste linac were investigated in this study using the available dosimetric tools in our clinic.

MP3 water phantom system

The MP3 system (PTW Freiburg, Germany) with PTW dosimetry diode type 60008 are used to beam profiles and depth dose measurements. MP3 system is based on the MP3 water tank, which is suitable for very large field measurements. Beam incidence may be vertical, horizontal or oblique. The horizontal detector moving range is 600 mm $\times$ 500 mm and the vertical range is 407.5 mm. Stepper motors are mounted close above the tank making it possible to adjust distances between the linac head and the

water surface as small as 120 mm. Stainless steel drive mechanics are used to minimize water perturbation and to preserve positioning accuracy during movement. They do not disturb or affect measurement accuracy [3].

Figure 3.2: Large size motorized 3D water phantom system for dose distribution measurement of radiation therapy beams [15]

The dosimetry diode was installed in the water phantom and their effective point of measurement positioned to the water surface by the TRUFIX Detector Positioning System.

The measurements were performed with the TANDEM Dual-Channel Electrometer and the beam data acquisition and analysis were done using MEPHYSTO mc^2 Software[15].

Dosimetry diode (type 60008- PTW)

The PTW dosimetry diode type 60008 is a waterproof p-type silicon diode detector designed for dose distribution measurements in high-energy photon and electron beams. Fields of applications are IMRT, stereotactic beams, brachytherapy and water phantom scanning. It is shielded against low-energy scattered photons by a thin metallic plate and has a cylindrical small sensitive volume shaped as a disk with an area of 1 mm^2 and a thickness of only 2.5 μm. This enables it to be used in small beams and to perform data acquisition with a very good spatial resolution. The excellent spatial resolution makes it possible to measure very precisely beam profiles even in the penumbra region

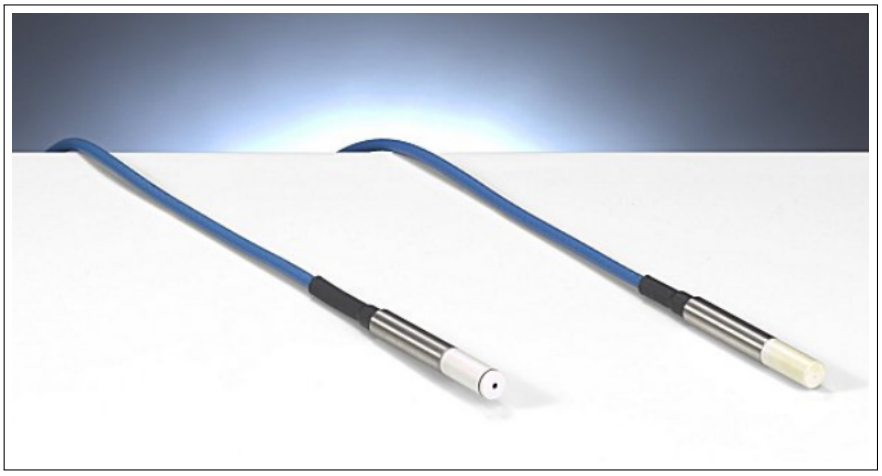

Figure 3.3: Dosimetry Diode Type 60008 [2]

of small fields. The superior energy response enables the user to perform accurate percentage depth dose measurements in small and large photon fields from 1×1 cm^2 till 40×40 cm^2. The dosimetry diodes are to be irradiated in axial direction [2].

Slab acrylic phantom and parallel plane chamber

Figure 3.4: Soft X-Ray Slab Phantom (PTW Freiburg, Germany)[15]

The slab acrylic phantom type 2962 and PTW parallel plane chamber type 23344 were used for dose measurements within the build-up region for 6 MV, 7 MV, 10 MV and 11 MV. The chamber is designed for use in solid state phantoms and field sizes upto 40 × 40 cm^2. The slab phantom is supplied with chamber adapter plate and

consists of 1 plate 1 mm thick, 2 plates each 2 mm thick, 2 plates each 5 mm thick and 5 plates each 10 mm thick. This combination enables the user to vary the measuring depth from the surface to a depth of 6 cm in increments of 1 mm [15].

3.1.3 Dosimetric verification systems

Delta^4 phantom

Delta^4 consists of 1069 p-type diodes in two orthogonal planes, as shown in Fig.3.5, inserted in a cylindrical polymethylmethacrylate (PMMA). The phantom is 22 cm in diameter, 40 cm in length and its mass density is 1.19 g/cm^3 with a relative electron density of 1.147. Each p-type diode has a cylindrical sensitive volume of 0.78 mm^2 area and a thickness of 0.05 mm. The detectors are spaced at 0.5 cm intervals in the central 6 cm $\times$ 6 cm area and at 1 cm intervals outside this area, and they cover an area of 20 cm $\times$ 20 cm in each plane (active area).

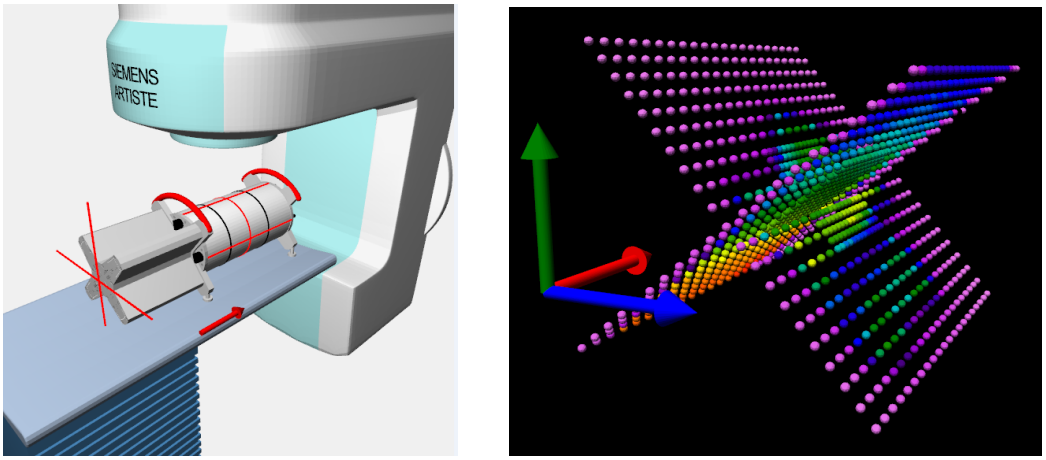

(a) (b)

Figure 3.5: a) Delta^4 phantom setup on patient couch. b) the arrangement of the diodes in two orthogonal planes, which are inserted in the phantom.

Delta^4 system is supplied with the inclinometer to measure the current gantry angle during verification of arc therapy treatments. The device records the measured dose synchronized with the accelerator pulses using a trigger signal from the accelerator. The measured dose is stored on a pulse-by-pulse basis, allows segment-by-segment analysis. Although the system has detectors in only two planes the associated computer software provides an interpolation algorithm that is capable of estimating doses at points where no detectors are present. This device also provides a novel technique for calculating the

dose in 3D, which has been described in the white paper of Gustafssonans [41]. The Delta^4 phantom is calibrated to absolute dose measurement using a farmer reference ion chamber for the specific linac, and can thus be used to measure absolute dose levels [1].

Octavius 4D

Octavius 4D is a 4D dosimetry system designed to verify IMRT and IMAT plans. It contains Octavius detector 729, Octavius 4D phantom and Verisoft software. Octavius detector 729 is a 2D detector array with 729 plane-parallel ion chambers. Each ion chamber is $5 \times 5 \times 5$ mm^3 in size, spacing 10 mm center-to-center. These chambers are located in a matrix of 27×27 providing a maximum field size of 27 cm $\times$ 27 cm. The octavius 729 array can handle increased dose rate up to 48 Gy/min. The Octavius 4D phantom is a motorized cylindrical, rotational phantom with a diameter of 32.0 cm and a length of 34.3 cm. The Octavius detector 729 is inserted into the Octavius 4D phantom. An external inclinometer mounted on the gantry provides

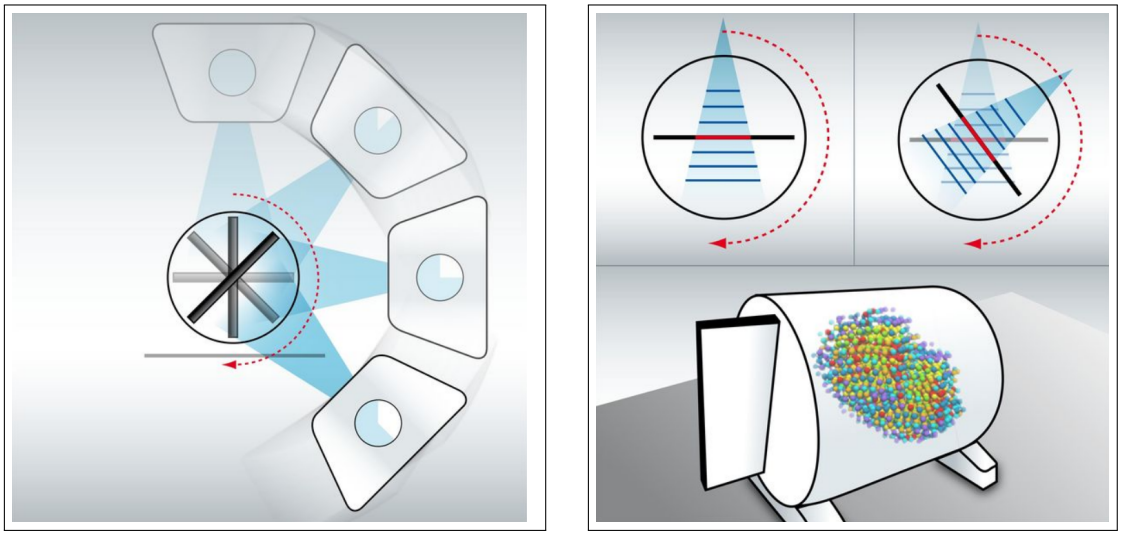

(a) (b)

Figure 3.6: (a) synchronous rotation of the Octavius 4D system with the gantry. The Octavius detector measures a dose plane for each gantry angle, thereby always remaining perpendicular to the incident beam. (b) The dose plane are measured for each gantry angle then the measured dose points are used for obtaining a 3D dose volume (red: measured dose plane, blue: calculated values) [4]

constant feedback on the actual gantry angle and allows the control unit to rotate the phantom accordingly, keeping the 2D array perpendicular to the beam axis at all times as illustrated in Fig.3.6.a. Thus the orthogonal beam output can be measured from

all angles with no need for angular corrections or detector calibrations to compensate for the directional response of its detector. The measured dose plane for each gantry angle is used to determine the dose values along the source-detector rays. To calculate these values, Octavius 4D applies a sophisticated algorithm developed by the DKFZ Heidelberg which is based on PDD curves measured for different field sizes for the accelerator and energy in use. All dose points measured are used for obtaining a 3D dose volume as shown in Fig.3.6.b. by applying a 3D dose reconstruction algorithm [18]. The capability 3D dose analysis of the VeriSoft software allows to analyze the measurement results superimposed on the patient's computed tomography (CT) scan and performs a volume analysis comparing the measured dose against the calculated dose for the entire phantom volume [60, 15].

3.1.4 Treatment planning systems

Computerized TPS are used in external beam radiation therapy to generate beam shapes and dose distributions with the intent to maximize tumour control and minimize normal tissue complications [65] .

In the present study two TPS are used to create the required treatment plans - Oncentra and RayStation planning systems. Oncentra planning system (v4.1, Nucletron by ELEKTA Company) has been used to create IMRT plans using FFF as well as IMRT plans using FF beams. The performance of the FFF beam as a new modality for producing IMRT plans was evaluated through creating IMRT-FFF plans and comparing it with the IMRT plans created by applying FF beams. The other TPS is RayStation planning system (RaySearch Laboratories AB, Stockholm, Sweden). RayStation planning system version 3.00 and 3.99 has been used to create mARC and IMRT plans, which were required to evaluate the mARC technique and compare it with IMRT.

Oncentra Masterplan treatment planning system

Oncentra TPS is one of the TPSs used in radiotherapy clinic at University of Leipzig, Germany. The Oncentra TPS is a fully featured external beam 3D planning system with IMRT planning capabilities. It is fully Digital Imaging and Communications in Medicine Standard (DICOM) compliant and includes a collapsed cone algorithm for

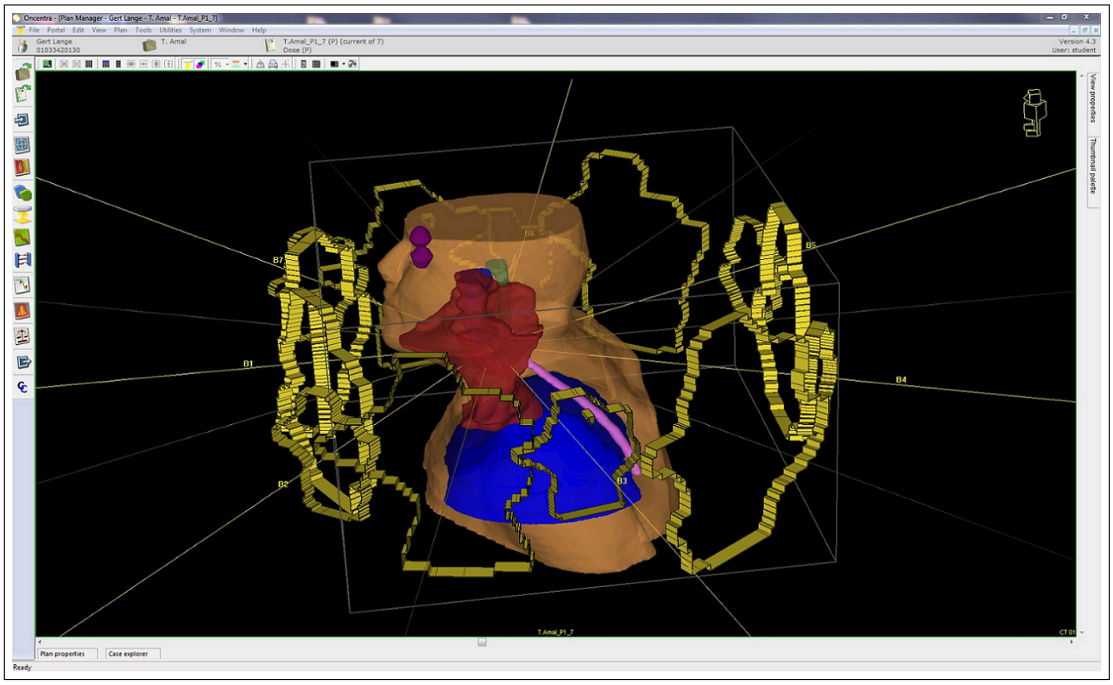

Figure 3.7: Oncentra Masterplan planning system

dose calculation. Accurate fluence modelling takes into account the exact shape of all beam-modifying devices as well as ensures the MLC leaf shapes and tongue and groove effects are accurately modelled [12].

IMRT (FF and FFF) plans required for the comparison study were performed with version 4.1. That version was commissioned with 6 MV and 10 MV FF beams, 7 MV and 11 MV FFF beams' data of Siemens Artiste linacs. To create IMRT plans the beam parameters are defined, then the IMRT plans are optimized with the option direct step and shoot (DSS) of the plan optimization activity after defining the objectives and the number of segments. The optimization process is started using a few iterations to find an initial set of CPs that meets the user and machine specific requirements. During the remaining iterations, the MLC leaf positions and segment weights are optimized [44].

RayStation treatment planning system

In 2012 RaySearch laboratories released RayStation planning system version 2.5 supporting all rotational arc capable linacs - (Elekta, Varian and Siemens) [8]. RayStation offers photon planning for all relevant delivery techniques, such as 3DCRT, S&S-IMRT, dynamic IMRT, modulated arcs and static arcs.

S&S-IMRT and mARC techniques are planned through an optimization procedure (inverse planning) where objectives and constraints for the desired dose are defined and the system produces the plan that matches these criteria best [13].

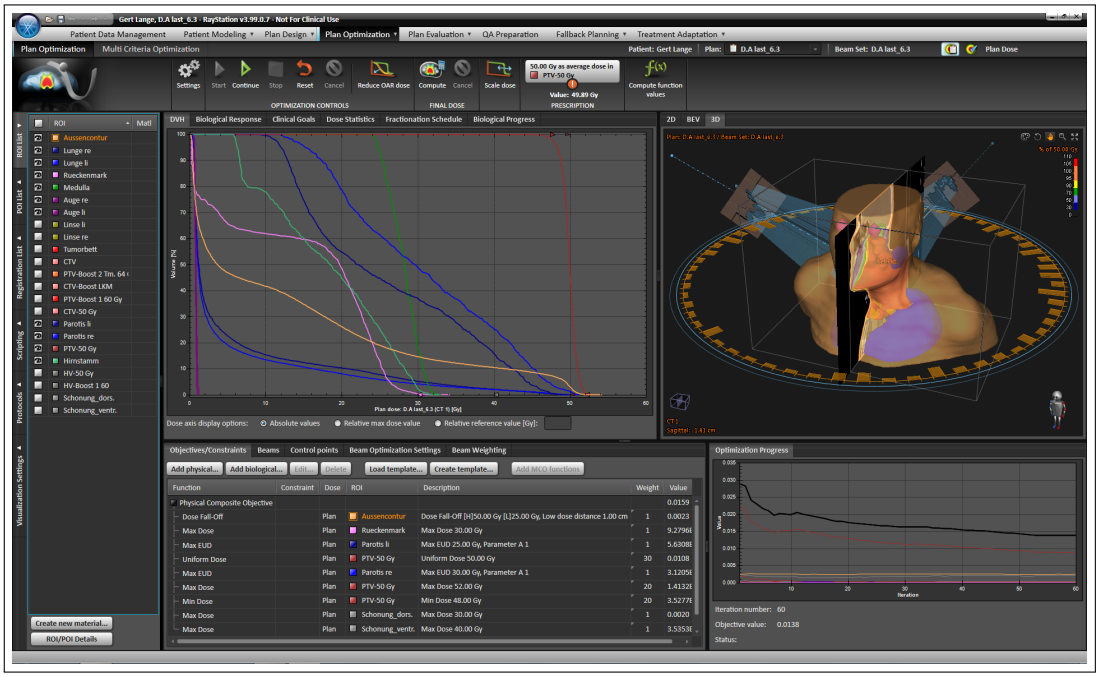

Figure 3.8: RayStation treatment planing system

RayStation TPS contains the collapsed cone photon dose calculation engine version 2.3 and RayArc modality. RayArc provides design and optimization of single or multiple-arc plans. Treatment plans are produced by direct and simultaneous optimization of all available mARC treatment parameters ensuring the fulfilment of accelerator constraints at the same time. The direct optimization of leaf positions and arc segment weights considering all machine limitations such as leaf speed, gantry speed and available dose rates make the optimized plan directly deliverable with no quality degrading post processing required [13]. The algorithm behind the optimization by RayStation as well as Oncentra Masterplane is the same, where the S&S-IMRT optimization module for Oncentra TPS comes from RaySearch.

RayArc introduces new optimization type VMAT and new group of VMAT specific optimization settings, which are used for mARC. The user sets up dose objectives in the same way as for S&S-IMRT optimization and starts an optimization. As input to the optimization the user can specify one or more arcs with any setting of gantry, couch, collimator, start and stop angles etc. The user can also set up one arc and have

RayArc create a dual arc plan where the second arc has the same setup as the first, but rotates in the opposite direction. The algorithm behind the dual arc feature strives to reduce leaf travel by distributing CPs between the two arcs based on the shapes of the segments. This generally leads to better target coverage and organ at risks (OARs) sparing for complex cases. The final result is a deliverable mARC plan.

By the time this work was finished the last upgrade of RayStation planning system is 4.5. We tested the principle performance of the first version of RayStation planing system (v.2.5) in our clinic after commissioning with the data of Artiste linac 7 MV and 11 MV FFF and later 10 MV FF was added. In the current study, RayStation TPS version 3.00 and version 3.99 are used to create the mARC and IMRT plans.

3.2 Methods

In this work the main dosimetric characteristics (depth dose curves, profiles, dose rate, surface dose) of unflattened 7 MV and 11 MV beams were determined and compared with that of 6 MV and 10 MV flat beams. These beams have been used to create IMRT treatment plans for IMRT-FF and IMRT-FFF comparison study. The plans required for the mARC planning study and the plan comparison of mARC with S&S-IMRT have been created by RayStation TPS using 7 MV, 11 MV FFF and 10 MV FF beams. For plan QA of IMRT and mARC plans, two different volumetric QA devices - Delta^4 and Octavius 4D have been used.

The measurements of 7 MV, 11 MV FFF and 10 MV FF were performed using Artiste digital linear accelerators and the acquisition of 6 MV FF data was done at another Artiste linac with an 6 MV FF beam before its upgrade to FFF mode.

All beams were calibrated under the same conditions, according to the German dosimetry protocol DIN 6800-2, (10×10 cm^2 field size, 90 cm SDD, 10 cm depth). The reference dose output at the central axis was the same for the corresponding energies (6 and 7 MV, and 10 and 11 MV, respectively).

All patients included in the treatment plans comparisons were selected from the list of the patients that had been treated before at the clinic of radiotherapy at University of Leipzig, Germany. Our strategy was to select patients who had tumors at different sites with different target complexity and volumes. The chosen clinical cases were

prostate, prostate with lymph nodes (prostate-LN) and head and neck (H&N). More details about these cases are given in sections 3.2.2 and 3.2.3.

3.2.1 Dosimetric parameters of FF and FFF beams

Depth dose curves and profiles of 6 MV FF, 7 MV FFF and 10 MV FF, 11 MV FFF were measured with a PTW MP3 Water-Tank (PTW Freiburg, Germany) and a PTW dosimetric diode (type 60008). The percentage depth dose (PDD) were measured on the central axis for open beams with field sizes from 1×1 cm^2 to 30×30 cm^2 at a source surface distance (SSD) of 90 cm. The dose profiles were normalized to the dose at central axis to demonstrate the changes due to removing the flattening filter.

The dose within the build-up region for 6 MV, 7 MV, 10 MV and 11 MV were measured using acrylic slab phantom PMMA and PTW parallel plane chamber type 23344. The chamber is designed for the use in solid state phantoms and field size up to 40 × 40 cm^2. The measurements of the dose build-up were started at 1 mm and ended at depth of dose maximum (d_{max}) with SSD of 100 cm. Acrylic phantom sheets of different thicknesses (1, 2, 5 and 10 mm) were combined enabling us to vary the measuring depth. The 1 mm thick acrylic phantom sheet was placed above the chamber and the absolute dose was measured at different sizes of open fields (3×3, 5×5, 10×10, 20×20 and 30×30 cm^2). The process was repeated for depths of 2, 3, 4, 5 and 15 mm for 6 MV and 7 MV and up to 25 mm for 10 MV and 11 MV.

3.2.2 Comparison of IMRT-FF and IMRT-FFF

IMRT-FF and IMRT-FFF treatment plan comparison study was performed for twenty patients who had tumors at different sites with different target complexity and volumes. The chosen clinical cases were 6 prostate patients with planning target volume (PTV) ranging from 165 to 237 cm^3, 6 prostate-LN patients with summation PTVs ranging from 922 to 1254 cm^3 and 8 H&N patients with summations PTVs ranging from 568 to 883 cm^3.

Two S&S-IMRT plans were created for each patient by applying seven beams with and without flattening filter for each case under the same optimization parameters and the same objectives. Energies of 10 MV FF and 11 MV FFF were used to cre-

ate the treatment plans for prostate and prostate-LN whereas 6 MV FF and 7 MV FFF were used for H&N plans. The prescribed treatment dose and fractionation of prostate, prostate-LN and H&N were 74 Gy/37 Fx, 50.4 Gy/25 Fx and 50 Gy/25 Fx, respectively.

All IMRT-FF and IMRT-FFF plans were created using TPS Oncentra masterplan V4.1. Dose distributions were calculated using the collapsed cone algorithm. The TPS was commissioned with beam data measured for the Artiste digital linear accelerators with 160 multileaf collimator operated with and without flattening filter.

3.2.3 mARC planning study

Before starting the mARC planning study, the performance of RayStation planning system to create mARC plans was tested for different clinical cases. We selected cases representing different sizes and different degrees of complexity to evaluate mARC technique and compare its performance with S&S-IMRT. Eighteen patients with tumors in different body regions (6 patients prostate, 6 patients prostate-LN and 6 patients H&N) were selected for this planning study from the list of the patients, who were treated before at our clinic. Various mARC plans with variant values of F.G.S (4°, 6° and 8°) - denoted in the following by SA (4), SA (6), SA (8) - and DA, and S&S-IMRT with seven and nine beams (7B and 9B) were created using RayStation planning system v.3.00 and v.3.99. Both versions of RayStation planning system produced identical dose distributions. The optimization of mARC and IMRT plans for each particular group of patients was performed with the same objectives and the planned dose of each patient was normalized to its PTV prescribed doses.

The number of segments is one of the optimization parameters of the IMRT treatment plan, which has an impact on plan quality and treatment efficiency. In case of mARC, the segments are known as arclets - defined by the number of OPs - as explained before in chapter two. Since mARC is a rotational technique based IMRT, the investigation of the influence of the number of arclets on mARC plan quality and mARC treatment efficiency is an important issue.

This comparison study is divided into three parts as illustrated in table 3.1.

1. Explanation of the effect of the number of arclets, by varying the F.G.S value, on

Table 3.1: The parts of mARC comparison study and the treatment plans created for the clinical cases included in each part.

Clinical Cases	F.G.S Effect	mARC and IMRT-FFF	mARC 10 MV FF and 11 MV FFF
Prostate-LN	SA (4) SA (6) SA (8)	SA (4) DA (6) IMRT 7B IMRT 9B	SA (4) SA (6) SA (8)
H&N	SA (4) SA (6) SA (8)	SA (4) DA (6) IMRT 7B IMRT 9B	
Prostate	SA (4) SA (8)	SA (4) SA (8) IMRT 7B IMRT 9B	SA (8)

the quality and the efficiency of the mARC treatment plan. This has been done through comparison of single arc plans with variant values of F.G.S. The value of F.G.S started with 4° because Siemens recommended that F.G.S should not be smaller than 4° in order to keep overall delivery times small [6]. The mARC plans SA (4), SA (6) and SA (8) were created for prostate-LN using 11 MV FFF beams and for H&N using 7 MV FFF beams. For prostate, SA (4) and SA (8) plans were created using 11 MV FFF.

2. Comparison between two different techniques of mARC (SA and DA) to evaluate their performance. Then both of them should be compared with S&S-IMRT 7B and 9B and estimated whether SA and DA are superior or equivalent to IMRT. For complex cases two arcs are supposed to achieve more plan modulation and hence better target coverage and more OARs sparing. Considering the result of the part 1, SA (4) was the optimal single arc plan so it was chosen and compared with the DA plans for prostate-LN and H&N as complex cases. We selected DA of F.G.S of 6° - DA (6) - because on one hand DA (4) lead to 180 arclets that need long TDT and on the other hand DA (8) has the same number of arclets as SA (4), which lead to comparable plan quality. Prostate is a simple small target and applying SA plan is sufficient to achieve an optimal plan. So there is no need to apply dual arc with more MU and longer treatment time. Therefore, the results of SA (4) and SA (8) were compared with IMRT 7B and IMRT 9B.

Table 3.2: Summery of the mARC and IMRT plans created for each group of patients.

Clinical Cases	Technique	No. of segments	Beam energy
Prostate	SA (4)	90	11 MV FFF
	SA (8)	45	11 MV FFF and 10 MV FF
	IMRT 7B	50	11 MV FFF
	IMRT 9B	50	11 MV FFF
Prostate-LN	SA (4)	90	11 MV FFF and 10 MV FF
	SA (6)	60	11 MV FFF and 10 MV FF
	SA (8)	45	11 MV FFF and 10 MV FF
	DA (6)	122	11 MV FFF
	IMRT 7B	60	11 MV FFF
	IMRT 9B	60	11 MV FFF
H&N	SA (4)	90	7 MV FFF
	SA (6)	60	7 MV FFF
	SA (8)	45	7 MV FFF
	DA (6)	122	7 MV FFF
	IMRT 7B	50	7 MV FFF
	IMRT 9B	50	7 MV FFF

3. Estimation of the performance of mARC plans in case of using FF and FFF beams. For this purpose, SA (4), SA (6) and SA (8) plans of prostate-LN, and SA (8) plans of prostate created by using 11 MV FFF were copied and optimized again by applying 10 MV FF.

All the single arc plans have the same setup, rotated in clockwise direction with the same arc span (358°), starting angle (181°), couch angle 0° and collimator angle 45° except prostate, where the collimator angle was 0°. The dual arc plans consisted of two coplanar arcs with F.G.S 6° [DA (6)], the first arc had the same setup as the previous single arcs and the second arc was created simultaneously during the optimization with the same setup of the first one but in counterclockwise direction. S&S IMRT treatment plans were created for each group of patients by applying 7 and 9 equal-spaced coplanar beams, respectively starting at gantry angle of 0° and with collimator angle of 0°. The maximum number of segments of the IMRT plans were set to be 50 for prostate and H&N and 60 segments for prostate-LN. A summary of mARC and IMRT plans which were created for each group of patients, the number of segments and the beam energy of each technique are listed in table 3.2.

3.2.4 Planning comparison parameters

In the current work two parameters, plan quality and treatment efficiency have been used to evaluate IMRT plans created by FF and FFF beams, evaluate the performance of mARC techniques and compare it with IMRT plans.

Plan quality

The plan quality was estimated by:

1. Visual examination of the dose distribution (CT slices) and evaluating the dose volume histogram (DVH) of each plan, which are important to decide whether plan is clinically acceptable.

2. Comparing clinical goals for PTVs and OARs with their calculated values. The clinical goals of PTVs and OARs are listed in table 3.3.

3. Calculating the homogeneity index (HI) and the conformity number (CN). Both act as an additional metric to measure the quality of the plans and facilitate the comparison between the applied techniques.

The HI describes the uniformity of the dose within the planning target volume. In the present work, the HI was calculated by using the formula 3.3 [85], which is the most commonly used formula in the literature. Kataria et al. [49] have calculated the HI of 99 patients who had tumors in different body regions using various formulae include the formula that is used int the present work. They found a high level of agreement between different formulae used for calculating the HI.

$$HI = \frac{(D_2 - D_{98})}{PD} 100 \tag{3.3}$$

where PD is the prescribed dose, minimum dose (D_{98}) is the minimum dose and maximum dose (D_2) is the maximum dose within the PTV. The lower the HI values the more homogeneous is the target dose.

Table 3.3: Clinical goals of PTVs and OARs. PTV clinical goals are average dose (D_{mean}) = prescribed dose, D_{98} define 95 % of the PD delivered to 98 % of the target volume and D_2 define 105 % of the PD delivered to 2 % of the target volume.

Clinial Cases	PTVs Clinical Goals	OARs	OARs Clinical Goals
Prostate	D_{mean} = 74 Gy $D_{98} \geq$ 70.3 Gy $D_2 \leqslant$ 77.7 Gy	Rectum	$D_{75} <$ 30 Gy
		Bladder	$D_{80} <$ 20 Gy $D_{60} <$ 40 Gy
		Femur L&R	D_1(Max.dose) $<$ 45 Gy
Prostate-LN	D_{mean} = 50.4 Gy $D_{98} \geq$ 47.88 Gy $D_2 \leqslant$ 52.9 Gy	Rectum	$D_{75} <$ 30 Gy
		Bladder	$D_{80} <$ 20 Gy $D_{60} <$ 40 Gy
		Femur L&R	D_1(Max.dose) $<$ 45 Gy
H&N	D_{mean} = 50 Gy $D_{98} \geq$ 47.5 Gy $D_2 \leqslant$ 52.5 Gy	Spinal Cord	D_1(Max.dose) $<$ 45 Gy
		Contralateral parotid	Mean dose $\leq$ 25 Gy
		Ipsilateral parotid	Mean dose $\leq$ 30 Gy

The reason for choosing D_{98} and D_2 to represent the minimum and maximum doses, respectively, is that the calculation of true minimum or maximum dose is sensitive to the dose-calculation parameters, such as grid size and grid placement, and the high-dose gradient that is common in IMRT [85]. In 2010, the recommendation of ICRU Report 83 was to use D_2, D_{98} and D_{mean} as parameters to describe the dose distribution within the PTV for IMRT techniques [16].

The CN suggested by Van't Riet et al. [79] was used as a tool to quantitatively assess the degree of dose conformity. It is defined as:

$$CN = \left(\frac{PTV_{RI}}{PTV}\right)\left(\frac{PTV_{RI}}{TV_{RI}}\right) \tag{3.4}$$

where PTV_{RI} is the target volume covered by the reference isodose, PTV is the planning target volume, TV_{RI} is the total volume within the reference isodose and the reference isodose is set to 95 % of the PD. The first term of the equation describes the quality of the coverage of the PTV and the second term refers to the volume of healthy tissue receiving a dose higher than or equal to the reference dose. The value of the CN is between 0 and 1. A value of 1 indicates optimal conformity representing a reference isodose covering the PTV without irradiation of healthy tissue with doses equal to or higher than the reference dose. On the other hand a value of 0 means no conformity at all.

In this work an additional PTV structure was drawn as PTV summation for the

cases with multiple PTVs (prostate-LN and H&N) taking into account the overlap between PTV volumes and therefore enabling a precise calculation of PTV clinical goals. The calculated values for the PTVs were used to calculate the HI.

Treatment efficiency

Treatment efficiency was measured by treatment delivery time and number of MU required for delivering the planned dose. The Artiste linacs in our clinic are calibrated under the reference conditions (field size (F.S) 10×10 cm^2, 100 cm SSD, d_{max}) to deliver approximately 1cGy/MU for all photon beam energies. The numbers of MU were calculated by the TPS. The treatment delivery time was measured without adding the time for patient set-up.

The statistical analysis of the results of the HI, the CN and the number of MU for each clinical case of each part of the present study was done using the matched-pair Wilcoxon Signed-Rank Test. This test is non-parametric test valid for non-normal distributed data. It calculates both a W-value and Z-value but only the W-value (summation of ranks) is calculated to evaluate the results if the size of the sample (N) is less than 10, as in the present work. If the value of W for $N < 10$ at $p \leqslant 0.05$ is 0, the difference is significant and if the value of $W > 0$ for $N < 10$ at $p \leqslant 0.05$, the difference is not significant. Wilcoxon Signed-Rank Test is calculated through the Origin software version 8.1.

3.2.5 Dosimetric verification

The treatment plans were verified using Delta^4 and Octavius 4D phantoms, which are recommended for plan verification with FF and FFF static and rotational beams. Both phantoms were tested and evaluated for IMRT and VMAT [42, 20, 69, 51, 78] and it was found that both devices shorten the time required for delivery verification due to their easy set-up and the ability of instantaneously reading, processing and analyzing the plan.

Delta^4 phantom was used to verify the mARC and IMRT plans for prostate and H&N. The selected H&N plans to verify using Delta^4 belong to patients of the volumes suited to its detection area - 20 cm × 20 cm per plane. For prostate-LN of large

treatment F.S, Octavius 4D was used because of its bigger active area - 27 cm × 27 cm. To compare the accuracy of the verification results of both systems, the plans of two patients of prostate and two patients of H&N were verified by both phantoms and the verification results were compared.

Inside the TPS all the treatment plans were transferred to both phantoms and recalculate the dose distribution. Each patient specific treatment plan and the planned dose distribution created for each phantom were imported into the Delta^4 program and the VeriSoft software in case of Octavius 4D as DICOM RT format. In parallel the calculated plans were exported from the RayStation TPS as DICOM file to Mosaiq v.2.5 then to linac's control console, which controls the planned dose delivery.

At the accelerator the measurement were performed after the setup of the phantom, which was positioned isocentrically on the treatment couch. During delivery the collected data were controlled by an inclinometer attached to the gantry to let the software register the measured dose with the current gantry angle. Each measured dose package is tagged with the currently measured gantry angle and the dose packages are sorted under the nearest CP. The angle resolution of the CPs is determined by the treatment plan. The verification was done by comparing the measured data with the planned dose calculated by the TPS for the phantom and imported in the software. The analysis of that comparison is performed using the comparison options of both systems like dose distribution in volume and profile. Furthermore, The evaluation methods, dose deviation, distance-to-agreement and gamma index are used. Local gamma is applied by VeriSoft and Delta^4 software. The gamma evaluation tool was used with dose deviation of 3 % and distance to agreement of 3 mm (3 %, 3mm).

Chapter 4

Results

4.1 Dosimetric characteristics of FF and FFF beams

Flattening filter removal results in non-uniform beam profiles, increases the dose rate and causes two additional effects: beam softening and reduction of the scattered radiation from the linac head. These effects lead to different characteristics of FFF photon beam, which consequently could affect the quality and efficiency of the IMRT treatment plans.

4.1.1 Dose rate

The flattening filter removes a large fraction of the primary photons from the beam, especially those close to the central axis. So the main effect expected due to removing the flattening filter is increasing the intensity of the photon beam at the central axis. Artiste linacs operated in FFF mode can produce dose rates up to 2000 MU/min regardless of the selected photon energy, 7 MV or 11 MV, in contrast to FF mode, where 300 MU/min are provided for 6 MV and 500 MU/min for 10 MV. Beam-on time should decrease as a result of the high dose rate of FFF beams. Reduced beam on time has a potential for decreasing total delivery time but there are also other parameters that affect the time of the treatment like the number of MU, the number of segments and number of MU per segment (MU/seg) for IMRT treatment. This will be discussed by exploring the treatment delivery time of the IMRT treatment plans using FF and FFF beams.

4.1.2 Dose profile

At megavoltage electron energies, radiation interaction between the accelerated electron beam and the X-ray target's nuclei produce bremsstrahlung X-rays, which are forward

peaked. The flattening filter is used to flatten the beam and its removal results in non-uniform beam profiles.

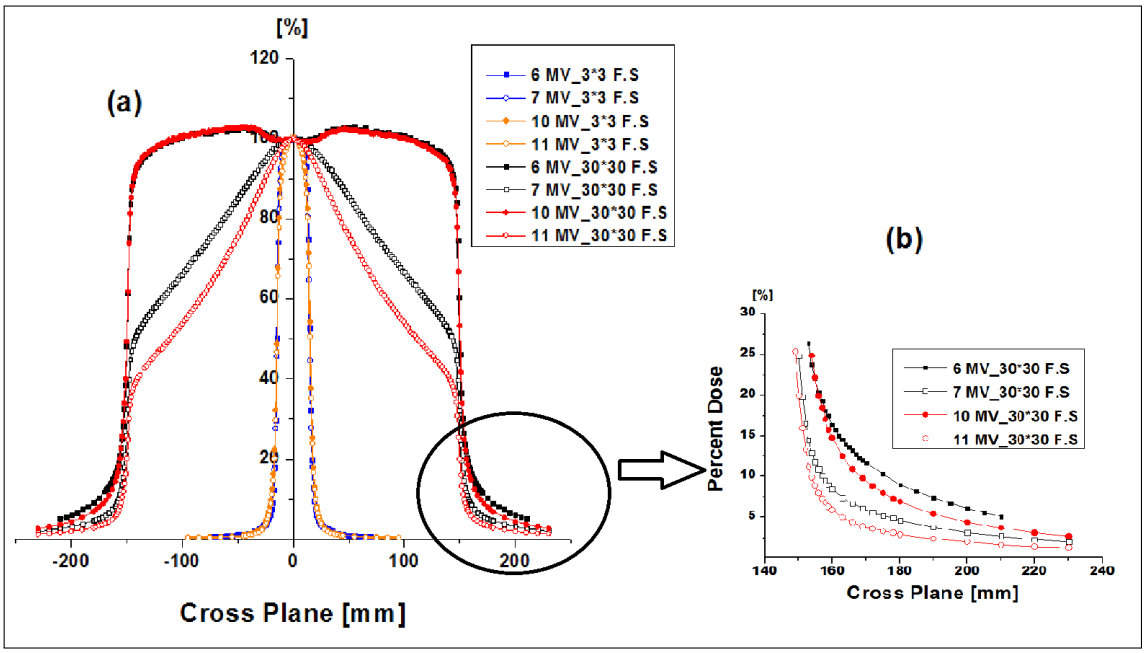

Figure 4.1: (a) Cross plane profiles of 6 MV, 10 MV FF and 7 M V, 11 MV FFF beams at field size 3×3 cm^2 and 30×30 cm^2 normalized to the dose at central axis. (b) Out-of-field dose at field size 30×30 cm^2 of 6 MV, 10 MV and 7 MV, 11 MV.

The dose profiles of 6 MV, 10 MV FF and 7 MV, 11 MV FFF beams were measured at field sizes ranging from 3×3 cm^2 to 30×30 cm^2 and normalized to the dose at central axis. Figure 4.1.a shows the dose profiles of FF and FFF beams. At 3×3 cm^2 as typical example of small field size, the profiles of the photon beams with and without flattening filter are similar for all measured photon beam energies. At 30×30 cm^2 as a typical example of large field size, the cone shape of the dose profiles of FFF beams differ significantly from those of FF beams. This cone shape of FFF beam profiles depends on the size of the field and the beam electron energy where the dose decreases with increasing distance away from the central axis for the same beam electron energy. For large field sizes, the higher the beam energy, the more peaked are the profiles. This is obvious in Fig.4.1.a where the lateral side of the profile of 11 MV beam is steeper than that of 7 MV and the central peak of the dose profile due to 11 MV is more tapered than that of 7 MV.

It can also be observed that at large field sizes the out-of-field doses due to FFF beams get less than that of FF beams, as shown in Fig.4.1.b, in consequence of the out-of-field scatter that is reduced due to removing the flattening filter.

4.1.3 Depth dose curve

The PDD curves of 6 MV, 10 MV FF and 7 MV, 11 MV FFF were measured and compared for different field sizes ranging from 1×1 cm^2 to 30×30 cm^2 and normalized to the depth of maximum dose for each measured field along the central axis. Figures 4.2 and 4.3 show PDD curves at reference F.S 10×10 cm^2 and examples of PDD curves of the small and large field sizes due to FF beams and their corresponding FFF beams. FFF beams of 7 MV and 11 MV produce PDD curves with similar characteristics to flattened beams of 6 MV and 10 MV as shown in Figs.4.2 and 4.3. We found that the depth of the d_{max} at reference F.S 10×10 cm^2 due to FF beams and their corresponding FFF beams have a slight diffrences, 3 mm betweem 6 MV and 7 MV and 5 mm between 10 MV and 11 MV. That could be explained by two competing effects due to inserting and removing the flattening filter. In case of FF beams the filter harden the beams leading to increase of the depth of d_{max} and the low energy scattered radiation reduces that depth. Removing the flattening filter adds the soft x-rays to the beam spectrum and eliminates a part of the scattered radiation.

At the exponential region of the PDD curve, a slight difference exhibits for dose fall-off between 6 and 7 MV, and 10 and 11 MV. Other investigators [28, 72, 81] registered a steeper dose fall-off of FFF beams at the exponential region than that of FF beams of the same electron energy because the addition of soft x-rays to the beam spectrum due to removing the flattening filter, lowers the mean energy of FFF beams. To avoid this effect Siemens introduced FFF beams with higher maximum energies (7 MV and 11 MV) than those used for FF beams (6 MV and 10 MV) to get a dose distribution close to FF beams and to keep the expected advantages of FFF beams at the same time.

Figures 4.2 and 4.3 show also that the PDD curves exhibit a dependence on the field size for both FF and FFF beams with increasing doses in the exponential region with increasing field size. It is also observed that the PDD curves of FF and FFF beams for 10×10 cm^2 are almost identical and there are only slight differences for smaller and larger fields.

The PDD curves show also deviations between FF and FFF beams in the buildup region. In order to describe these differences in more detail, measurements with another

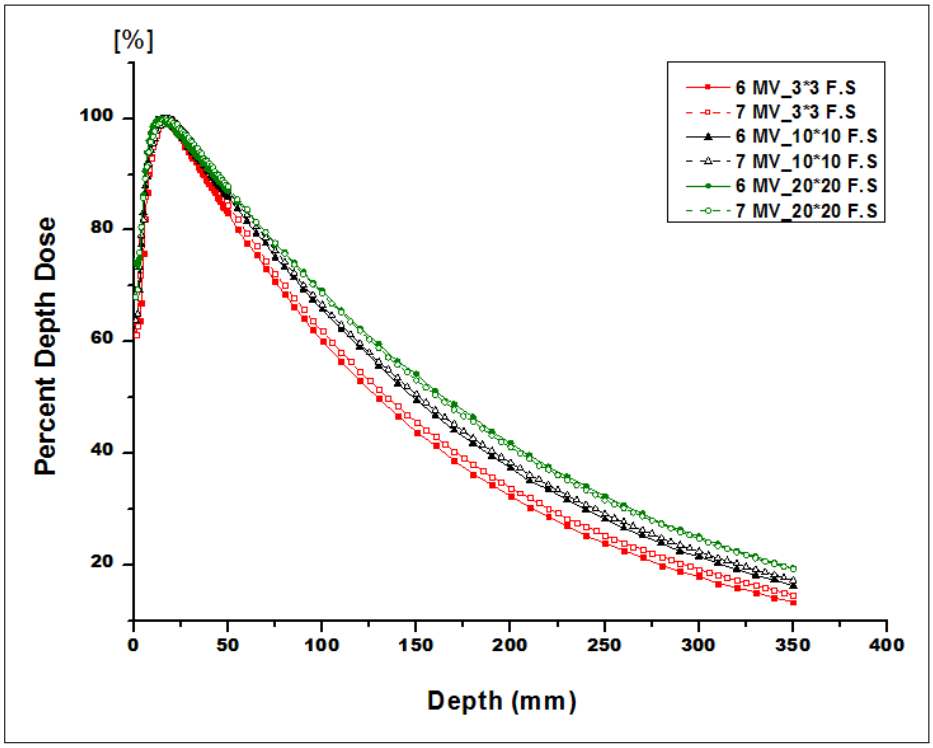

Figure 4.2: PDD curves of 6 MV FF (solid lines) compared with 7 MV FFF beam (dotted lines) for field sizes 3×3 cm^2, 10×10 cm^2 and 30×30 cm^2 at SSD 90 cm.

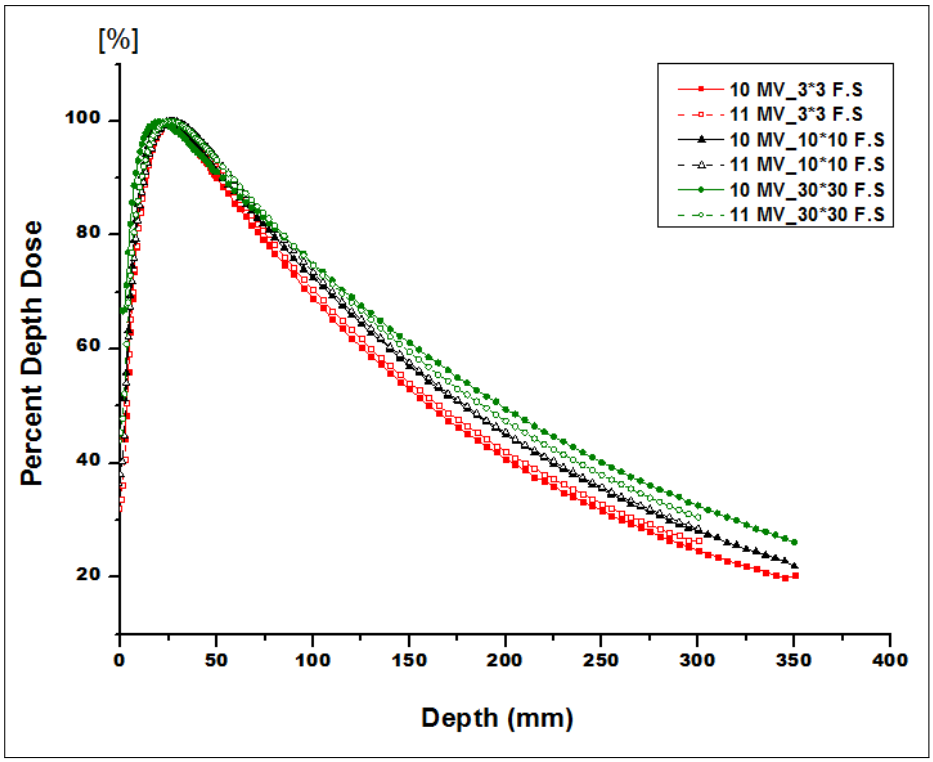

Figure 4.3: PDD curves in water of 10 MV FF (solid lines) compared with 11 MV FFF beam (dotted lines) for field sizes 3×3 cm^2, 10×10 cm^2 and 30×30 cm^2 at SSD 90 cm.

detector (PTW parallel plate ionization chamber Type 23344) along the depth axis were performed for all FF and FFF beams and for various field sizes.

4.1.4 Dose in buildup region

On the one hand the flattening filter hardens the beam and it is a source of the low energy scattered radiation. Removing the flattening filter from the linac reduces this scattered radiation and the electron contamination produced by the filter. The low energy component in FFF beams might affect the dose distribution close to the surface. Therefore, it is important to measure the dose in buildup region produced by FF and FFF photon beams to estimate the changes which result from the removal of the flattening filter. The measurements were performed using PTW parallel plate ionization chamber Type 23344 along the depth axis for all FF and FFF beams and for various F.Ss. The buildup curves of 7 MV and 11 MV FFF were plotted and compared with its corresponding 6 MV and 10 MV FF. The measured doses in the buildup region of the same field sizes and at different depths for FF and FFF beams were normalized to the dose at d_{max} of each field size. Figures 4.4 and 4.5 show the buildup curves of each pair of energy and Figs.4.6 and 4.7 show the relation between field size and relative buildup dose (measured dose normalized to the d_{max} at the reference depth of the field size 10×10 cm^2).

According to these figures a slight increase of the buildup dose is observed at field sizes smaller than 10×10 cm^2 for the FFF photon beams in comparison with FF beams. That is because the FFF beams include more low energy components and hence softer energy spectra, which lead to increased dose in the buildup region. For field sizes larger than 10×10 cm^2 the buildup doses in FF photon beams are higher than that of FFF beams and that is because the scattered radiation due to the flattening filter is increasing with field size. This means that the scattered radiation at large field sizes due to FF beams affects the dose in the buildup region more than the beam softening leading to an increase of the dose buildup of the FFF beams. This is clearly evident through the calculation of the dose ratio of the largest field size (30×30 cm^2) to the smallest field size (3×3 cm^2) at each depth for each electron energy, these dose ratio calculations are listed in table 4.1.

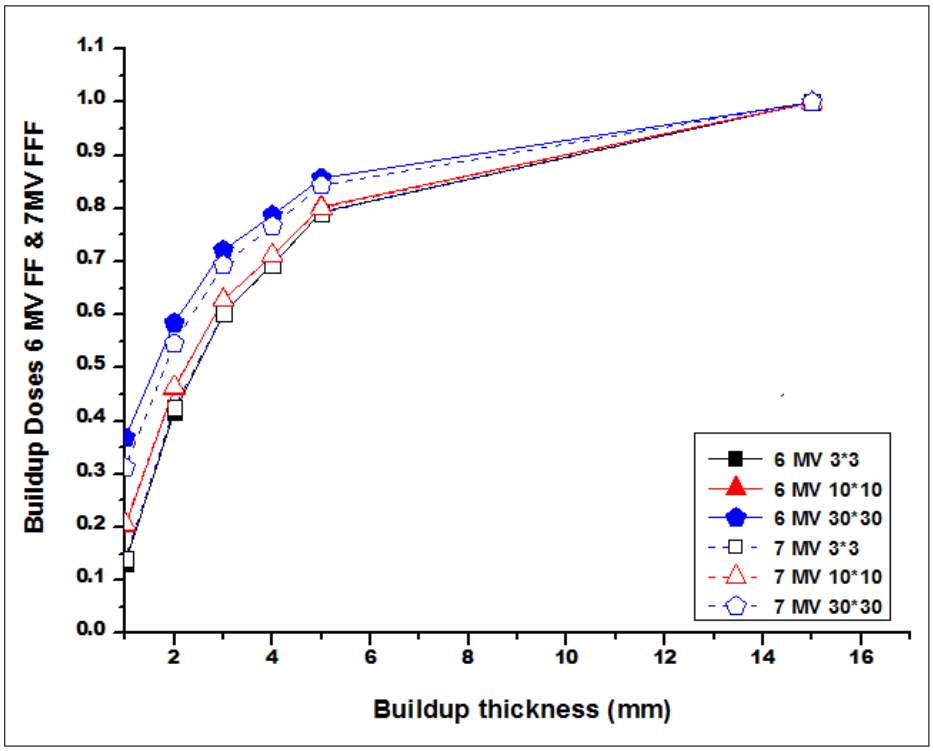

Figure 4.4: Build-up curves 6 MV FF and 7 MV FFF for different field sizes measured in solid water normalized to the maximum dose of each field size.

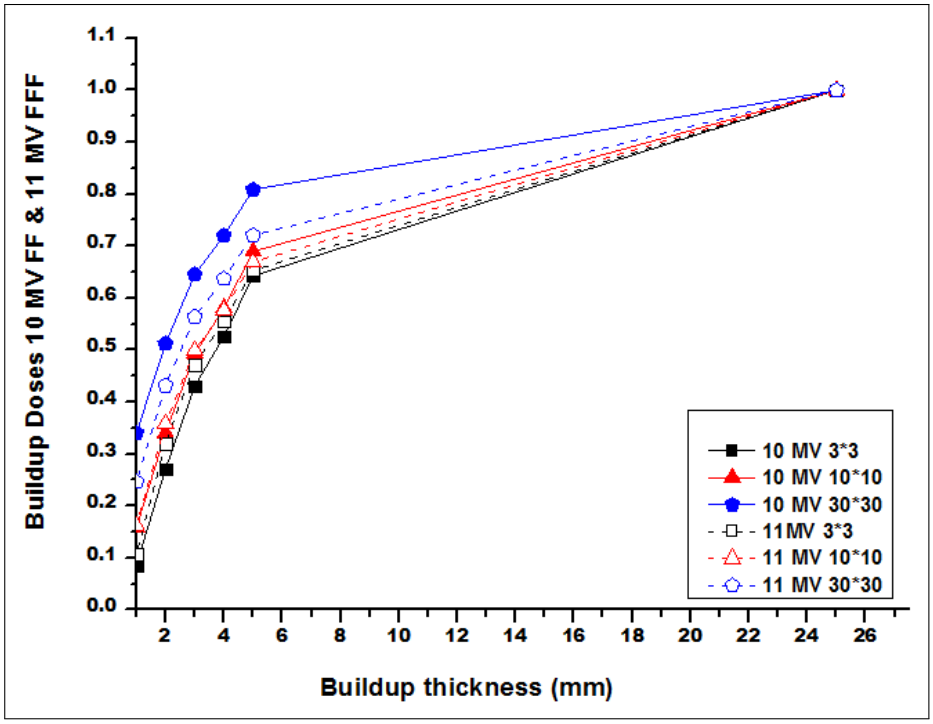

Figure 4.5: Build-up curves of 10 MV FF and 11 MV FFF for different field sizes measured in solid water normalized to the maximum dose of each field size.

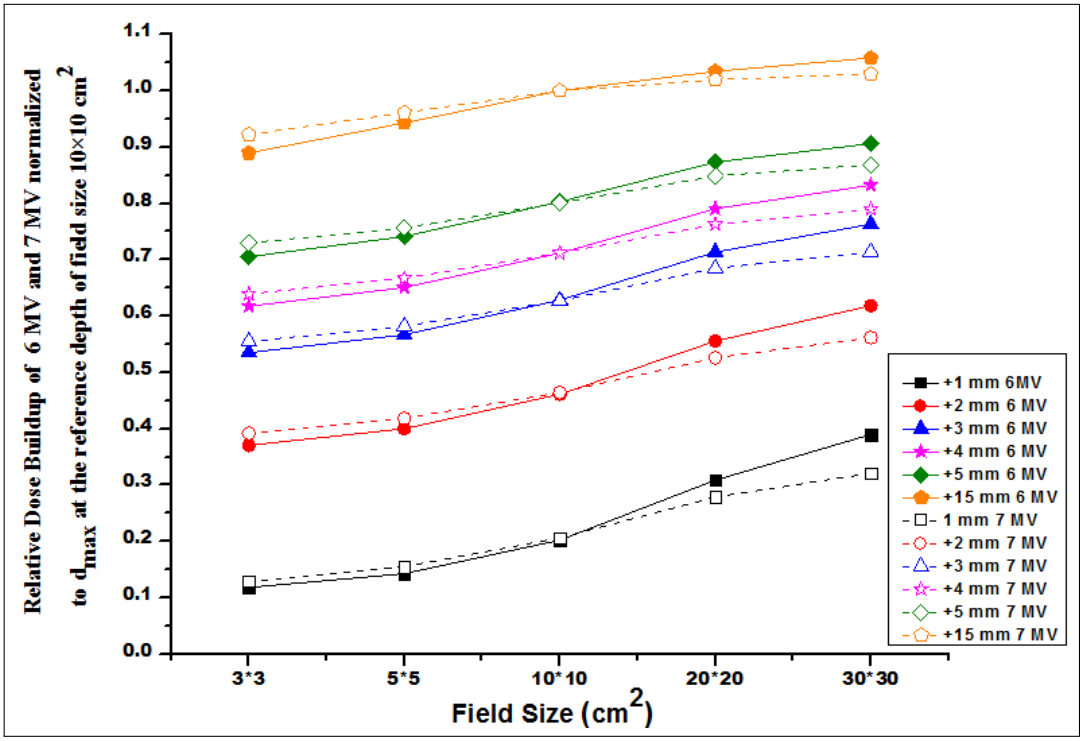

Figure 4.6: Relative dose buildup of 6 MV FF and 7 MV FFF normalized to d_{max} at field size 10×10 cm^2.

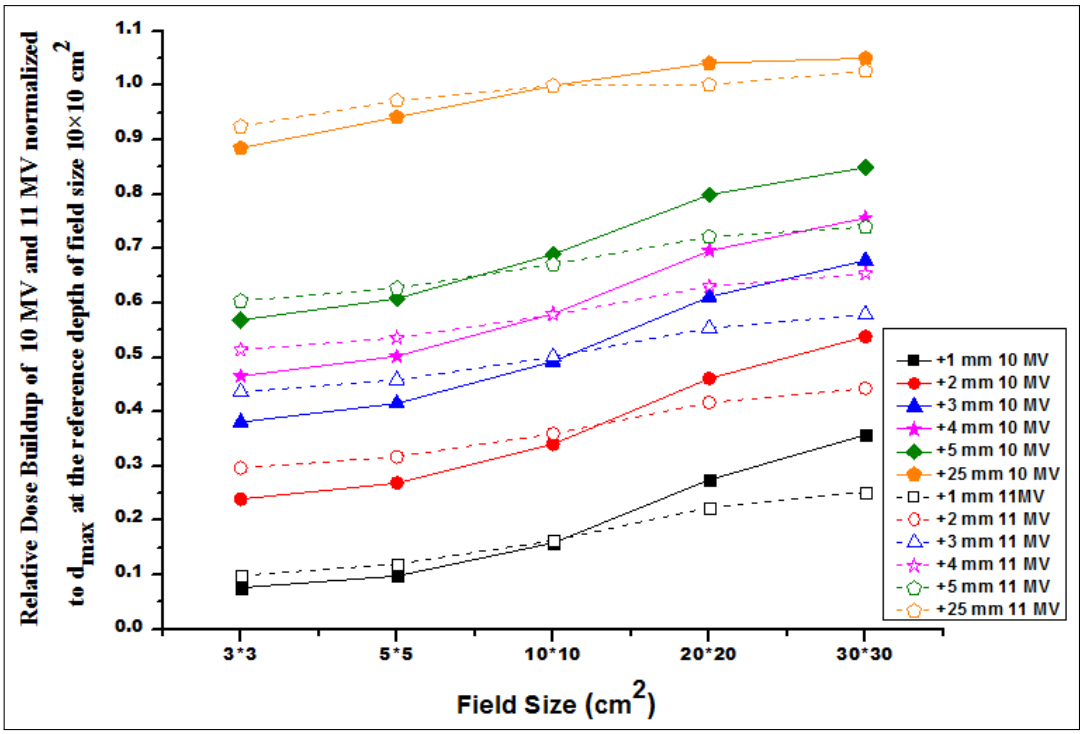

Figure 4.7: Relative dose buildup of 10 MV FF and 11 MV FFF normalized to d_{max} at field size 10×10 cm^2.

Table 4.1: Dose ratio of the largest field size (30×30 cm^2) to the smallest field size (3×3 cm^2) at each depth for each electron energy.

Depth (mm)	6 MV	7 MV	10 MV	11 MV
1	3.3	2.5	4.6	2.5
2	1.67	1.4	2.25	1.5
3	1.4	1.28	1.8	1.3
4	1.3	1.23	1.6	1.27
5	1.28	1.2	1.5	1.23
15	1.19	1.1	-	-
25	-	-	1.18	1.1

According to Figs.4.6, 4.7 and table 4.1, dose in buildup region due to FFF beams is less field size dependent in comparison with that due to FF beams. Furthermore, the difference between the dose ratio of the largest to smallest field size in case of 6 MV and 7 MV beams is less than the difference between the 10 MV and 11 MV, respectively.

4.2 Comparison of IMRT-FF and IMRT-FFF

A comparison between the IMRT plans using FF and FFF photon beams was performed for twenty patients with different tumour sites, target complexity and volumes. The chosen clinical cases were 6 patients with irradiation of the prostate only, 6 patients with irradiation of the prostate and the regional lymph nodes (prostate-LN) and 8 patients with cancer in the head and neck (H&N) region. As mentioned before, two parameters were used to assess the results of this comparison study: plan quality and treatment efficiency.

4.2.1 Plan quality

DVHs analysis and PTV clinical goals

The IMRT plans were optimized with the same objectives for each group of patients. Examples of dose distribution of transversal CT sections and DVHs of the prostate, prostate-LN and H&N due to FF and FFF IMRT plans are shown in Figs.4.8, 4.9 and 4.10.

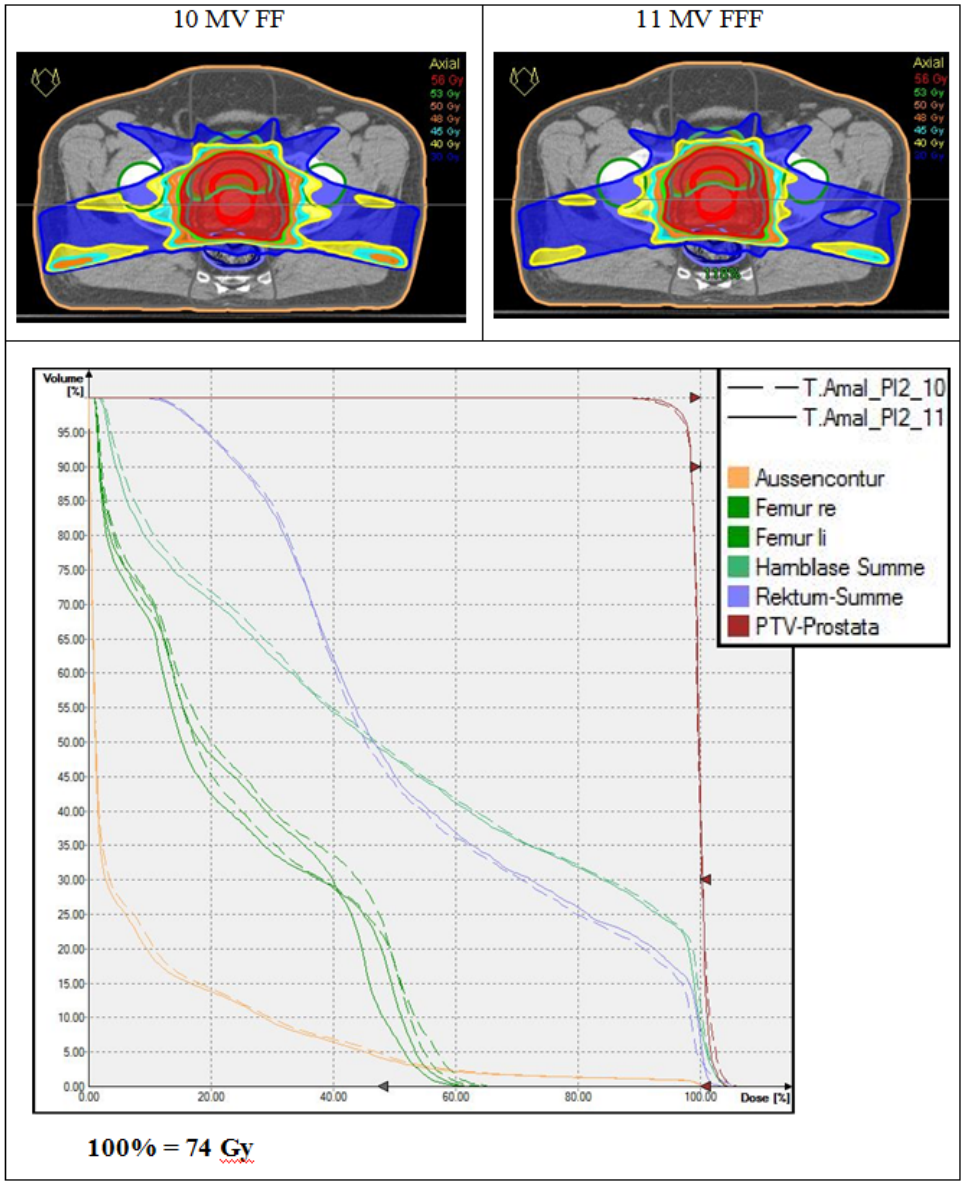

Figure 4.8: Dose distribution and DVH comparison between IMRT plans created with 7 beams for prostate, FF (dashed line) and FFF (solid line).

DVH comparison, the visual examination of dose distributions and the calculated values of the clinical goals show that both IMRT modalities (FF and FFF)can deliver clinically acceptable plans for all cases. Both modalities achieve the dose distribution within the PTVs with negligible differences. Dose distribution to the OARs, rectum, bladder and femoral heads for prostate and prostate-LN patients, and spinal cord, ipsilateral and contralateral parotid for H&N patients were nearly the same.

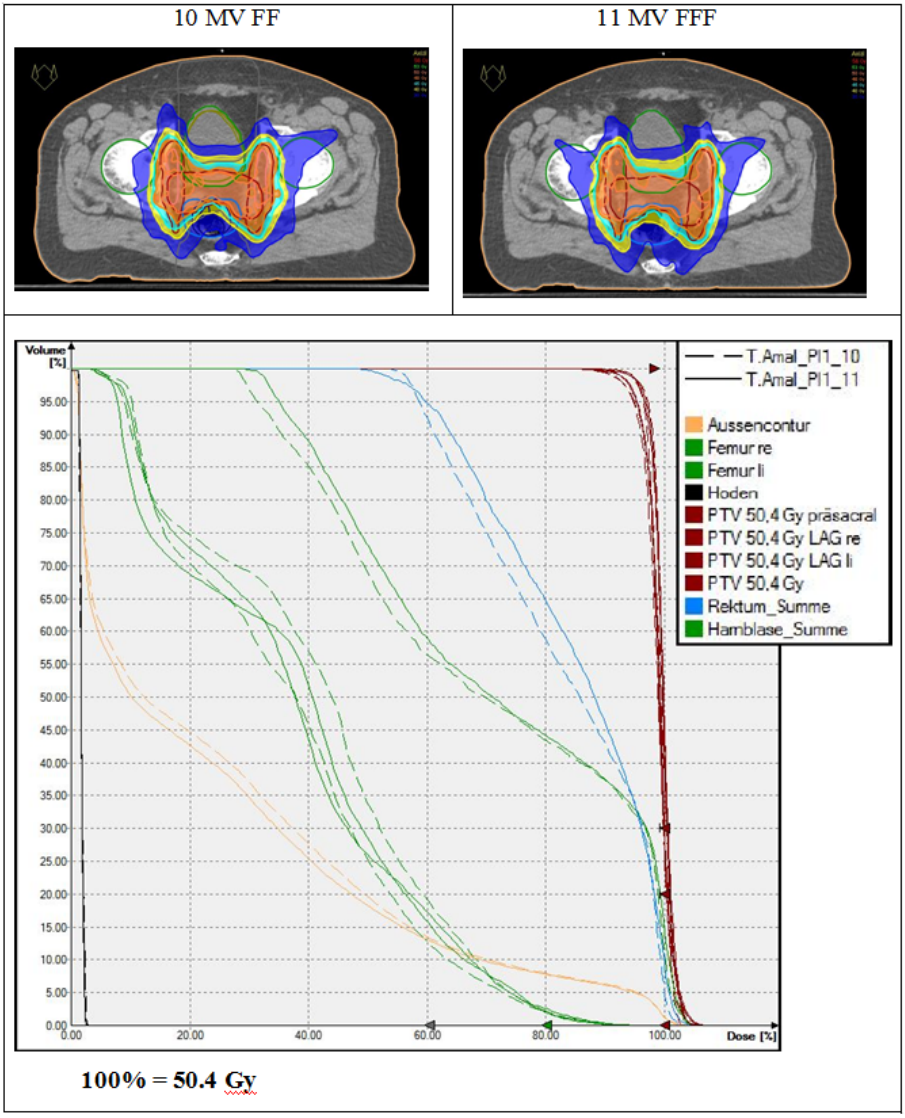

Figure 4.9: Dose distribution and DVH comparison between IMRT plans created with 7 beams for prostate-LN, FF (dashed line) and FFF (solid line).

The estimated plan values of D_{mean}, D_{98} and D_2 of PTV are compared with the PTV clinical goals in table 4.2. IMRT-FF and IMRT-FFF achieve the PTV clinical goals of all cases except the minimum dose of some prostate-LN patients because the volume of the bladder and rectum included in PTV varied from patient to patient.

OAR clinical goals of the prostate, prostate-LN and H&N are listed in table 4.3 in comparison with the results of each technique. For prostate, both IMRT techniques achieve the OARs clinical goals but the bladder of some patients was spared more using IMRT-FFF. For prostate-LN as illustrated in table 4.3, IMRT-FF and IMRT-FFF can spare the femur and achieve the clinical goal $D_{60} < 40$ Gy for the bladder for all patients. Both IMRT modalities could not achieve the clinical goals $D_{80} < 20$ Gy

for the bladder and $D_{75} < 30$ Gy for the rectum for all patients but sometimes values near the clinical goals could be achieved depending on the volume of the bladder and rectum included in the PTV. In case of H&N patients, spinal cord is spared by IMRT-FF and IMRT-FFF, while the contralateral and ipsilateral parotid are not spared for all patients by both modalities depending on how both parotids are close to the PTV or overlapped with it.

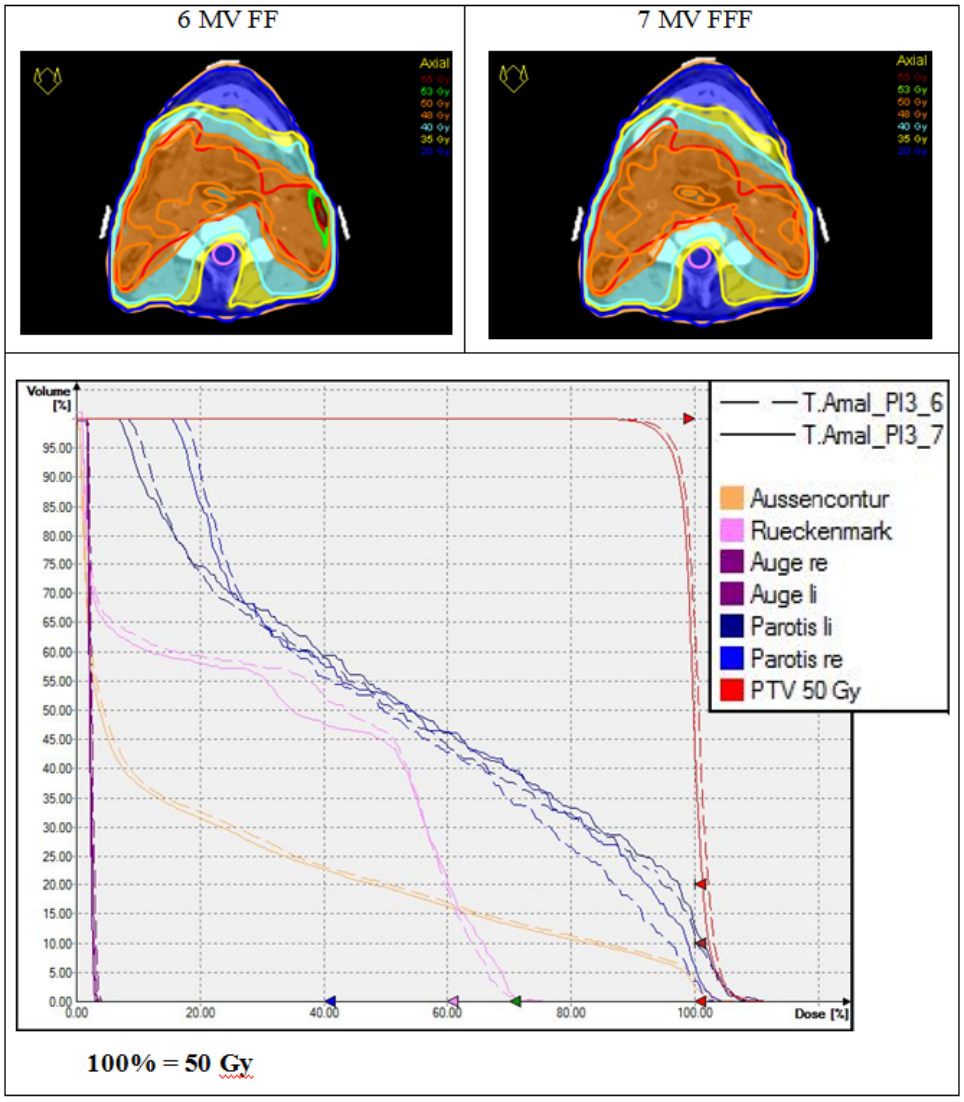

Figure 4.10: Dose distribution and DVH comparison between IMRT plans created with 7 beams for H&N, FF (dashed line) and FFF (solid line).

Table 4.2: Target average (D_{mean}), minimum(D_{98}) and maximum (D_2) dose of the prostate, prostate-LN and H&N plans

Clinial Cases	PTVs Clinical Goals	IMRT-FF	IMRT-FFF
Prostate	D $_{mean}$ = 74.00 Gy	73.95 ±0.04 (73.88 - 74.00)	73.94 ±0.04 (73.88 -73.97)
	$D_{98} \geq$ 70.30 Gy	70.80 ±0.87 (69.25 - 71.84)	71.75 ±0.36 (71.33 - 72.20)
	$D_2 \leqslant$ 77.70 Gy	76.34 ±0.50 (77.10 - 75.63)	75.90 ±0.30 (75.44 - 76.24)
Prostate-LN	D $_{mean}$ = 50.40 Gy	50.02 ±0.30 (49.70 - 50.45)	50.20 ±0.20 (49.80 - 50.40)
	$D_{98} \geq$ 47.88 Gy	47.30 ±0.80 (46.30 - 48.43)	47.70 ±0.70 (46.70 - 48.50)
	$D_2 \leqslant$ 52.90 Gy	52.00 ±0.60 (50.94 - 52.47)	52.30 ±0.50 (51.57 - 52.95)
H&N	D $_{mean}$ = 50.00 Gy	50.10 ±0.30 (49.92 - 50.60)	50.10 ±0.20 (49.94 - 50.60)
	$D_{98} \geq$ 47.50 Gy	47.81 ±0.73 (47.08 - 49.20)	47.70 ±0.60 (47.05 - 48.70)
	$D_2 \leqslant$ 52.50 Gy	52.20 ±0.45 (51.64 - 53.04)	52.30 ±0.35 (51.80 - 52.80)

Table 4.3: The clinical goals of OARs of the prostate, prostate-LN, H&N and the calculated values due to each techniques.

OAR	Clinical Goals	IMRT-FF	IMRT-FFF
Prostate			
Rectum	$D_{75} <$ 30 Gy	22.00 – 26.40	20.60 – 25.00
Bladder	$D_{80} <$ 20 Gy	1.10 – 14.40	1.00 – 11.70
	$D_{60} <$ 40 Gy	1.80 – 37.00	1.50 – 32.40
Femur L&R	D_1(Max.dose) < 45 Gy	41.30 – 45.00	40.00 – 44.00
Prostate-LN			
Rectum	$D_{75} <$ 30 Gy	32.00 – 40.00	32.30 – 40.80
Bladder	$D_{80} <$ 20 Gy	21.80 – 31.30	21.50 – 32.00
	$D_{60} <$ 40 Gy	28.00 – 38.80	28.00 – 37.60
Femur L&R	D_1 (Max.dose) < 45 Gy	39.20 – 45.00	36.00 – 43.60
H&N			
Spinal Cord	D_1(Max.dose) < 45 Gy	30.30 – 39.20	32.20 – 39.50
Contralat.parotid	Mean dose $\leq$ 25 Gy	16.50 – 31.40	15.00 – 31.00
Ipsilat.parotid	Mean dose $\leq$ 30 Gy	21.00 – 42.20	20.70 – 42.20

Homogeneity index (HI)

Figure 4.11 shows the values of the HI, which were calculated for IMRT plans using FF and FFF beams for prostate, prostate-LN and H&N. The HI of the prostate for IMRT-FFF plans are lower than for IMRT-FF plans, that means the dose distribution within the PTV is more homogeneous by applying FFF beams. The difference between both samples is tested statistically by paired sample Wilcoxon Signed Rank Test and we found that the difference is significant where the value of W at $p \leqslant 0.05$ is 0. At the same time, Fig.4.11 shows that the IMRT plans for prostate, smallest target volumes in this study, achieve the smallest values of HI regardless of using photon beams with or without flattening filter.

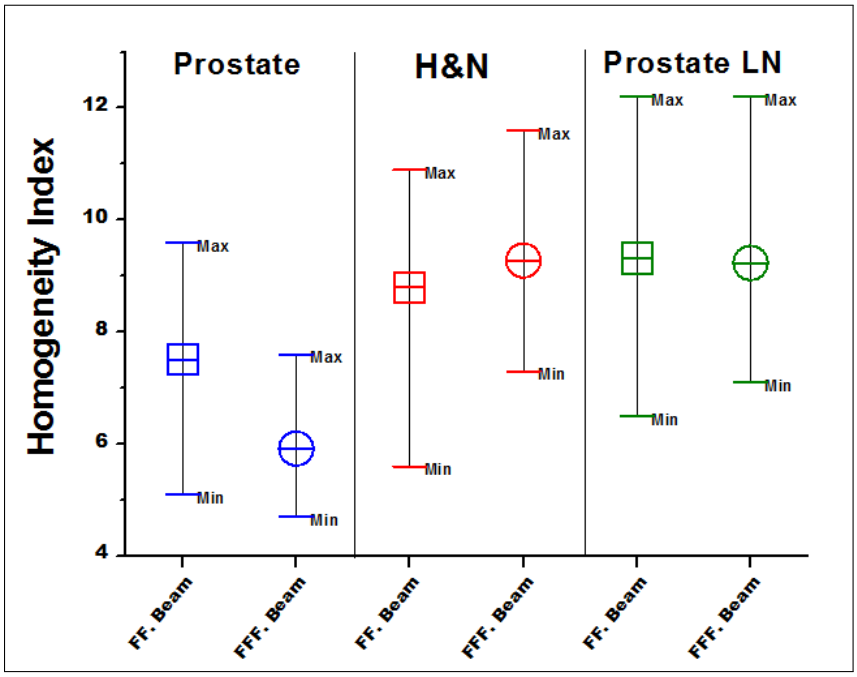

Figure 4.11: HI of IMRT plans of the clinical cases used in this work using FF and FFF beam.**

The HI of the H&N and prostate-LN plans indicate that FF and FFF beams produce IMRT plans with nearly the same homogeneity within the PTV. These differences are not statistically significant where the critical values of W are 3 and 2 at $p \leqslant 0.05$ for H&N and prostate-LN, respectively.

** The box charts represent the minimum, the maximum and the mean values of the results

Conformity number (CN)

According to equation 3.4, CN values close to 1 mean better PTV coverage and less irradiation for the healthy tissues. As shown in Fig.4.12, IMRT-FFF plans have better conformity than IMRT FF plans for all clinical cases. CN results were tested using paired sample Wilcoxon Signed Rank Test and we found the value of W at $p \leqslant 0.05$ is 0 for prostate-LN and H&N which means that IMRT-FFF plans achieve better conformity with significant difference than those created with FF beams. Considering the dose to the OARs, these statistically significant differences are not clinically important. For prostate, however, the dose conformity of IMRT-FFF plans is better than that of IMRT-FF plans, the difference is not significant where $W = 1$ at $p \leqslant 0.05$.

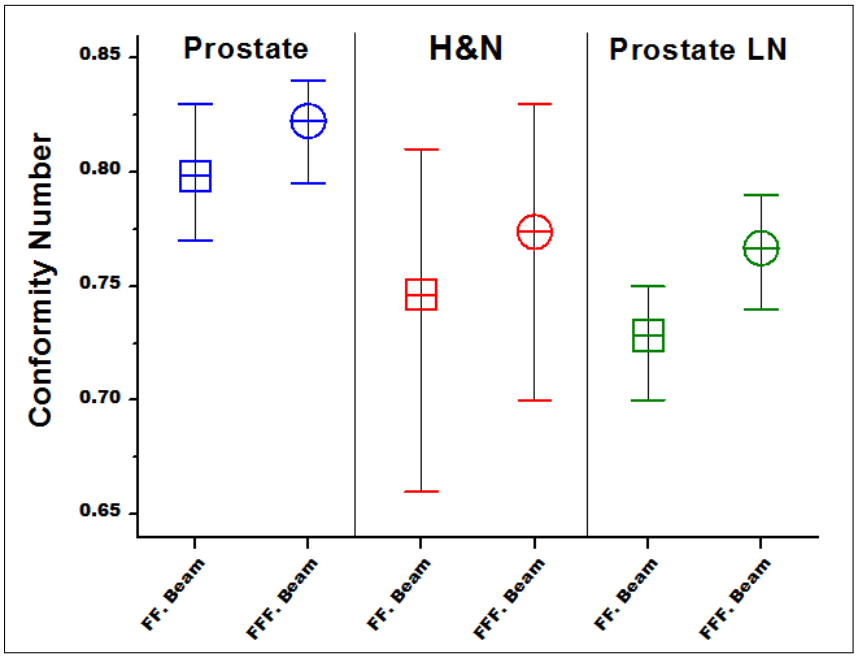

Figure 4.12: CN of IMRT plans of the clinical cases used in this work using FF and FFF beam.**

4.2.2 Treatment efficiency

Number of MUs

As shown in Fig.4.13, IMRT treatment plans using FFF beams for the chosen clinical cases need more number of MU per fraction (MU/Fx) than IMRT treatment plans using FF beams to deliver the same PD and the difference between both techniques is statistically significant. That could be explained by looking at the beam profiles of the FF and FFF beams as shown in Fig.4.1. The profiles of the FFF beams are

conical in shape and the dose at the lateral sides is lower than that at the central axis. This reduction of the lateral dose increases with increasing the photon energy and the field size. Therefore, with increasing PTV volume the numbers of required MU should increase. This result is explained in more details in Fig.4.14. The relative difference of the number of MU/Fx (FFF to FF) increases with the increasing volume of the PTV. Prostate plans having small PTVs (165 to 237 cm^3) show only relative difference of the MU/Fx between 20 % and 32 %. H&N plans with larger PTVs (568 to 883 cm^3) have relative differences of the MU/Fx ranging from 36 % to 85 %. The prostate-LN cases have the largest PTVs (922 to 1254 cm^3) in this study. For the prostate-LN cases, the numbers of the MU/Fx are higher for FFF techniques by 79 % to 114 %. These results indicate that in case of IMRT-FFF the larger PTVs require more MU to compensate for the lower dose in the lateral parts of the FFF beams.

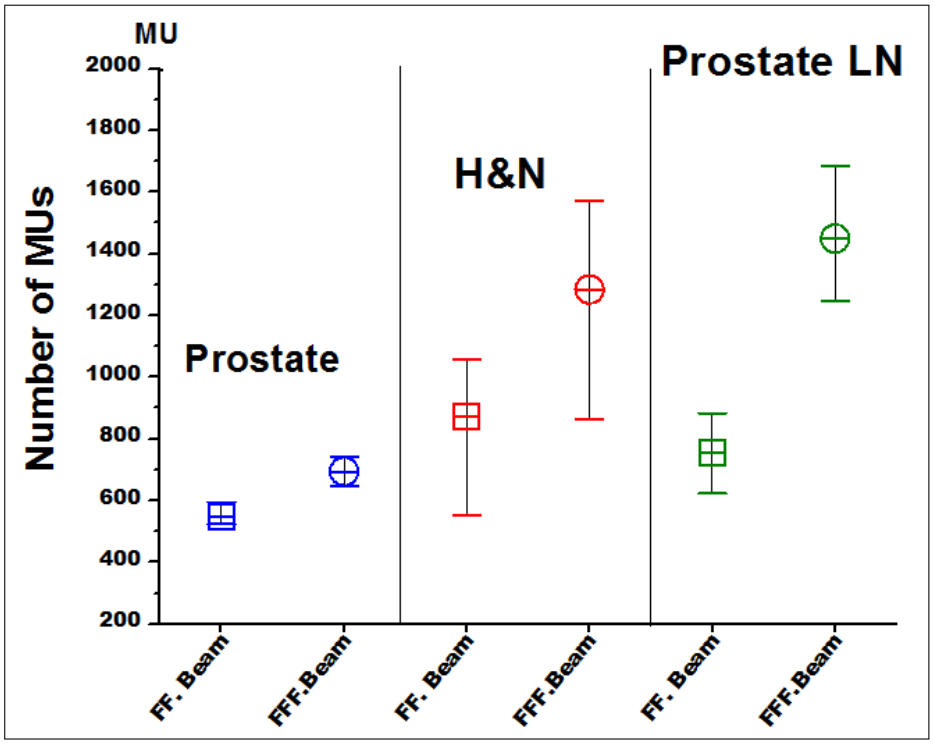

Figure 4.13: The number of the MU/Fx of the IMRT plans using FF and FFF beam.**

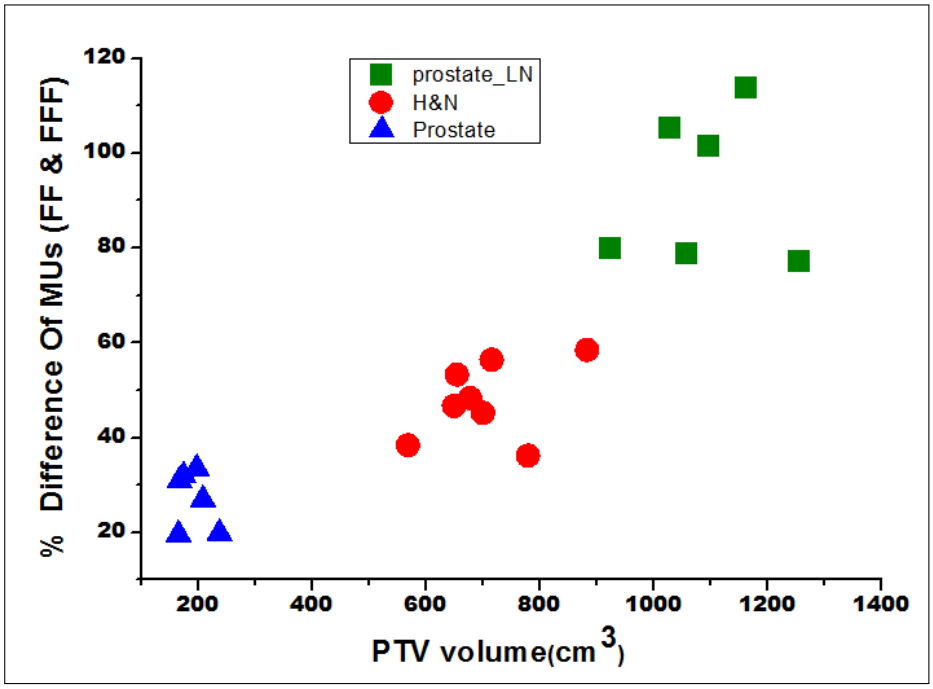

Figure 4.14: The relation between the volume of the PTV and the relative difference of the number of the MU/Fx for IMRT plans using FF and FFF beam.

Treatment delivery time

In this study, S&S-IMRT technique has been used to create treatment plans using FF and FFF beams. For prostate and H&N, 2 Gy/Fx were delivered and 1.8 Gy/Fx for prostate-LN. The Artiste linacs in our clinic have been calibrated to deliver about 1 cGy/MU for FF and FFF photon beam energies. Two examples for each group of patients included in this study are listed in table 4.4. Each of two examples represent the minimum and maximum values of the MU/Fx for a particular group. The percentage difference of the number of MU, the number of segments and the TDT between IMRT-FF and IMRT-FFF plans related to that of the IMRT plans created by FF beams were calculated. It is observed that the TDT of the IMRT plan depends not only on the output dose rate of the linac but also on the required number of the MU, the number of segments and their complexity causing an increase of the leaf travel time between the segments. When the numbers of the segments of both IMRT-FF and IMRT-FFF plans are the same as in case of the H&N or with only slight difference as for prostate-LN (6.7 - 10 %), the difference in TDT is affected by the large difference of MU. In case of H&N, the MU of the IMRT-FFF were around 50 % more than the MU required for IMRT-FF leading to the same TDT. In case of prostate-LN, the TDT of the IMRT-

FFF plans exceeded that of IMRT-FF by 13.8 to 21.6 % and the percentage difference of the number of the MU was 80 % to 114 %. In case of prostate, it is observed that the low difference of the MU (19.6 %) and the low difference in the number of segments (9 %) between IMRT-FFF and IMRT-FF followed by shorter TDT for the IMRT-FFF than that of the IMRT-FF plans by 20 %, like patient-1. The opposite is observed for patient-2 where the TDT of IMRT-FFF plan is longer than that of IMRT-FF by 25 %. That is because not only the number of the MU required for IMRT-FFF increased but also the number of segments increased by 43 % than that of IMRT-FF plan.

Table 4.4: The percentage difference of the TDT related to the percentage difference of the required MU and the number of segments. Examples of the clinical cases used in the current study.

Clinical Case	Examples	MU (FF)	MU (FFF)	% diff MU	Seg.No (FF)	Seg.No (FFF)	% diff Seg.No	TDT (FF) min	TDT (FFF) min	% diff TDT
H&N	Patient_1	1058	1572	48.50 %	99	98	-1 %	13:00	13:00	0 %
	Patient_2	781	1238	58.50 %	99	98	-1 %	12:00	12:30	4 %
Prostate-LN	Patient_1	623	1122	80 %	89	98	10 %	10:08	11:34	13.80 %
	Patient_2	599	1280	114 %	91	97	6.70 %	10:55	13:15	21.60 %
Prostate	Patient_1	541	647	19.60 %	75	82	9 %	10:00	8:00	-20 %
	Patient_2	545	692	27 %	65	93	43 %	8:00	10:00	25 %

4.3 mARC

4.3.1 Final gantry spacing (F.G.S)

Plan quality

Final gantry spacing (F.G.S) is the main planning parameter that influences the plan quality and the treatment efficiency of the mARC delivery where the number of the optimization points (OP) - arclets or segments - is determined by the value of the F.G.S. As recommended by Siemens the smallest value of the F.G.S should not be less than 4° and this value produces 90 arclets for a complete arc. Increasing the value of the F.G.S decreases the number of the arclets.

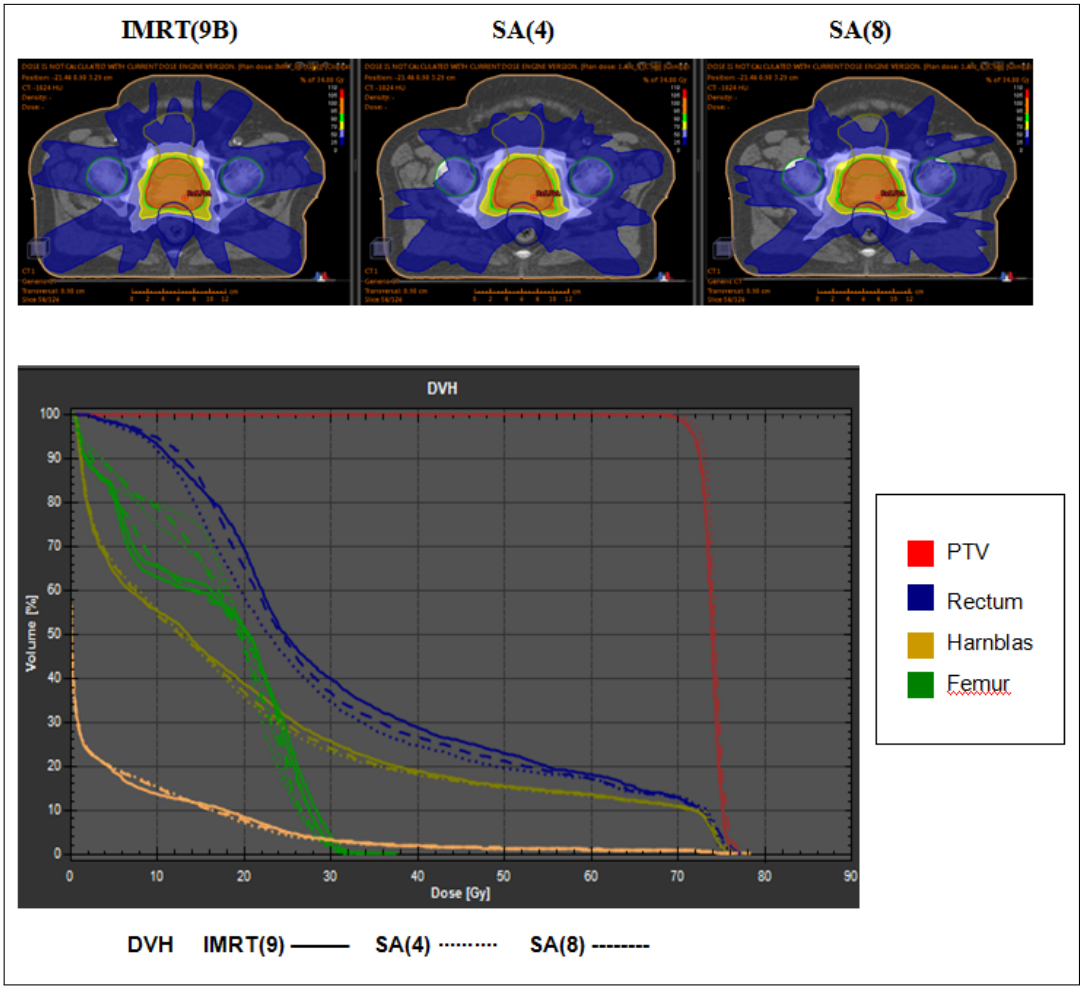

Figure 4.15: Dose distribution and DVH comparison between IMRT and mARC (SA (4) and SA (8)) plans created with 11 MV FFF beams for a prostate case.

To investigate the effect of the F.G.S, the plan quality and treatment efficiency of complete SA plans with different F.G.S values (4°, 6° and 8°) for prostate-LN and

H&N cases have been compared. For prostate, SA plans with F.G.S values of 4° and 8° have been compared. The influence of increasing the F.G.S value is clearly observed by the examination of the dose distribution through CT sections and DVHs. Examples of dose distributions in transversal CT sections and DVHs of prostate, prostate-LN and H&N of the created SA plans are shown in Figs.4.15, 4.16 and 4.17. In case of prostate-LN, SA (4) achieve the best PTV and OARs dose distribution whereas SA (6) and SA (8) led to PTV hot and cold spots and higher doses for OARs. For H&N, the visual examinations of the dose distributions through the CT sections and DVHs for SA (4) and SA (6) show nearly the same PTV dose distribution while SA (8) leads to hot spots inside the PTV. The dose distribution within the OARs (spinal cord, ipsilateral and contralateral parotid) of the H&N patients were nearly the same using SA plans of the F.G.S (4°, 6° and 8°).

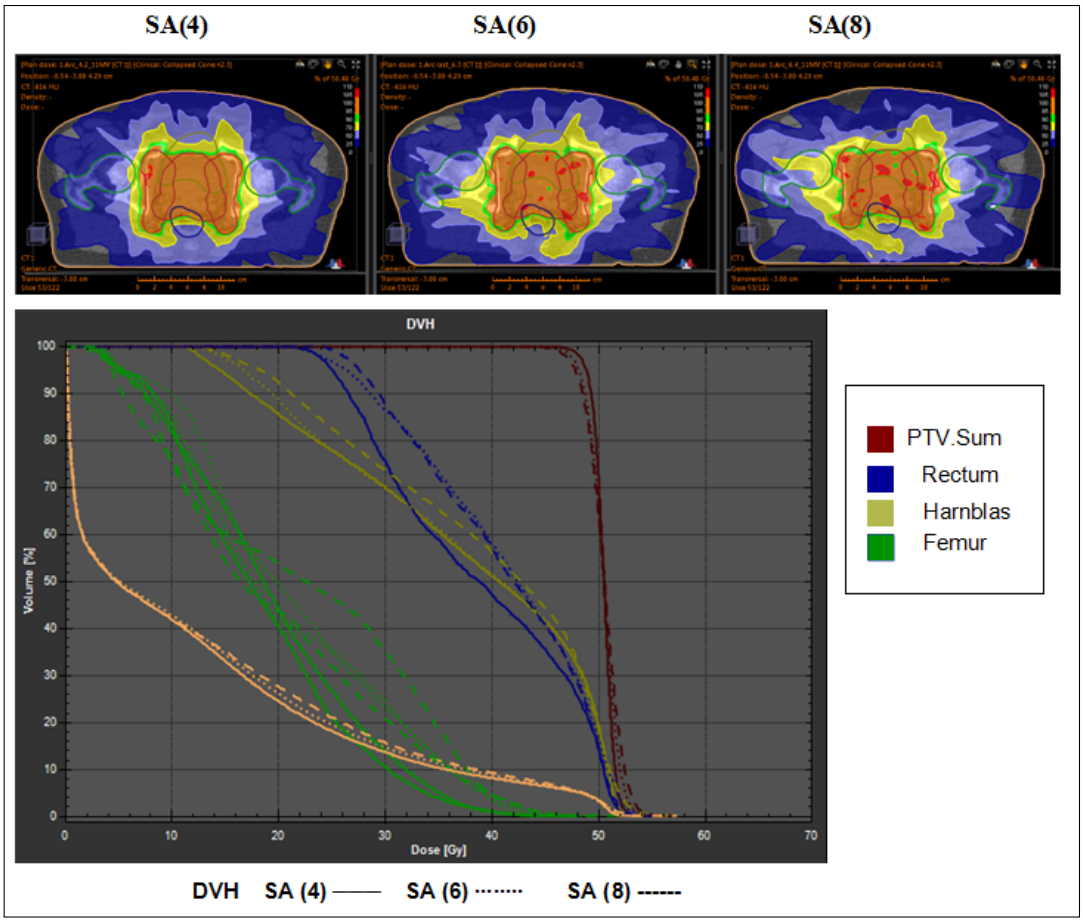

Figure 4.16: Dose distribution and DVH comparison comparison between SA (4), SA (6) and SA (8) plans created with 11 MV FFF beams for a prostate-LN case.

The achievement of PTV and OARs clinical goals, and the values of CN and HI prove the results of the visual examination of the dose distribution. The reference

values of the PTV clinical goals (D_{mean}, D_{98}, and D_2) and the average of the calculated plan values for all SA plans for all groups of patients are listed in table 4.5. For prostate-LN and H&N, SA (4) fulfilled the PTV clinical goals for all patients. SA (6) achieved the PTV clinical goals only for some cases but failed to achieve them for the others. The SA (8) plans achieve the clinical goal for D_{mean} of the prostate-LN but do not fulfil that of H&N. For the same patients, SA (8) plans failed to achieve the minimum and maximum dose of the PTV clinical goals.

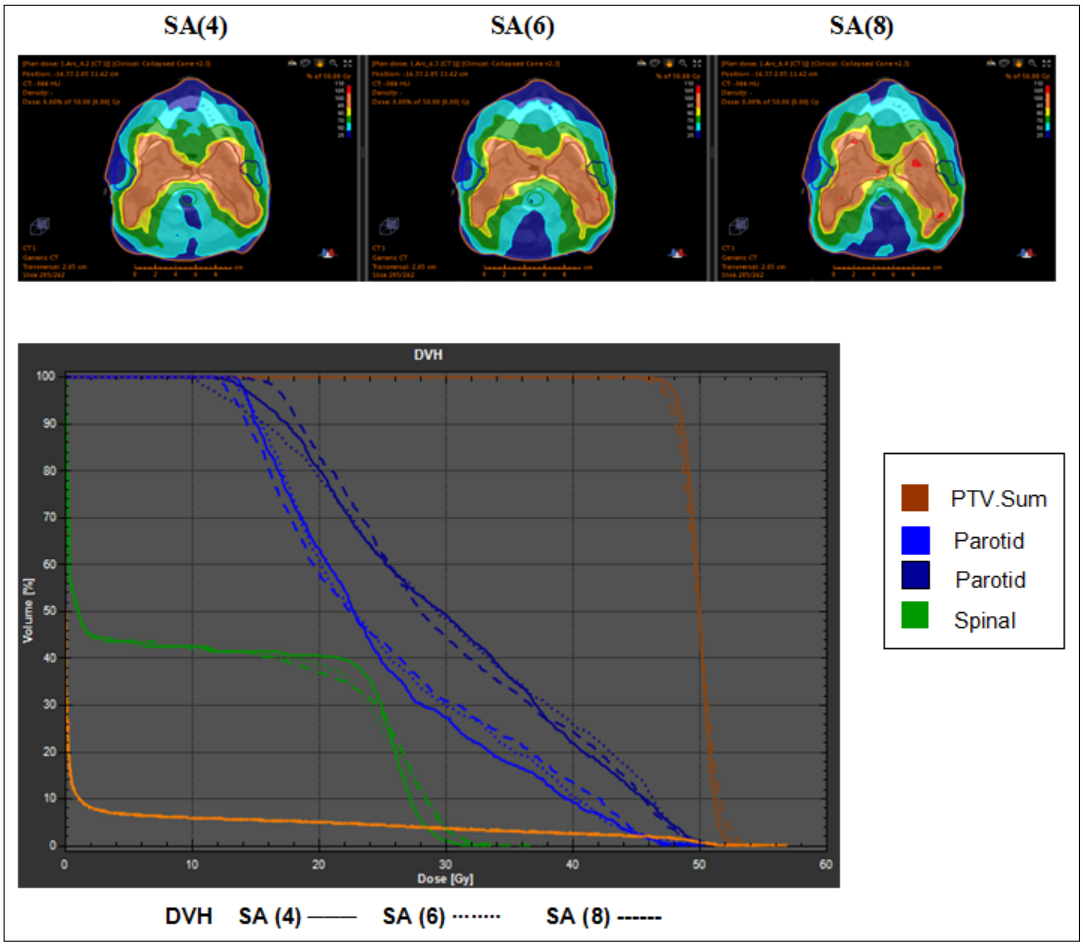

Figure 4.17: Dose distribution and DVH comparison between SA (4), SA (6) and SA (8) plans created with 7 MV FFF beams for a H&N case.

The OAR clinical goals of the prostate, prostate-LN and H&N are listed in table 4.6 in comparison with the results for each technique. All mARC techniques can spare the femur for prostate and prostate-LN. The bladder and rectum are spared for all prostate patients except for only one the rectum is not spared enough. For prostate-LN, the clinical goals $D_{75} < 30$ Gy of the rectum and $D_{80} < 20$ Gy of the bladder are not fulfilled for all patients but $D_{60} < 40$ Gy is achieved for all patients. In case of H&N,

mARC techniques can spare the spinal cord but SA (4) gives a lower maximum dose to it than SA (6) and SA (8). The contralateral and ipsilateral parotids could be spared but not for all patients. These results indicate that the sparing of OARs depend on how they are near to or included in the PTV and the changing of F.G.S value from 4° to 8° has no great effect on achieving the OARs clinical goals.

Table 4.5: The PTV clinical goals for target average dose (D_{mean}), minimum dose (D_{98}) and maximum dose (D_2) of the prostate, prostate-LN and H&N, in comparison with the calculated values of each technique (average of the calculated values), its standard deviation and (minimum-maximum).

Clinial Cases	PTVs Clinical Goals	SA (4) (Gy)	SA (6) (Gy)	SA (8) (Gy)	DA (6) (Gy)	IMRT (7B) (Gy)	IMRT (9B) (Gy)
Prostate	D $_{mean}$ = 74 Gy	74.16 ±0.14 (73.90 - 74.30)		74.07 ±0.06 (73.90 - 74.14)		73.90 ±0.13 (73.70 - 74.05)	73.80 ±0.10 (73.70 - 73.90)
	$D_{98} \geq$ 70.30 Gy	71.40 ±0.67 (70.10 - 71.90)		70.70 ±0.50 (69.80 - 71.14)		70.80 ±0.75 (69.60 - 71.80)	70.70 ±0.70 (69.40 - 71.40)
	$D_2 \leqslant$ 77.70 Gy	76.00 ±0.30 (75.06 - 76.50)		76.60 ±0.40 (76.10-77.30)		76.00 ± 0.20 (75.70 - 76.40)	75.90 ±0.24 (75.50 - 76.20)
Prostate-LN	D $_{mean}$ = 50.40 Gy	50.40	50.40	50.40 ±0.06 (50.30 - 50.50)	50.48 ±0.04 (50.30 - 50.50)	50.27 ±0.08 (50.20 - 50.40)	50.25 ±0.05 (50.20 - 50.30)
	$D_{98} \geq$ 47.88 Gy	48.00 ±0.20 (47.50 - 48.20)	47.50 ± 0.25 (47.20 - 47.80)	46.89 ±0.30 (46.50 - 47.20)	48.10 ±0.14 (47.90 - 48.30)	47.60 ±0.13 (47.50 - 47.85)	47.88 ±0.30 (47.30 - 48.25)
	$D_2 \leqslant$ 52.90 Gy	52.26 ±0.12 (52.20 - 52.50)	52.80 ±0.25 (52.50 - 53.10)	53.43 ±0.30 (53.40 - 53.90)	52.20 ±0.26 (51.70 - 52.40)	52.30 ±0.13 (52.30 - 52.50)	52.24 ±0.30 (51.90 - 52.70)
H&N	D $_{mean}$ = 50 Gy	49.93 ±0.02 (49.90 - 49.95)	49.91 ±0.07 (49.80 - 50.03)	49.80 ±0.08 (49.70 - 49.90)	49.90 ±0.05 (49.80 - 49.94)	49.92 ±0.05 (49.86 - 49.97)	49.92 ±0.06 (49.84 - 50.00)
	$D_{98} \geq$ 47.50 Gy	47.76 ±0.15 (47.70 - 48.06)	47.06 ±0.34 (46.50 - 47.50)	46.27 ± 0.42 (45.80 - 46.80)	47.68 ±0.22 (47.45- 48.00)	47.56 ±0.13 (47.40 - 47.70)	47.58 ±0.017 (47.30 - 47.80)
	$D_2 \leqslant$ 52.50 Gy	51.70 ±0.15 (51.50 - 51.87)	52.30 ±0.24 (52.00 - 52.60)	52.90 ±0.30 (52.50 - 53.30)	51.70 ±0.20 (51.70 - 51.90)	51.83 ±0.13 (51.70 - 52.00)	51.70 ±0.24 (51.30 - 51.90)

Table 4.6: The clinical goals of OARs of prostate, prostate-LN, H&N and the calculated values due to each technique.

OAR	Clinical Goals	SA (4) (Gy)	SA (6) (Gy)	SA (8) (Gy)	DA (6) (Gy)	IMRT (7B) (Gy)	IMRT (9B) (Gy)
Prostate							
Rectum	$D_{75} < 30$ Gy	4.00 - 32.30		4.00 - 34.60		4.00 - 34.90	4.00 - 34.80
Bladder	$D_{80} < 20$ Gy	0.90 - 5.60		0.90 - 6.00		0.84 - 5.00	0.85 - 5.00
	$D_{60} < 40$ Gy	1.40 - 20.50		1.40 - 19.00		1.40 - 18.40	1.40 - 18.40
Femur L&R	D_1(Max.dose) < 45 Gy	29.00 - 30.80		29.50 - 30.70		26.50 - 31.00	28.00- 31.00
prostate-LN							
Rectum	$D_{75} < 30$ Gy	22.00 - 33.00	23.50 - 33.80	22.00 - 34.00	23.00 - 33.30	25.00 - 31.50	24.00 - 31.40
Bladder	$D_{80} < 20$ Gy	19.00 - 31.00	20.00 - 27.00	23.00 - 28.70	20.00 - 30.00	21.00 - 26.00	19.00 - 26.00
	$D_{60} < 40$ Gy	28.00 - 37.20	28.00 - 38.00	32.00 - 39.60	28.00 - 36.30	31.00 - 36.50	29.00 - 37.60
Femur L&R	D_1 (Max.dose) < 45 Gy	35.00 - 41.00	37.00 - 42.00	40.00 - 44.00	34.00 - 390.00	30.00 - 40.50	34.00 - 41.00
H&N							
Spinal Cord	D_1(Max.dose) < 45 Gy	25.60 - 31.40	27.00 - 34.50	31.40 - 34.50	28.30 - 31.50	31.60 - 34.50	30.80 - 33.40
Contralat.parotid	Mean dose ≤ 25 Gy	24.00 - 25.60	23.00 - 27.00	25.60 - 27.70	24.00 - 26.60	24.00 - 25.70	23.00 - 26.50
Ipsilatparotid	Mean dose ≤ 30 Gy	26.00 - 45.70	26.00 - 46.00	28.00 - 45.00	26.50 - 44.00	26.60 - 45.30	26.40 - 45.70

As shown in Figs.4.18, 4.19 and 4.20 the conformity and homogeneity are getting worse with increasing the F.G.S. value for all cases. The CN and HI of SA (4) are the best and SA (6) achieves CN and HI better than SA (8). According to the Wilcoxon Signed-Rank Test, in case of prostate-LN, there are statistically significant differences of the CN and the HI between SA (4) and both of SA (6) and SA (8), also between SA (6) and SA (8) where the W-value is 0 at $p \leqslant 0.05$. For H&N cases the situation is the same as in prostate-LN except the values of the CN due to SA (4) do not differ significantly from that of SA (6), the W-value is 6.5 at $p \leqslant 0.05$.

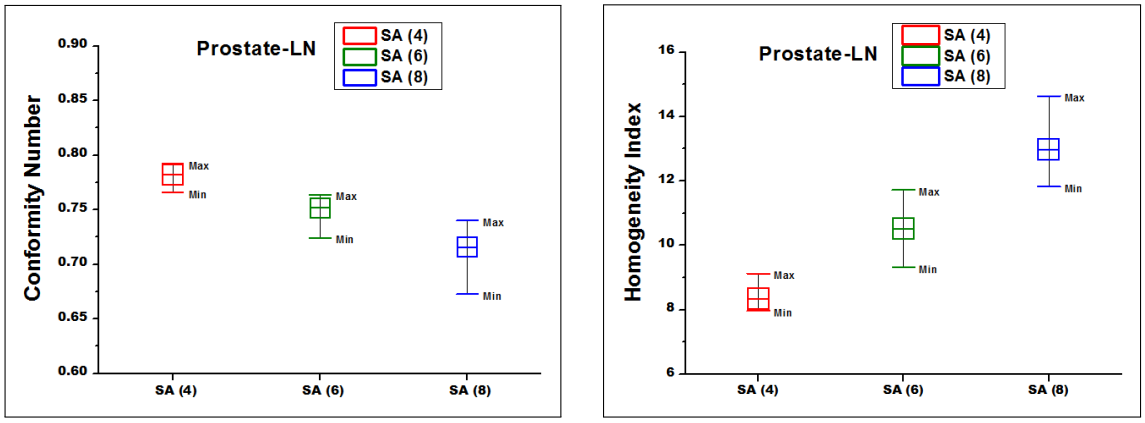

(a) (b)

Figure 4.18: CN & HI of prostate-LN SA plans with F.G.S (4°, 6° and 8°) 11 MV FFF beam.**

In case of prostate, as small and homogeneous PTV, SA plans created with F.G.S of 4° and 8° led to nearly the same dose distribution and achieve the PTV and OARs clinical goals as shown in Fig.4.15, and table 4.5 and 4.6. The CN and HI of SA (4) in comparison with SA (8) for prostate are represented in Fig.4.20. The HI of SA (4) was better than that of SA (8) with mean difference of 23.5 % and the difference between them is statistically significant (the W-value is 0 at $p \leqslant 0.05$). For CN, the Wilcoxon Signed-Rank Test could not be applied because our sample are six patients and that is the minimum limit to apply that test but two patients got identical CN values for SA (4) and SA (8) leading to prevent the test from being applied.

** The box charts represent the minimum, the maximum and the mean values of the results

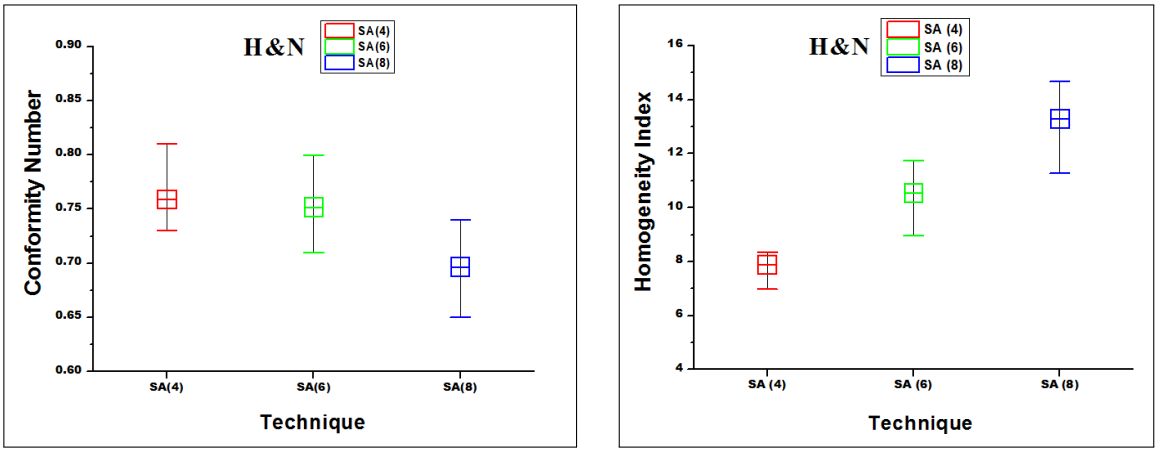

(a) (b)

Figure 4.19: CN & HI of H&N SA plans with F.G.S (4°, 6° and 8°) 7 MV FFF beam.**

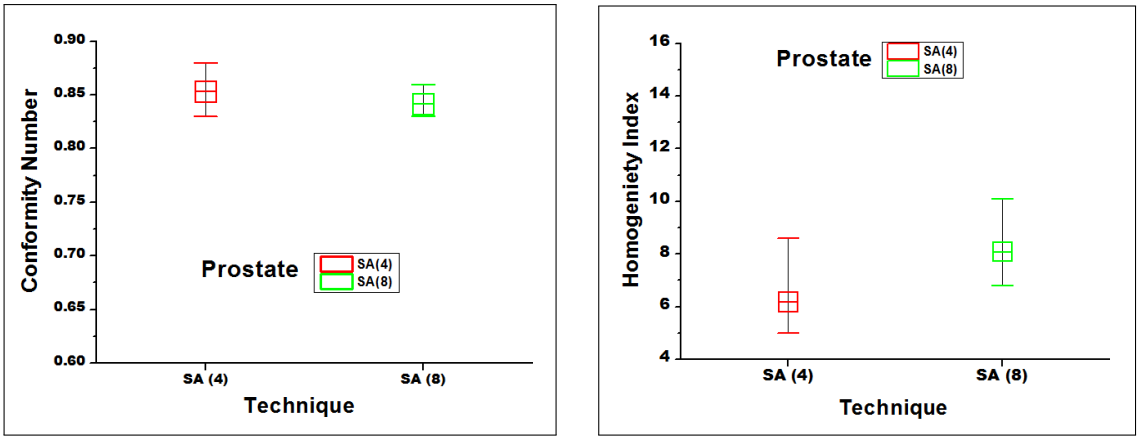

(a) (b)

Figure 4.20: CN & HI of prostate SA plans with F.G.S (4°, 8°) using 11 MV FFF beam.**

Treatment efficiency

The number of MU and the TDT required to deliver the prescribed dose of each plan created with SA (4), SA (6) and SA (8) for prostate, prostate-LN and H&N were measured and listed in table 4.7. As shown in that table, the lowest number of MUs and the shortest TDT were registered for SA (8) in comparison with SA (6) and SA (4) for all patients. These results indicate that the larger the F.G.S, the more efficient is the plan. It is observed that the F.G.S has a minor effect on the plan's MU but TDT is reduced by around 40 % when SA (8) of 45 arclets is used instead of SA (4) of 90 arclets. Basically, TDT depends on the gantry speed, which is calculated by the accelerator firmware using many parameters depending on the value of the F.G.S. These parameters are: 1) The effective beam-off gantry angle of the previous arclet.

Table 4.7: The mean, minimum and maximum values of the number of MUs and the measured TDT times of SA (4), SA (6) and SA (8) for prostate-LN and H&N. SA (4) and SA (8) for prostate.

clinical case	Prostate		Prostate-LN		H&N	
Technique	MUs	TDT (min)	MUs	TDT (min)	MUs	TDT (min)
SA (4)	650 ±71 (560 - 766)	6:22 (6:00 - 6:50)	961 ±137 (772 - 1170)	8:26 (8:12 - 8:52)	794 ±49 (743 - 861)	8:10 (7:50 - 8:30)
SA (6)			882 ±148 (715 - 1144)	6:10 (6:00 - 6:25)	728 ±58 (664 - 805)	6:02 (6:00 - 6:10)
SA (8)	554 ±44 (497 - 609)	3:30 (3:18 - 3:40)	827 ±123 (649 - 964)	4:46 (4:38 - 5:00)	736 ±89 (603 - 818)	4:41 (4:30 - 4:48)

2) The nominal beam-on gantry angle and the beam-off gantry angle of the current arclet, which are defined by the treatment planning system. 3) The longest of the required times to adjust MLC shape. 4) The nominal beam-on time, which mainly depends on the total amount of the arclet MU and the nominal dose rate [7]. Increasing the number of the arclets means increasing the MLCs movement to shape arclet by arclet and hence affecting the TDT. The complexity of the arclets shapes also plays a role. The longer the required times to adjust MLC shape, the lower is the gantry speed leading to longer TDT.

4.3.2 mARC and IMRT

Plan quality

Figures 4.15, 4.21 and 4.22 show examples of the dose distribution and DVHs for the IMRT 9B and the mARC plans. In Fig.4.15, IMRT 9B, SA (4) and SA (8) for prostate are compared. In Figs.4.21 and 4.22, IMRT 9B, SA (4) and DA (6) for prostate-LN and H&N are compared. The visual examination of the dose distribution of the transversal CT sections and the DVHs of the IMRT and the mARC plans show that all plans are clinically acceptable for all patients. The rectum and the bladder as OARs of the prostate-LN and the spinal cord of the H&N can sometimes be spared more using mARC techniques. Tables 4.5 and 4.6 show the clinical goals of the PTV and the OARs of each clinical case, which have been used as reference values in comparison with the calculated values obtained by each technique for each particular group of patients.

For prostate, as shown in table 4.5, all techniques achieve the D_{mean} clinical goal of the PTV (74 Gy) with standard deviation not more than ±0.14 Gy. The calculated PTVs' maximum doses did not exceed the clinical goals - the estimated D_2 values for all techniques were less than 77.7 Gy. The mean value of the calculated PTV minimum doses for all techniques achieve the PTV clinical goal $D_{98} \geq 70.3$ Gy (only one patient did not fulfil the clinical goals).

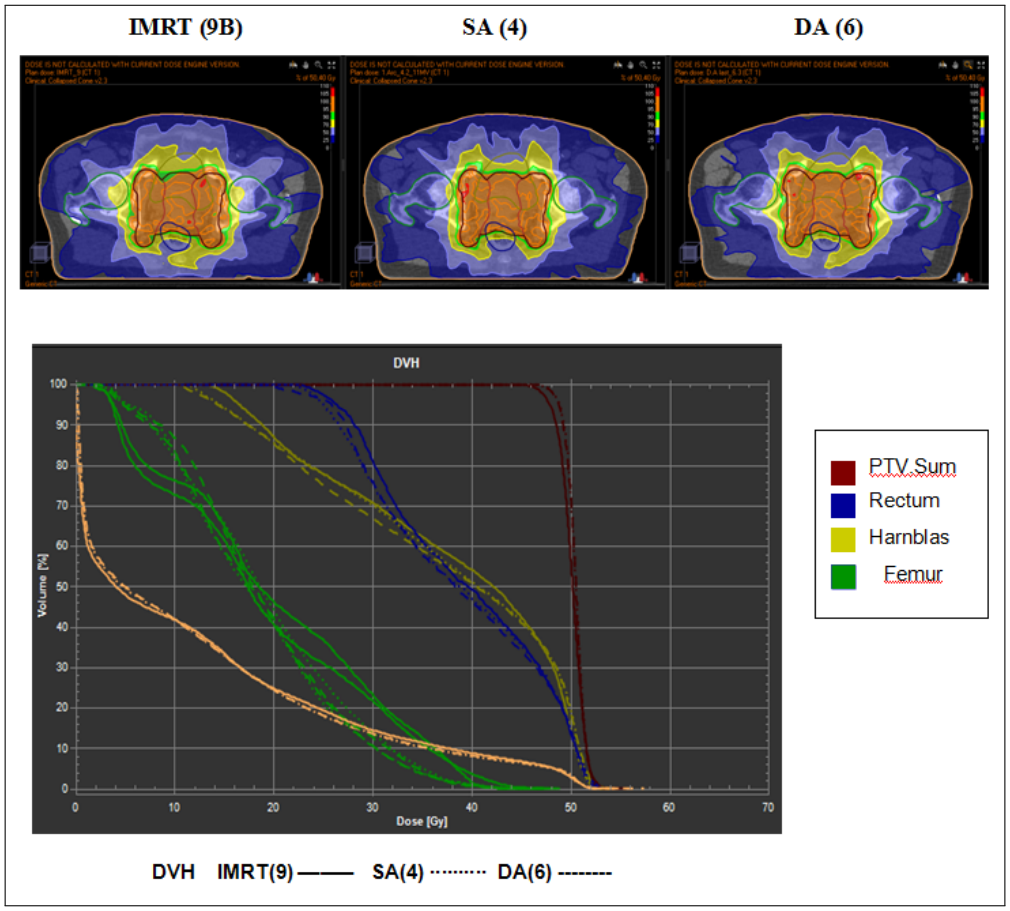

Figure 4.21: Dose distribution and DVH comparison between IMRT and mARC (SA (4) and DA (6)) plans created with 11 MV FFF beams for prostate-LN

For prostate-LN, mARC plans SA (4) and SA (6) could achieve all clinical goals for the PTV. The PTV average dose and the minimum dose for IMRT 7B are on average 50.27 and 47.6 Gy, respectively and for IMRT 9B are on average 50.25 and 47.88 Gy, respectively. The calculated maximum doses of the IMRT 7B and 9B plans did not exceed the clinical goal ($D_2 \leqslant 52.5$ Gy).

For H&N, the PTV average dose clinical goal is 50 Gy and the calculated values by SA (4), DA (6), IMRT 7B and 9B plans are between 49.8 to 50 Gy. The PTV

clinical goals of the minimum and the maximum doses have been fulfilled by all of those techniques.

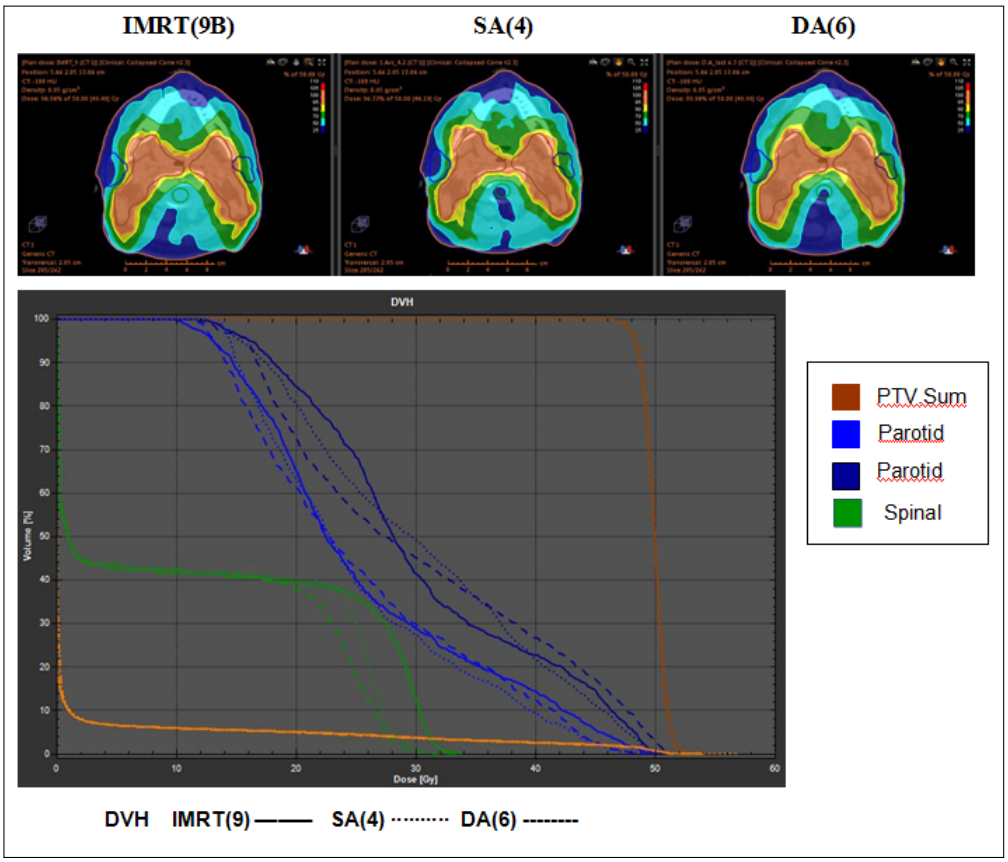

Figure 4.22: Dose distribution and DVH comparison between IMRT and mARC (SA (4) and DA (6)) plans created with 7 MV for H&N.

The OARs of all patients could be sufficiently spared by all techniques, which are used in this part of the study, with some exceptions. When a large volume of the OARs overlapped with the PTV or is close to it, the OARs clinical goals could not be achieved. In case of prostate, the rectum, the bladder and the femur are spared by all techniques except in one patient where the rectum received a higher dose than that of the clinical goal $D_{75} < 30$ Gy by 2.3 Gy for SA (4) and by approximately 5 Gy for the other techniques. In case of prostate-LN, not all of the OARs clinical goals are fulfilled for all patients. The clinical goals $D_{75} < 30$ Gy for the rectum and $D_{80} < 20$ Gy for the bladder could not be achieved by all techniques, but $D_{60} < 40$ Gy for the bladder and $D_1 < 45$ Gy for the femur are fulfilled by all techniques. In case of H&N, the achievement of the clinical goals of contralateral parotid and ipsilateral parotid differ from patient to patient depending on whether their volume is included in or close to the PTV. The spinal cord can be spared by all techniques with more sparing in case

of the mARC plans.

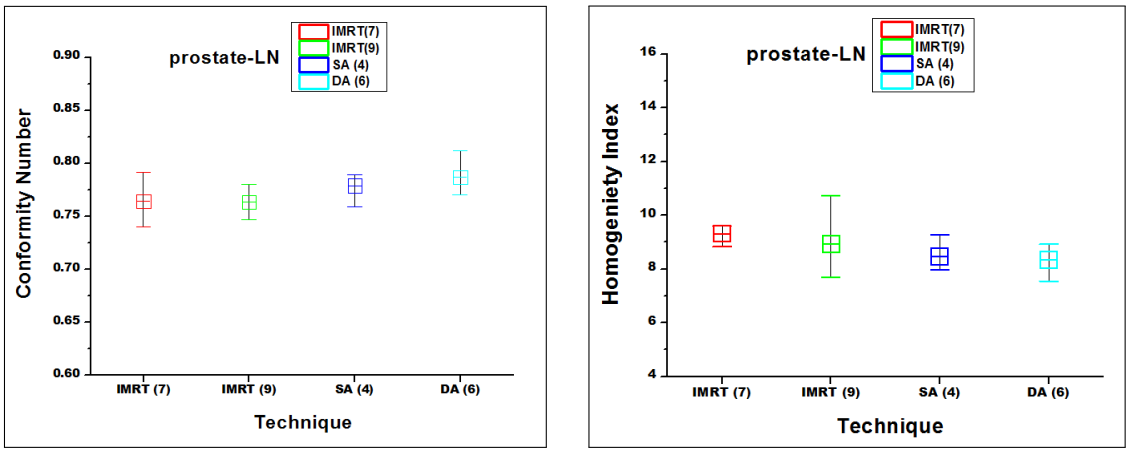

(a) (b)

Figure 4.23: CN & HI of the prostate-LN using IMRT 7B and 9B, and mARC SA (4) & DA (6).**

Like the comparable results of the dose distribution, DVHs and the clinical goals of the PTV and the OARs between mARC and IMRT plans, also mARC plans of the prostate-LN, H&N and prostate resulted in comparable PTV dose homogeneity and dose conformity with IMRT plans as shown in Figs.4.23, 4.24 and 4.25. The mean differences of the CN between mARC and IMRT plans for prostate-LN, H&N and prostate are less than 3 %, 0.9 % and 1.7 %, respectively. These differences are not statistically significant.

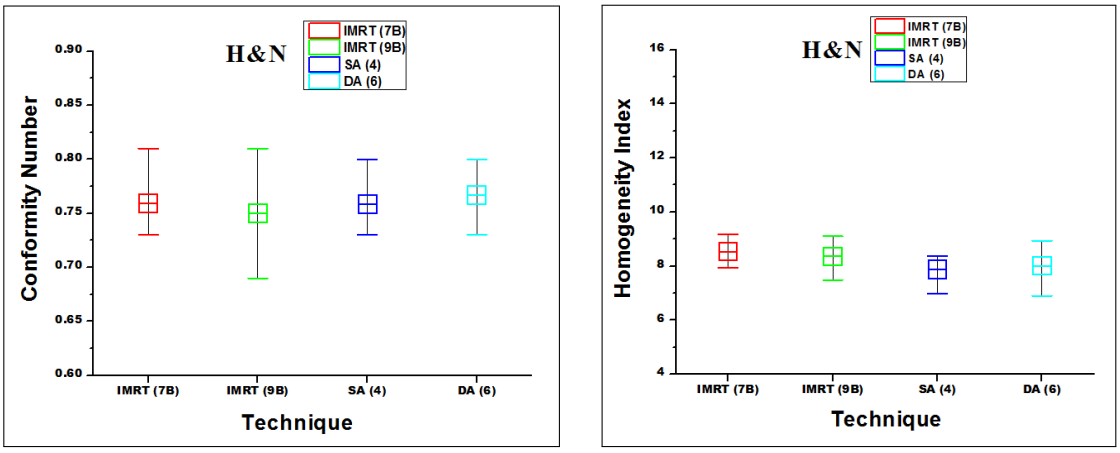

(a) (b)

Figure 4.24: CN & HI of H&N using IMRT 7B and 9B and mARC $\big($SA (4) & DA (6)$\big)$.**

The value of the HI of prostate-LN for SA (4) and DA (6) indicates better homogeneity than IMRT 7B with mean differences of 9 % and 10.2 %, respectively and these differences are statistically significant, the W-value is 0 at $p \leqslant 0.05$. When we

compared the HI of SA (4) and DA (6) with IMRT 9B, we found the mean differences are 4.5 % and 6.5 %, respectively. These differences are not statistically significant where W-values are 7 and 6, respectively at p $\leqslant$ 0.05. For H&N, the HI due to mARC is better than for IMRT with mean differences less than 7.5 % and these differences again are not statistically significant (W-value between SA (4), DA (6) and IMRT 9B is 6, between SA (4)-IMRT 7B is 2, and between DA (6)-IMRT 7B is 3 at p $\leqslant$ 0.05). In case of prostate, as shown in Fig.4.25, SA (4) plans achieve better HI than IMRT 7B and 9B plans with mean differences of 10.7 % and 11.7 %, respectively. The dose homogeneity of SA (8) plans is worse than that of both IMRT plans 7B and 9B with the mean differences of the HI 16.8 % and 15.4 %, respectively. The differences between the HI of SA (4) and IMRT 7B and 9B plans are not statistically significant (W-values are 2 and 1, respectively at p $\leqslant$ 0.05). For SA (8) and IMRT 7B plans the differences are not statistically significant (W-value is 1 at p $\leqslant$ 0.05) but between SA (8) and IMRT 9B plans the HI is significantly different W-value is 0 at p $\leqslant$ 0.05).

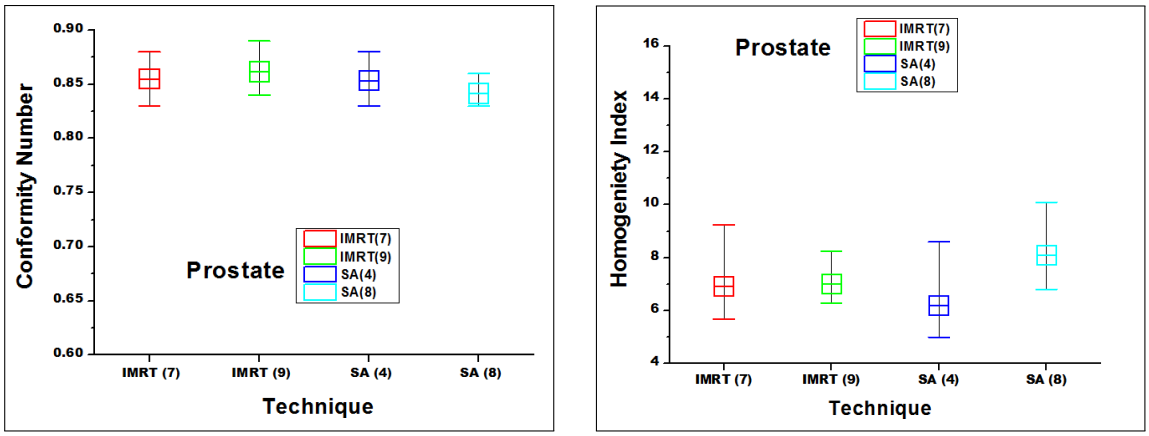

(a) (b)

Figure 4.25: CN & HI of the prostate using IMRT 7B and 9B and mARC (SA (4) & SA (8)).**

Comparable results for the plan quality parameters between SA (4) and DA (6) plans can be observed for both prostate-LN and H&N patients where SA (4) and DA (6) produce the optimal plan using mARC technique.

Treatment efficiency

1- Number of MUs

Figure 4.26 shows the number of the MU for all patient groups of all techniques.

Despite SA (4) has the largest number of arclets (90) as a SA plan, it produces lower number of MU than that of the IMRT 7B and 9B plans of 60 and 50 segments in case of prostate-LN and H&N, respectively. Furthermore, SA (4) requires fewer MU than DA (6) with 122 arclets. For prostate-LN, the differences between the number of the MU for SA (4) and IMRT 7B, IMRT 9B and DA (6) plans are 19 %, 14.3 % and 7.5 % respectively. The differences between the number of MU of SA (4) on one hand and IMRT 7B and 9B on the other hand are statistically significant (W-value is 0 at p $\leqslant$ 0.05) but there is no significant difference between SA (4) and DA (6) plans where W-value is 3 at p $\leqslant$ 0.05. In case of H&N, there is no significant difference between the number of the MU of SA (4) plans and IMRT 7B, IMRT 9B and DA (6) plans (W is 4.5, 3 and 3 at p $\leqslant$ 0.05). For prostate, the number of the MU required for delivering SA (8) is lower than that required for SA (4) and IMRT 7B and 9B plans by 17 %, 19 % and 21 %, respectively with significant difference (W-value is 0 at p $\leqslant$ 0.05). There is no significant difference between the number of the MU of SA (4) and IMRT 7B and 9B plans where W values are 9 and 4, respectively at p $\leqslant$ 0.05.

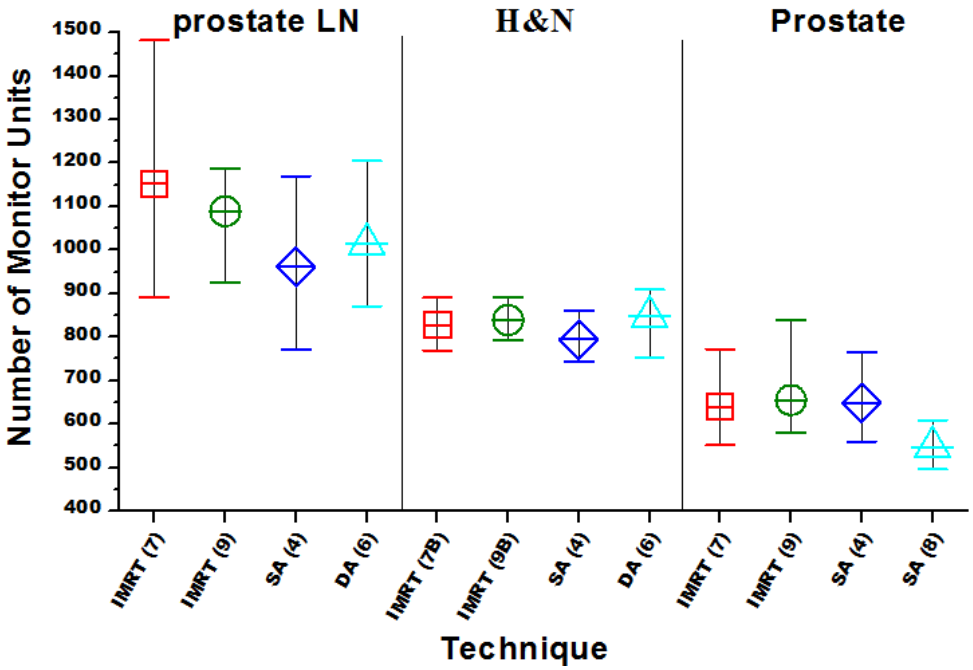

Figure 4.26: Number of MUs for SA (4), IMRT 7B and 9B plans of all cases, DA (6) plans of prostate-LN and H&N and SA(8) plans for prostate.**

2- Treatment delivery time

The measured TDT time of SA (4) and SA (8) of prostate and SA (4) and DA (6) of prostate-LN and H&N in comparison with the TDT of the IMRT 7B and 9B of all cases

Table 4.8: The measured TDT time of SA (4) and SA (8) plans for prostate and SA (4) and DA (6) plans for prostate-LN and H&N in comparison with the TDT of the IMRT 7B and 9B of all cases. In this table the mean, minimum and maximum TDT are listed.

Clinical case	Prostate	Prostate-LN	H&N
Technique	TDT (min)	TDT (min)	TDT (min)
SA (4)	6:22 (6:00 - 6:50)	8:26 (8:12 - 8:52)	8:10 (7:50 - 8:30)
SA (8)	3:31 (3:18 - 3:40)	4:46 (4:38 - 5:00)	4:41 4:30 - 4:48
DA (6)	-	9:10 (8:35 - 9:56)	10:45 (10:00 - 12:00)
IMRT 7B	5:51 (5:40 - 6:05)	7:52 (7:50 - 7:58)	6:30 (6:20 - 6:40)
IMRT 9B	6:21 (6:15 - 6:30)	8:00 (7:57 - 8:00)	6:47 (6:38 - 6:55)

are listed in table 4.8. For prostate, reducing treatment time is the main advantage of using mARC technique over IMRT. TDT of SA (8) plans of 45 arclets was 3:18 to 3:40 minutes and the TDT of IMRT 7B and 9B plans with 50 segments was 5:40 to 6:30 min. Despite SA (4) and IMRT 9B plans were created with 90 arclets and 45 segments, respectively, the measured TDTs of them are the same.

In case of prostate-LN, the TDT of SA (4) and DA (6) plans are comparable with that of the IMRT 7B and 9B.

In case of H&N, as shown in table 4.8, in contrast to prostate and prostate-LN, the TDTs required to deliver IMRT plans were less than those of SA (4) and DA (6) plans. This result can be explained by the number of the arclets that is larger than the number of the IMRT segments. Furthermore the PTV complexity leads to complex shapes of the arclets and hence longer time is required for MLC to adjust the arclets shapes leading to lower gantry speed and long treatment time.

4.3.3 Comparison of mARC 10 MV FF and 11 MV FFF plans

Plan quality

We investigated the effect of FF and FFF beams on mARC plans by creating SA plans with different values of F.G.S, 4°, 6° and 8°, for prostate-LN and SA plans with F.G.S 8° for prostate using 10 MV FF and 11 MV FFF beams. In this study, the prescribed doses for prostate and prostate-LN were 2 Gy/Fx and 1.8 Gy/Fx, respectively. The

artiste linacs in our clinic have been calibrated to deliver about 1 cGy/Mu under reference conditions (100 cm SSD, depth = d_{max}, 10 cm × 10 cm F.S) for FF and FFF photon beam energies.

As mentioned before, SA plan with F.G.S 4° is the optimal mARC plan. For prostate-LN, as shown in Fig.4.27, SA (4) leads to nearly the same conformity and PTV dose homogeneity whether using FF or FFF beam. The mARC plans - SA (6) and SA (8) - using 10 MV FF lead to better dose conformity than 11 MV FFF with only small differences which are not statistically significant - W value is 3 at $p \leqslant 0.05$. The HI of SA (6) and SA (8) plans of FF beams are better than that of FFF beams with differences of 11.4 % and 15 %, respectively and the differences are statistically significant where W value is 0 at $p \leqslant 0.05$. It was also found that the SA (6) FFF plans with 60 arclets and SA (8) FF plans with 45 arclets achieve comparable PTV dose homogeneity where there is no significant difference between the HI of both - W value is 3 at $p \leqslant 0.05$ and the mean is difference 5.4 %. This plan comparison between SA plans for prostate-LN prove that the change in the F.G.S value has the same effect on the dose conformity and homogeneity of the mARC plan whether applying FF or FFF beams. The values of CN and HI indicate that for prostate-LN the gradual increase in F.G.S value leads to a gradual decrease in the dose conformity and homogeneity of the mARC plans with statistically significant difference.

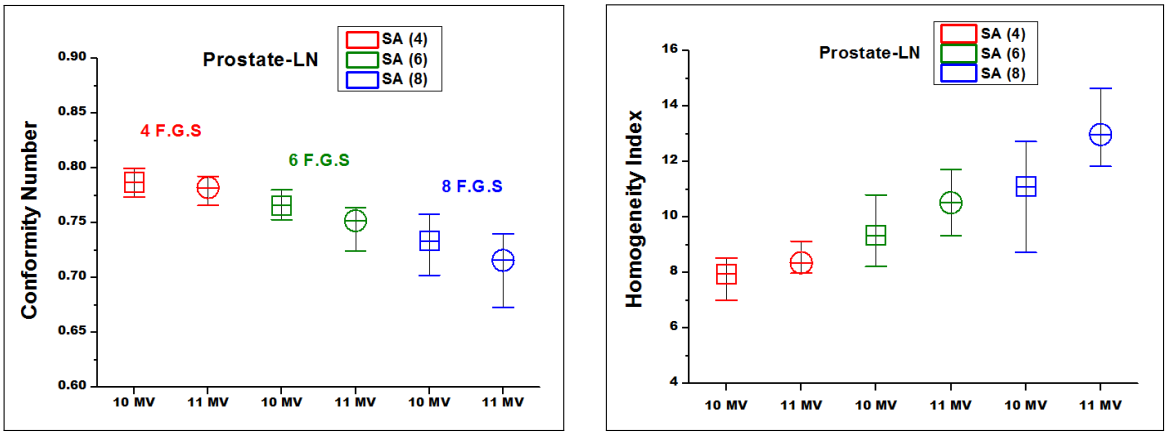

(a) (b)

Figure 4.27: CN and HI of the prostate-LN SA plans [SA (4), SA (6) and SA (8)] using 10 MV FF beam and 11 MV FFF beam.**

In case of prostate, as a small homogeneous PTV, SA (8) plans created with 10 MV FF and 11 MV FFF achieve nearly the same homogeneity and conformity as shown in Fig.4.28 for CN and HI.

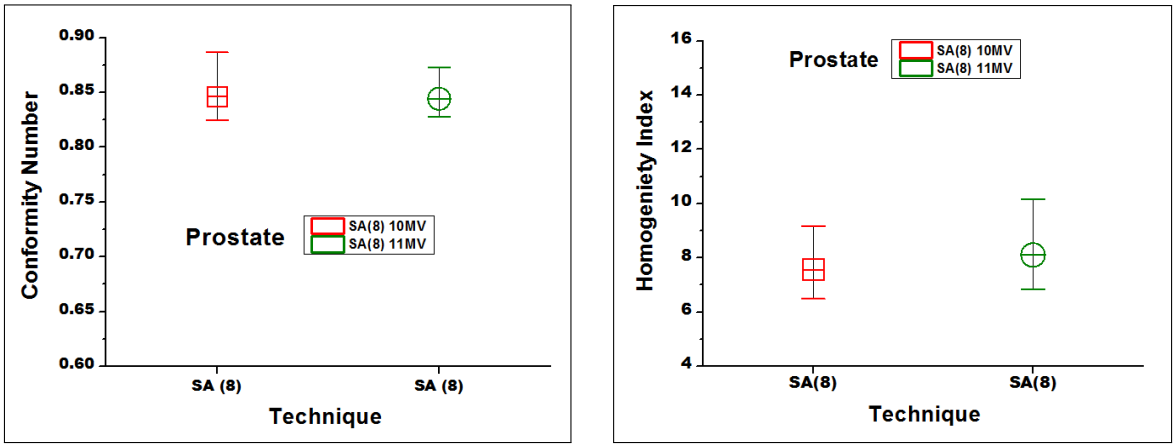

(a) (b)

Figure 4.28: CN and HI of the prostate SA (8) plans 10 MV FF and 11 MV.**

Treatment efficiency

The number of MU and the TDT required to deliver mARC plans for prostate-LN and prostate using FF and FFF beams are listed in table 4.9. Our results show a reduction in the MU/Fx and shorter TDT with increasing the F.G.S for both FF and FFF beams. The smaller number of MU/Fx is required to deliver the same PD for each treatment plan by applying FF beams instead of the FFF beams . The average of the number of MU/Fx for each group of mARC plans using FF and FFF beams and their relative differences (FFF to FF) have been calculated. In case of prostate-LN, the relative differences were 52 % for SA (4) and SA (6) and 60 % for SA (8). In case of prostate, the relative difference due to SA (8) was 19 %. The difference between MU/Fx due to FF and FFF beams for all mARC plans is statistically significant. TDT required to deliver mARC-FFF plans is decreased by not more than 1 min over mARC-FF plans.

Table 4.9: Number of MUs and measured TDT per fraction for mARC plans (10 MV FF, 11 MV FFF) in case of prostate-LN (SA (4), SA (6), SA (8)) and prostate (SA (8)).

Clinical case	Beam energy	SA (4)		SA (6)		SA (8)	
		MU	TDT(min)	MU	TDT(min)	MU	TDT(min)
Prostate-LN	10 MV FF	612 ±73 (525 - 723)	8:56 (8:34 - 9:18)	577 ±65 (490 - 648)	6:40 (6:30 - 6:59)	512 ±77 (400 - 609)	5:13 (5:12 - 5:13)
	11 MV FFF	933 ±139 (772 - 1132)	8:26 (8:12 - 8:52)	878 ±152 (715 - 1144)	6:10 (6:00 - 6:25)	819 ±133 (649 - 964)	4:46 (4:38 - 5:00)
Prostate	10 MV FF					466 ±25 (431 - 501)	4:07 (4:00 - 4:18)
	11 MV FFF					554 ±44 (497 - 609)	3:22 (3:18 - 3:40)

4.3.4 Plan verifications

Pretreatment QA for mARC and IMRT plans were done using Delta^4 and Octavius 4D phantoms. In case of Delta^4, since the detectors cover an area of 20 cm $\times$ 20 cm in each plane (active area), its ability to measure large treatment field sizes in a single isocentric set-up (in the present study, prostate-LN) is limited. For treatment fields longer than 20 cm the system offers the possibility to do two consecutive measurements of the same plan with different phantom offset and merge the data afterwards. The purpose is to cover a much larger area but this leads to repeat the measurement for the same patient, which requires longer time to verify the plan. Therefore, we have used Delta^4 to verify the treatment plans of the prostate and H&N of the field sizes suitable for its limits and Octavius 4D with 27 $\times$ 27 cm^2 detector surface was used for prostate-LN. The comparison options of both system used to compare the dose distribution between the treatment and verified plans as described in material and methods. The comparison resulted in a good agreement using both verification systems. The pass rate of the gamma evaluation of the plans verification are presented in table 4.10 using criteria of 3 % dose deviation and 3 mm DTA. The detectors of the dose range 10 % to 500 % of the maximum absorbed dose were included during measurements. All the QA plans achieve the 3D gamma criteria (gamma value $\leqslant$ 1) with pass rate 95 %.

Table 4.10: Pass rate of gamma values $\leqslant$ 1 of prostate and H&N using Delta^4 and of prostate-LN using Octavius 4D

Clinical case	Beam energy	SA (4)	SA (6)	SA (8)	DA (6)	IMRT 7B	IMRT 9B
Prostate (Delta^4)	10 MV FF	-	-	99.6 ±0.2	-	-	
	11 MV FFF	97.3 ±1.6		97.8 ±1.4		98.3 ±0.8	97.7 ±0.7
Prostate-LN (Octavius 4D)	10 MV FF	97.1 ±0.5	96.5 ±1.2	96.2 ±0.9	-	-	-
	11 MV FFF	97.4 ±0.2	96.8 ±0.4	96.6 ±0.8	96.9 ±0.2	94.9±0.7	95 ±1
H&N (Delta^4)	7 MV FFF	98.2 ±0.6	98.1 ±1.2	97.6 ±1.8	98.4 ±1	99.3 ±0.4	99.3 ±0.3

Chapter 5

Discussion

5.1 Dosimetric parameters of FF and FFF beams

This present work investigates the dosimetric characteristics of FFF beams produced by Artiste linacs, and their effect on IMRT plans and compares it with that of FF beams. The flattening filter is used to flatten the forward peaked bremsstrahlung distribution of megavoltage photons, but it is at the same time one of the linac head components responsible for a significant part of scattered radiation. Thus, removing the flattening filter affects the dosimetric features of the photon beam by two main factors, the alteration of the bremsstrahlung spectrum and the reduction of scattered radiation from the head of the linac. The current study is focusses on dose rate, beam profile and PDD curve with their components (buildup region, d_{max}, and exponential fall-off region) as main dosimetric characteristics of the photon beam. Reduction of leakage radiation by about 50 % due to FFF beams was reported by other investigators [28, 52], but we did not investigate this in this work.

The Artiste linac is operated in FFF mode to produce high dose rate (2000 MU/min) photon beams of 7 MV and 11 MV. This high dose rate is the main advantage of removing the flattening filter, by which a large fraction of primary photons is removed from the beam especially those close to the central axis.

The geometry of the flattening filter has an effect on the dose profile. Therefore, removing the flattening filter produces FFF beam profiles with new shapes and dosimetric features especially at large F.Ss. The profile of an FFF beam at large F.Ss as shown in Fig.4.1 is characterized by highest dose value at the middle and low dose at the lateral side relative to the dose at the central axis. This conical shape of the profile is more pronounced for higher energy. Furthermore, the out-of-field dose close to the field edge is reduced due to flattening filter removal because the flattening filter is

responsible for a significant part of the extra focally scattered radiation. Reducing the out-of-field dose may reduce the risk of inducing a secondary malignancy to the organs out of the treatment field. Stephen et al. [55] and Kragl et al. [53] studied the impact of unflattened beams on the out-of-field dose for open fields and IMRT plans. Stephen et al. applied 6 MV FF and FFF beams to prostate using Varian 2100 accelerator. Kragl et al. created IMRT treatment plans for prostate and H&N using 6 and 10 MV FF and FFF beams of Elekta Precise linac. They have found that the out-of-field dose was generally reduced following removal of the flattening filter. At distances within a few cm ($\sim < 3$ cm) and beyond approximately 15 cm from the edge of the field, the dose tends to be lower for the FFF mode, although the effect depends on the field size and depth. Kragl et al. added that the relative difference between peripheral doses of flattened and unflattened beams was more pronounced when the beam energy was increased from 6 to 10 MV and that could be seen from our results for 7 and 11 MV as shown in Fig.4.1.a.

We investigated the PDD curves at reference, small and large F.S between FF and FFF beams. We found that the PDD curves at reference F.S between 6 and 7 MV, and 10 and 11 MV are almost identical. Slight differences at the buildup region between FF and FFF beams and the depths of d_{max} are shifted some mm to higher depth for FFF beams. That agreement between PDD curves and the shift of the depths of d_{max} is related to Siemens philosophy for Artiste linacs, which aims to increase the maximum photon energy in bremsstrahlung spectrum by using higher energy of the electron. The PDD curves of FFF beams exhibit a slight steeper dose fall-off in the exponential region as shown in Figs.4.2 and 4.3. This is because the amount of the scattered radiation on the central axis decreased due to FFF beams. At the same depth the doses in the buildup region due to FF and FFF beams are increased with increasing the F.S, but for FFF beams this variation was less than that of FF beams where the scattered radiation due to the flattening filter is field size dependent and has a larger effect than the soft x-ray spectra of FFF beams. This difference in dose in the buildup region decreases with increasing depth and it may not be clinically important. Cashmore showed the same results when he measured the dose in buildup region for field sizes ranging from 3×3 to 30×30 cm^2 at 3 cm depth using an Elekta Precise linear accelerator running at 6 MV FF and FFF photon beams [28]. Wang et al. [83] reported similar results at

small field sizes (2×2 cm^2 to 10×10 cm^2). He investigated the surface dose produced by 6 MV and 10 MV FF and FFF photon beams at small field sizes using Varian TrueBeam linear accelerators.

Other investigators used Varian linac [81, 72] or Elekta [52, 28] linacs with the same electron energy for FFF and FF beams. They found that the FFF beams for Varian and Elekta linacs [52, 28] produce PDD curves steeper than that of FF beams at the exponential region. Cashmore J [28] compare the PDDs of 6 MV FF and FFF photon beams produced by Elekta Precise linac with the PDDs of 5 MV FF (on the central axis depth dose for photon), which are registered in the supplement of British Journal of Radiology (BJR 25). He demonstrated a good match of the used beam specification parameters between 6 MV FFF and 5 MV FF where the lack of beam hardening due to 6 MV FFF beams is seen as an energy decrease to approximately of 5 MV. This supports the the philosophy of Siemens to introduce FFF beams with higher maximum energies (7 MV and 11 MV) than those used for FF beams (6 MV and 10 MV) to avoid the softening effect of removing the flattening filter. In that way Siemens keeps the characteristics of the flattened beams and gets the advantages of FFF beam.

Our results of the measurements of the dosimetric characteristics, PDD curves, beam profiles and dose rate of the 6 MV FF and 7 MV FFF photon beams of Siemens Artiste linac are in agreement with the results of Dzierma et al. [35] who only presented the beam characteristics of Artiste linac equipped with 7 MV FFF and compared it with a normal flat 6 MV beam of the same machine. As shown before, our investigations evaluate not only 6 FF and 7 FFF beams, but also 10 FF and 11 FFF beams with similar findings.

5.2 IMRT-FF and IMRT-FFF

The IMRT plan comparison using FF and FFF beams was performed to evaluate the effect of the dosimetric characteristics of FFF beams on the plan quality and treatment efficiency. For these investigations, we selected three groups of patients, which represent typical tumor sites treated with IMRT technique. These groups were prostate, prostate-LN and H&N patients. The IMRT-FF and IMRT-FFF were created for each group of patients under the same optimization parameters and the same objective functions.

The parameters used to evaluate the plan quality were dose distribution, DVHs analysis and how the PTV and OARss clinical goals could be achieved, in addition to HI and CN. The HI and CN as additional indicators of the plan quality should only be used once a satisfactory plan has been achieved on the basis of the dose distribution along the treatment volumes and normal structures [49].

For the chosen cases in this study, prostate, prostate-LN and H&N, the dose distribution, DVHs, and achievement of PTVs and OARs clinical goals for IMRT-FF and IMRT-FFF were comparable.

IMRT technique uses multiple beams with non-uniform fluence modulated by MLC and incident from different directions. the desired dose distribution in the target is achieved after optimizing and superimposing these beams. Therefore, a homogeneous dose distribution could be delivered to the target regardless of using FF or FFF beams. That is evident through the DVHs, visual examination of the dose distributions, achievement of the PTV and OARs clinical goals in addition to the values of HI and CN. We found that the value of the HI even for large and complex tumor sites - prostate-LN and H&N, were comparable and for prostate the IMRT-FFF exhibited more homogeneous dose distribution than IMRT-FF. Our hypothesis is, however, that FFF beams have inhomogeneous fluence distribution, we get homogeneous dose distribution within the PTV because of the superposition of the beam segments.

The IMRT-FFF plans for all clinical cases were more conformal than IMRT-FF plans with no significant difference for prostate but for prostate-LN and H&N patients the differences were statistically significant. That can be understood through the influence of removing the flattening filter on the dose profile of photon beams. The out-of-field doses of FFF-beams are lower than that of FF-beams especially for F.Ss larger than 10×10 cm^2 and subsequently less dose is delivered to the surrounding tissues and OARs leading to more conformal plans. Although, there were some differences for HI and CN between IMRT-FFF and FF, both IMRT plans are clinically acceptable considering the other plan comparison parameters.

Treatment efficiency was estimated by the number of MU and the TDT of the plans. IMRT plans created using FFF beam need more MUs than that of the IMRT plans using FF beam to deliver the same prescribed dose especially for large PTVs like prostate-LN and H&N. That could be explained according to the beam profiles of the

FF and FFF beams, Fig. 4.1, where with increasing the photon energy and the field size, the lateral dose decreases. Therefore, increasing the PTV volume requires more MUs per field to compensate for the lower dose in the lateral part of the beam in case of FFF beams.

The TDT of IMRT has a complex relation between many parameters. Reducing Beam-on time as a result of the high dose rate of FFF has a potential for decreasing total delivery time but the TDT of IMRT is not only influenced by the dose rate, which depends on the operating mode of the linac (FF or FFF), but also by the total number of MUs, the number of fields, the number of segments and the leaf travel time from one segment to another depending on the shape of the segments in addition to gantry speed, and the waiting time required for checking the MLC positions of the next segment. The TDT is affected by the number of MU/seg too, which determines the applied dose rate for each segment. The maximum output dose rate of Artiste operating in FFF mode is 2000 MU/min but in order to maintain the dose linearity for segments with low MU, the Control Console will automatically switch from the high dose rate to the low dose rate of 500 MU/min for segments with a dose less than 10 MU [7]. That might increase the overall TDT of IMRT-FFF plans. According to the result of the current study, IMRT plans using FFF beams produce a higher numbers of MUs with relative difference to IMRT-FF beams ranging from 19 to 114 %. Furthermore, a part of segments has a number of MUs less than 10 MU/seg. Both effects might balance the high dose rate of FFF beams, which was expected to cause a reduction in the TDT. Thus, the IMRT-FFF plans delivered by Artiste linacs required TDT differing from -20 % to +25 % than TDT of IMRT-FF plans depending on the site, volume and complexity of the tumor and the relative difference of total number of MUs and number of segments.

Comparison with the previous studies

Many previous studies that performed planning studies for IMRT-FFF and IMRT-FF plans using different linacs and TPS [36, 72, 80] showed comparable results between both techniques for different tumor sites. To our knowledge, only a few planning studies for different tumor sites have been done using Artiste linacs operated in FF and FFF

mode. So, we compared our results with the previous studies regardless which TPS and linacs were used. Dzierma et al. [36] performed treatment plans for hypopharynx cancer using Philips Pinnacle3 V9.2 and 9.4 (Philips healthcare, Amsterdam). The measurements were done for 6 MV FF and 7 MV FFF of Artiste linacs. Dzierma et al. found that the treatment plans of 70 segments created by both modalities achieved good plan quality and more MUs in agreement with our results. On the other hand, they registered shorter treatment times for IMRT-FFF plans (-16 % to -30 %) for H&N patients where we found the same TDT. This difference in the results of TDT resulted from the use of a different TPS, which might generate segments with smarter arrangement than Oncentra planning system does, leading to a reduction in TDT. Stathakis [72] and Vassiliev [80] performed their IMRT planning studies using Pinnacle3 (Philips Medical Milpitas, CA) and Eclipse version 8.0 (Varian Medical Systems), which were commissioned by the data of Varian 23 EX and Clinac 21 EX (Varian Medical Systems), respectively. They also reported no substantial differences of DVH and isodose distribution for prostate and H&N using 6 MV and 18 MV FF and FFF beams. Since Vassiliev did not recalibrate the MUs/dose after removing the flattening filter, he registered a reduction in the MUs of the plans on average by a factor of 2.0 at 6 MV FFF and by a factor of 2.6 at 18 MV FFF. Stathakis reported that the IMRT plans created by FFF photon beams required less MUs. We did not register that reduction in the MUs for IMRT-FFF plans because the Artiste linacs in our clinic have been calibrated to deliver the same dose per MU for the FF photon beam energies and their corresponding FFF beams under the same conditions, according to the German dosimetry protocol DIN 6800-2, (10×10 cm^2 field size, 90 cm SDD, 10 cm depth).

5.3 mARC

The aim of developing radiotherapy treatment techniques is to improve the plan quality and treatment efficiency. The main advantage of modulated arc therapy is shortening the TDT, which allows to treat more patients per machine or to reduce the working hours. Furthermore, it reduces the risk of patient movement and increases the patient's comfort. Recent studies of different VMAT techniques have shown that a plan quality comparable to IMRT could be achieved even with a reduction of the number of MUs

and shorter TDT [82, 22, 64].

mARC is a novel technique of arc therapy. It has special properties in comparison with other VMAT techniques so it was important to study mARC features and its variable plan parameters and how they affect the plan quality and treatment efficiency of different types of cancer. We included patients with tumors of different volumes and levels of complexity to explain how mARC deals with this variety.

In mARC, the treatment dose is delivered by a number of arclets (segments) controlled by the chosen value of F.G.S, which expresses the angle spacing within the arc. F.G.S is the main parameter influencing the plan quality and treatment efficiency. We found that gradual increase in F.G.S leads to gradually decreasing in PTV dose coverage, conformity and homogeneity. Increasing F.G.S value restricts the beam modulation because the spaces within the arc increase and the numbers of OP decrease. On the other hand, a small value of F.G.S means more arclets leading to more PTV dose homogeneity and better conformity but at the cost of more MUs and longer TDT. That is evident in case of SA (4), which are the optimal single arc plans for all patients but with higher number of MUs and longest TDT.

It was necessary to compare different options of mARC plans with each other for different targets to evaluate their performance and compare them with IMRT plans to find out the differences. Our strategy was to investigate the plan quality and treatment efficiency of the optimal SA plan and DA plan and to compare them with each other and with IMRT 7B and 9B plans. For prostate-LN and H&N, SA (4) and DA (6) were created. For prostate, as a homogeneous small PTV, only SA (4) and SA (8) plans were applied since DA for that target did not improve the treatment significantly but prolonged the TDT. All mARC and IMRT plans were clinically acceptable and the plan qualities of all mARC plans were comparable with each other and with IMRT plans.

Treatment efficiency is a common comparison parameter of IMRT and VMAT techniques. The TDT of mARC plan is affected mainly by the gantry speed between the arclets, which depends on the number of the arclets and the arclets complexity. The more complex the arclets shapes, the longer the time required for MLC leaves movement, the lower is the gantry speed. The gantry speed also depends on the MU/arclet where the more the dose per arclet, the slower is the gantry. In case of mARC, the

gantry movement is continuous, which plays a role in shortening the TDT, whereas in case of S&S-IMRT, the gantry moves only between the beams and the MLC adjusts the segments shapes within the beam. As we found, the time required for the gantry movement is approximately two minutes for IMRT 7B or 9B plan.

For prostate-LN and H&N, despite the SA (4) and DA (6) plans were delivered with a high number of arclets in comparison to the number of segments for IMRT plans (90 and 122 arclets, vs. 60 IMRT segments for prostate-LN and 50 for H&N, respectively), they require nearly the same or a lower number of MUs. In case of prostate-LN as large PTV, the TDT for SA (4) and IMRT plans is nearly the same, but it is longer for the DA (6) by about one minute. These results can be understood by considering the the continuous movement of the gantry in case of mARC and the gantry movement between the IMRT beams, which takes approximately two minutes. The required time for the gantry movement in case of IMRT to some extent is compensated by a smaller number of IMRT segments. The TDT of DA (6) is longer than that of SA (4) because the DA (6) is delivered with 32 arclets more than SA (4). In case of H&N as a complex and relatively large PTV, the TDT required to deliver SA (4) and DA (6) plans are longer than that of IMRT plans by around 2:30 and 4:00 minutes, respectively. This might be caused by the PTV volume and its complexity leading to slowing down of the gantry speed between the arclets where the MLC needs more time to adjust the arclets shapes.

For prostate, the treatment efficiency of SA (4) with 90 arclets is comparable with that of IMRT plans of 50 segments. The SA (8) plans in comparison to IMRT plans are more efficient despite they have been produced with nearly the same number of arclets and segments - 45 and 50, respectively. The average number of MUs and TDT are reduced for SA (8) plans by 17 % and 40 %, respectively. Similarly, as shown in table 4.7 and 4.8, SA (6) plans with 60 arclets required shorter TDT than IMRT plans with 60 and 50 segments for prostate-LN and H&N, respectively. The shorter TDT of SA (8) and SA (6) plans is related to the lower number of MUs and the continuous movement of the gantry.

Recently, FFF beams have been implemented and evaluated in the linacs and they are already in clinical use in many hospitals all over the world. Removal of the flattening filter results in a higher dose rate, head scatter reduction, lower peripheral dose and

shorter beam-on-time. After introducing VMAT technique, many vendors apply FFF beams for arc therapy as well as for IMRT. It has been expected that the combination between the advantages of FFF beam and the way of arc delivery would produce more efficient plans.

In this study 10 MV FF and 11 MV FFF beams were applied to produce SA plans for prostate and prostate-LN. As mentioned before, for small F.S, both FF and FFF beams have similar beam profiles. Therefore, in case of prostate, the plan quality did not change whether using FF or FFF beams to create mARC plans because in that case the PTV is small and regular. The effect of FF and FFF beams on mARC plans is more evident in case of complex and large PTVs. In our example of prostate-LN, SA (4) - the optimal single arc plan - produces nearly the same CN and HI whether using FF or FFF beams. The dose homogeneity of SA (6) and SA (8) plans due to FF beams are better than their corresponding FFF plans. The SA (6) FFF plans with 60 arclets achieve dose homogeneity nearly similar to that of SA (8) FF with 45 arclets, Fig. 4.27, which is related to the cone shape profile of the FFF beam that need more modulation (i.e. more arclets) to produce comparable dose homogeneity.

mARC-FFF plans need more MUs than mARC-FF to deliver the same prescribed dose especially for large PTVs. It is evident that the prostate as a small PTV exhibit only a small difference in monitor units between mARC plans created with 10 MV FF and 11 MV FFF, while mARC plans created with 11 MV FFF for prostate-LN require higher MU/Fx as shown in table 4.9. As mentioned before, at large field sizes the cone shape of the FFF beam profile has lower dose at its lateral part than the dose at the central axis, which is compensated by more MUs.

Despite the dose rate increased from 500 MU/min to 2000 MU/min due to flattening filter removal, TDT of mARC plans for prostate and prostate-LN is decreased by not more than 1 min using FFF beams instead of FF beams. In case of mARC delivery, the dose rate in FFF mode is variable depending on the number of MU/arclet and it can be slowed down till 500 MU/min. For the arclet with low MUs, the linac firmware automatically reduces the dose rate for better linearity. This reduction of the dose rate will improve the dose linearity with the minor drawback of increasing slightly the overall treatment time [7]. The TDT of mARC-FFF is also influenced by the higher number of MUs and more complex shapes of the arclets that lead to an increase of leave

travel times. All these parameters can slow down the gantry speed, and consequently mARC-FFF plans require longer TDT .

The treatment plan verification of mARC (FF and FFF) and IMRT plans calculated by RayStation have been done using Delta^4 and Octavius 4D. In general, Delta^4 and Octavius 4D are efficient dosimetric devices to perform patient specific QA for mARC and IMRT. For tumors with large field sizes (more than 20 cm^2), their treatment plans can not be verified using Delta^4 because of its limited active area. This leads to measure the plan with long field size as two plans to cover its whole area and that increase the measurement time and that is why we used Octavius to verify the treatment plans of prostate-LN. A very good accuracy of mARC delivery is obtained with Artiste linac using Delta^4 or Octavius 4D.

Comparison with the previous studies

Only few non-systematic comparison studies [48, 37, 34] have been done between mARC and S&S-IMRT. Several studies [22, 76, 68, 39, 64] have investigated the plan quality and treatment efficiency for VMAT and RapidArc treatment in comparison with IMRT. All of these studies for VMAT, RapidArc and mARC techniques have achieved clinically acceptable plans of qualities comparable with that of IMRT. These studies have shown no observable decrease in the number of MUs but they conclude that the main advantage of all volumetric arc techniques over IMRT is a reduction in TDT.

Teoh et al. [76] have discussed the use of VMAT techniques in practice and review the available data, till 2011 in their review article, from planning and clinical outcome studies in various tumor sites including those that have been studied in the present work. The reviewed data conclude that for most tumor sites, VMAT and fixed field IMRT will produce largely equivalent plan quality. The absolute difference in dosimetric parameters reported as statistically significant in some of the planning studies is relatively small and may not be clinically important.

Peters et al. [64] have evaluated Eclipse TPS (v.11.0.39) to create VMAT planning for Elekta linac. They have created S&S-IMRT plans for 162 patients with different tumor sites using an older version of Eclipse TPS (v.8.6) then the VMAT plans were compared with the S&S-IMRT plans. Depending on the tumor region, 5 to 9 coplanar

fields were chosen in comparison with partial, one or two arcs. The results of this study have demonstrated that the quality achieved for single and double arc VMAT plans is comparable to that of fixed-field S&S-IMRT for a variety of tumor sites. Furthermore, plans with two arcs provide better dose distributions than plans with one arc. Additionally, the reduced treatment time and smaller number of MUs, (approximately 30% smaller compared to IMRT) are the major advantages of VMAT. For prostate-LN, the reduction in the number of MUs was comparable with our results where our mARC plans reduced the MUs by not more than 20% compared to IMRT.

Daniel et al. [39] have compared VMAT treatment plans for 120 patients of different tumors sites, among them 20 prostate and 20 H&N, generated using Eclipse TPS (v. 11) for both 6 MV and 10 MV of FF and FFF mode. Their data showed that FF and FFF beams in most of the cases resulted in equivalent VMAT plans regarding both target coverage and OARs sparing. They have reported a higher number of MUs for VMAT-FFF and shorter TDT with less than 10 second for prostate. This is supported by our results with more reduction for TDT where we have registered approximately 45 second.

In general, the results of the current work for mARC technique are in principle agreement with the previous studies for VMAT/RapidArc. However there are some differences because mARC is a special version of VMAT with different way of plan optimization and dose delivery. Also, each study used different tumor sites, planning systems, linacs and planning approaches.

Like us, Dzierma et al. [34] have evaluated mARC techniques in comparison with S&S-IMRT using FF and FFF beams delivered at the Artiste linac. They have used different energies (6 MV FF and 7 MV FFF) and TPS (Prowess Panther v.5.10r2) to perform the mARC and IMRT plans for ten prostate patients treated with 76 Gy. For mARC plans, they have used one complete arc with 36 OP, which is equivalent to 10° F.G.S, whereas the IMRT plans consisted of 11 beams with a total of 33 segments or less. They have found only small differences in plan quality between the treatment plans created by 6 MV FF and 7 MV FFF beams, using IMRT or mARC and all these plans were clinically accepted. They have observed that the TDT for both techniques is reduced by about 50 seconds in case of FFF beams. Furthermore, they observed that the TDT of mARC in comparison to that of IMRT is reduced by half. Our results

are in good agreement with their results indicating that applying mARC for prostate with the number of arclets equal to the IMRT segments produce clinically acceptable plans with similar plan quality to that of IMRT plans and reduce the TDT by half.

Summary

Dissertation for the academic degree of

Dr.rer.med

IMRT and Rotational IMRT (mARC) Using Flat and Unflat Photon Beams

Submitted by

Amal Nabil Atef Sheta

completed at

Univerisity of Leipzig

Department of Radiation Therapy

supervised by

Prof. Dr. Ulrich Wolf

Prof. Dr. med. Thomas Kuhnt

01.2016

Flattening filters have been inserted into the beam path of the linacs to produce a uniform fluence and make it suitable for clinical use but it causes reduction of the dose rate and undesirable issues like photon scatter, electron contamination and leakage radiation. Despite the removal of the flattening filter produces non-uniform beams, modern radiotherapy treatment techniques, have interest in using flattening filter free (FFF) photon beams because of its benefits, e.g., high dose rate, reduced scattered and leakage radiation. Hypofractionated radiotherapy is interested in the high dose rate of FFF beams to shorten the treatment delivery time (TDT) especially the FFF beams have acceptable flatness at small field sizes. The radiotherapy techniques that deliver intensity-modulated beams (IMBs), e.g., Tomotherapy, intensity modulated radiation therapy (IMRT) and volumetric modulated arc therapy (VMAT), can use non-uniform FFF beams whereas the beam modulation using MLC and optimization algorithms produce homogeneous dose to the target such that of the FF beams.

Summary

The present work deals with Steep and Shoot (S&S)-IMRT and rotational IMRT (mARC). mARC is the VMAT version developed by Siemens for Artiste linacs. In contradiction to other VMAT techniques the radiation is only switched on in small angular intervals that is called arclets. During RAD ON the shapes of the MLC don't change. In the gap between two arclets radiation is off and the MLC contour is set for the next arclet. With mARC, like all VMAT techniques, the planer can use complete or partial arcs and single arc (SA), dual arcs (DA) or multiple arcs to achieve the best plan.

In 2011 the radiotherapy clinic of Leipzig University was equipped with two digital Artiste linacs. Both linacs provide 7 MV and 11 MV FFF beams of variable dose rates ranging from 500 to 2000 MU/min and 10 MV FF beams of 500 MU/min. In 2012, both Artiste linac were upgraded to apply mARC treatment.

This work is divided into three parts:

1. Determination of the main dosimetric characteristics (depth dose curves, profiles, dose rate, surface dose) of 7 MV and 11 MV FFF beams of Artiste digital linacs from Siemens and comparison with those of 6 MV and 10 MV FF beams.

2. Comparison of IMRT treatment plans of simple and complex-shaped target volumes using photon beams with and without flattening filter

3. A treatment planning comparison of mARC and S&S-IMRT to estimate the performance of various mARC techniques (single arc (SA) and dual arc (DA)) for tumor sites of different complexity and volumes and compare their performance with S&S-IMRT with static beams. The study also explains the effect of the final gantry spacing (F.G.S) on the quality and efficiency of the mARC treatment plan. The mARC plans created by FF and FFF beams were evaluated to know which technique is the best.

In addition to the planning study, the plan quality assurance (QA) of IMRT and mARC plans were done using two different volumetric QA devices, Delta^4 with two perpendicular array diode detectors and Octavius 4D as an electronic array of ion chambers. This dosimetric verification aimed to evaluate the accuracy of mARC delivery as a new technique in the clinic, the possibility of the plan verification with both

phantoms to verify IMRT and mARC plans.

The dosimetric characteristics of FFF beams 7 MV and 11 MV produced by Artiste digital linac were estimated and compared with their corresponding 6 MV and 10 MV FF beams. A PTW MP3 Water-Tank (PTW Freiburg, Germany) and a PTW dosimetry diode (type 60008) were used to determine percentage depth dose curves (PDDs) and beam profiles. The dose within the buildup region for 6 MV, 7 MV, 10 MV and 11 MV were measured using acrylic slab phantom (PMMA) and a parallel plate ionization chamber (Type 23344, PTW). Twenty patients with different tumor sites of different target complexity and volumes were selected to perform the IMRT-FF and IMRT-FFF plan comparison study using the treatment planning system Oncentra masterplan (V 4.1, Nucletron, ELEKTA). Another Eighteen patients were selected to evaluate the performance of various mARC techniques in comparison to S&S-IMRT by using RayStation treatment planning system (V 3.00 and 3.99, RaySearch Laboratories, Sweden). The chosen clinical cases were prostate, prostate with lymph nodes (LN) and head and neck (H&N). The comparison parameters were plan quality and treatment efficiency. The Artiste linacs in our clinic are calibrated under the reference conditions (field size 10×10 cm^2, 100 cm SSD, d_{max}) to deliver approximately 1 cGy/MU for all photon beam energies. The numbers of MU were calculated by the treatment planning system. The treatment delivery time was measured without adding the time for patient set-up.

The main dosimetric features of photon beams from Artiste linac (Siemens) operated with and without a flattening filter were measured and compared. The main effect of removing the flattening filter was getting photon beams with higher dose rate. Artiste linac in FFF mode produces high dose rate (2000 MU/min) for both 7 MV and 11 MV beams. The shape of the profiles of FFF beams was affected by the field size and the photon beam energy. The beams profiles of FFF beams are conical in shape at large field sizes and more tapered for 11 MV. The beam profile was slightly different at small field sizes for the FF and FFF photon beams for all electron energies. The FFF photon beams produce PDD curves with similar characteristics to FF photon beams and the differences at the build-up region between them are clinically insignificant. The FFF beams produce acceptable IMRT plans and comparable with that created by FF beams. IMRT-FFF plans need more MUs to deliver the same prescribed dose.

The TDT of IMRT-FFF is different than TDT of IMRT-FF plans by -20 % to +25 %, depending on the site, volume and complexity of the tumor. Also the relative difference of both MUs and number of segments between IMRT-FF and IMRT-FFF plans affects the TDT.

mARC as a novel arc therapy technique can deliver a comparable dose distributions to IMRT treatment delivery. The main advantage of mARC technique is the possibility to shorten the TDT, which allows to treat more patients per machine or to reduce the working hours. Furthermore, it reduces the risk of patient movement and increases the patient's comfort. The arc is delivered over a number of arclets (segments) controlled by the chosen value of F.G.S, which determine the number of optimization points (OP). Therefore, F.G.S is the main planning parameter that influences the plan quality and treatment efficiency of mARC delivery. As we found, gradual increase in F.G.S lead to gradually decreasing in the plan quality. On the other hand, a small value of F.G.S means more arclets and better plan optimization leading to more PTV dose homogeneity and better conformity but the cost will be more MUs and increasing of TDT. That is evident in case of SA with F.G.S of 4°(SA (4)), which is the optimal single arc plan for all patients but with higher number of MUs and longest TDT.

The effect of the FF and FFF beams on the mARC plans depends on the F.G.S and the complexity of the PTV. SA (4) is the optimal mARC plan for all patients whether using FF or FFF beams. For large and complex PTV, prostate-LN, by increasing the F.G.S, the FF beam produce mARC plan with better PTV dose homogeneity than that due to FFF beam. In case of prostate as a small homogeneous PTV, SA (8) plans created with 10 MV FF and 11 MV FFF achieve nearly the same dose conformity (CN) and PTV dose homogeneity. mARC-FFF plans need more MUs than mARC-FF to deliver the same prescribed dose especially for large PTV. TDT of mARC plans is decreased by not more than 45 seconds using FFF beams instead of FF beams.

A very good accuracy of mARC and IMRT delivery was obtained with Artiste linac using Delta^4 and Octavious 4D. In general, both systems are efficient dosimetric devices to perform patient specific QA for mARC and IMRT.

Finally, mARC has a variety options to create clinically acceptable treatment plans with comparable dose distribution with IMRT, so the planer should evaluate each case to decide which technique will be suitable to create the best plan.

Bibliography

[1] *Delta^4 manual (ScandiDos, Uppsala, Sweden).*

[2] Dosimetry diode type 60008 - PTW. `http://www.ptw.de/dosimetry_diodes00.html`.

[3] MP3 water phantom system. `http://www.ptw.de/mp3_phantom_tank.html`.

[4] Octavius 4D system. `http://www.ptw.de/typo3temp/pics/a25a9ed1d9.jpg`.

[5] Raysearch white paper - volumetric modulated arc therapy (VMAT) optimization in raystation. 2009.

[6] *Artiste mARC Treatment Planning Guide.* Siemens AG, Print NO:T2-000.640.32.01.02, 2012.

[7] *Digital Linear Accelerator Physics Primer.* Siemens AG, Print NO:T2-000.621.28.02.02, 2012.

[8] Raystation 2.5 released. `http://www.raysearchlabs.com/en/About-RaySearch/History/`, 2012.

[9] First rotational IMRT treatment with a siemens artiste linear accelerator and raystation. `http://www.raysearchlabs.com/en/About-RaySearch/Press-room1/`, 2014.

[10] Varian treatment planning support for siemens modulated Arc (mARC) treatments to be highlighted at 2014 ASTRO meeting in san francisco. `http://investors.varian.com/newsreleases`, 2014.

[11] Cancer, key facts. `http://www.who.int/mediacentre/factsheets/fs297/en/`, 2015.

[12] Oncentra external beam treatment planning system. `http://www.elekta.com`, 2015.

[13] Photon planning in raystation. `http://www.raysearchlabs.com/en/RayStation/PhotonPlanning/`, 2015.

[14] Proarc. `http://www.prowess.com/submnu-proarc-141.html`, 2015.

[15] *PTW Catalogs of Radiation Medicin QA solutions.* PTW, D587.211.00/07 2015-02, 2015.

[16] ICRU Report 83. [prescribing, recording, and reporting photon-beam intensity-modulated radiation therapy (IMRT)]. *Journal of ICRU*, 10(1), 2010.

[17] John R Adler Jr, SD Chang, MJ Murphy, J Doty, P Geis, and SL Hancock. The cyberknife: a frameless robotic system for radiosurgery. *Stereotactic and functional neurosurgery*, 69(1-4):124–128, 1997.

[18] B Allgaier, E Schüle, and J Würfel. Dose reconstruction in the octavius 4d phantom and in the patient without using dose information from the tps. *PTW, Freiburg, Germany*, 2013.

[19] James L Bedford. Treatment planning for volumetric modulated arc therapy. *Medical physics*, 36(11):5128–5138, 2009.

[20] James L Bedford, Young K Lee, Philip Wai, Christopher P South, and Alan P Warrington. Evaluation of the delta4 phantom for IMRT and VMAT verification. *Physics in medicine and biology*, 54(9):N167, 2009.

[21] Stanly H Benedict, David J Schlesinger, Steven J Goetsch, and Brian D Kavanagh. *Stereotactic Radiosurgery and Stereotactic Body Radiation Therap*. CRC Press, 2015.

[22] Anders Bertelsen, Christian R Hansen, Jørgen Johansen, and Carsten Brink. Single arc volumetric modulated arc therapy of head and neck cancer. *Radiotherapy and Oncology*, 95(2):142–148, 2010.

[23] Thomas Bortfeld, Rupert Schmidt-Ullrich, Wilfried De Neve, and David E Wazer. *Image-guided IMRT*. Cambridge Univ Press, 2006.

[24] Thomas R Bortfeld, Darren L Kahler, Timothy J Waldron, and Arthur L Boyer. X-ray field compensation with multileaf collimators. *International Journal of Radiation Oncology* Biology* Physics*, 28(3):723–730, 1994.

[25] Luther W Brady, HP Heilmann, and M Molls. *New technologies in radiation oncology*. Springer, 2006.

[26] Karl Bzdusek, Henrik Friberger, Kjell Eriksson, Björn Hårdemark, David Robinson, and Michael Kaus. Development and evaluation of an efficient approach to volumetric arc therapy planning. *Medical physics*, 36(6):2328–2339, 2009.

[27] C Cameron. Sweeping-window arc therapy: an implementation of rotational IMRT with automatic beam-weight calculation. *Physics in medicine and biology*, 50(18):4317, 2005.

[28] Jason Cashmore. The characterization of unflattened photon beams from a 6 MV linear accelerator. *Physics in medicine and biology*, 53(7):1933, 2008.

[29] X Yu Cedric, X Allen Li, Lijun Ma, Dongjun Chen, Shahid Naqvi, David Shepard, Mehrdad Sarfaraz, Timothy W Holmes, Mohan Suntharalingam, and Carl M Mansfield. Clinical implementation of intensity-modulated arc therapy. *International Journal of Radiation Oncology* Biology* Physics*, 53(2):453–463, 2002.

[30] X Yu Cedric and Grace Tang. Intensity-modulated arc therapy: principles, technologies and clinical implementation. *Physics in medicine and biology*, 56(5):R31, 2011.

[31] Varatharaj Chandraraj, Sotirios Stathakis, Ravikumar Manickam, Carlos Esquivel, Sanjay S Supe, and Nikos Papanikolaou. Comparison of four commercial devices for rapidarc and sliding window IMRT QA. *Journal of Applied Clinical Medical Physics*, 12(2), 2011.

[32] Steven D Chang and John R Adler. Robotics and radiosurgery–the cyberknife. *Stereotactic and functional neurosurgery*, 76(3-4):204–208, 2000.

[33] SM Crooks, Xiaodong Wu, C Takita, M Watzich, and Lei Xing. Aperture modulated arc therapy. *Physics in medicine and biology*, 48(10):1333, 2003.

[34] Yvonne Dzierma, Katharina Bell, Jan Palm, Frank Nuesken, Norbert Licht, and Christian Rübe. mARC vs. IMRT radiotherapy of the prostate with flat and flattening-filter-free beam energies. *Radiation Oncology*, 9(1):250, 2014.

[35] Yvonne Dzierma, Norbert Licht, Frank Nuesken, and Christian Rübe. Beam properties and stability of a flattening-filter free 7 MV beam-an overview. *Medical physics*, 39(5):2595–2602, 2012.

[36] Yvonne Dzierma, Frank G Nuesken, Jochen Fleckenstein, Patrick Melchior, Norbert P Licht, and Christian Rübe. Comparative planning of flattening-filter-free and flat beam IMRT for hypopharynx cancer as a function of beam and segment number. *PloS one*, 9(4):e94371, 2014.

[37] Yvonne Dzierma, Frank G Nuesken, Stephanie Kremp, Jan Palm, Norbert P Licht, Christian Rübe, et al. Commissioning and first clinical application of mARC treatment. *Strahlentherapie und Onkologie*, 190(11):1046–1052, 2014.

[38] MA Earl, DM Shepard, S Naqvi, XA Li, and CX Yu. Inverse planning for intensity-modulated arc therapy using direct aperture optimization. *Physics in medicine and biology*, 48(8):1075, 2003.

[39] Daniel Gasic, Lars Ohlhues, N Patrik Brodin, Lotte S Fog, Tobias Pommer, Jens P Bangsgaard, and Per Munck af Rosenschöld. A treatment planning and delivery comparison of volumetric modulated arc therapy with or without flattening filter for gliomas, brain metastases, prostate, head/neck and early stage lung cancer. *Acta Oncologica*, 53(8):1005–1011, 2014.

[40] Dietmar Georg, Tommy Knöös, and Brendan McClean. Current status and future perspective of flattening filter free photon beamsa). *Medical physics*, 38(3):1280–1293, 2011.

[41] Anders Gustafsson. Patient dose calculation based on scandidos delta^{4PT} measurements, 2013.

[42] Alonso N Gutiérrez and Oscar Calvo. Diode arrays and qa of advanced techniques. In *Journal of Physics-Conference Series*, volume 250, page 012049, 2010.

[43] Edward C Halperin, Luther W Brady, David E Wazer, and Carlos A Perez. *Perez and Brady's Principles and Practice of Radiation Oncology*. Lippincott Williams & Wilkins, 2013.

[44] Bjorn Hardemark, A Liander, H Rehbinder, and J Löf. Direct machine parameter optimization with raymachine in pinnacle. *Ray-Search White Paper*, 2003.

[45] Rebecca M Howell, Stephen F Kry, Eric Burgett, Nolan E Hertel, and David S Followill. Secondary neutron spectra from modern varian, siemens, and elekta linacs with multileaf collimators. *Medical physics*, 36(9):4027–4038, 2009.

[46] Robert Jeraj, Thomas R Mackie, John Balog, and Gustavo Olivera. Dose calibration of nonconventional treatment systems applied to helical tomotherapy. *Medical physics*, 32(2):570–577, 2005.

[47] Robert Jeraj, Thomas R Mackie, John Balog, Gustavo Olivera, Dave Pearson, Jeff Kapatoes, Ken Ruchala, and Paul Reckwerdt. Radiation characteristics of helical tomotherapy. *Medical physics*, 31(2):396–404, 2004.

[48] Kristofer Kainz, Guang-Pei Chen, Yu-Wen Chang, Douglas Prah, X Sharon Qi, Himanshu P Shukla, Johannes Stahl, and X Allen Li. A planning and delivery study of a rotational IMRT technique with burst delivery. *Medical physics*, 38(9):5104–5118, 2011.

[49] Tejinder Kataria, Kuldeep Sharma, Vikraman Subramani, KP Karrthick, and Shyam S Bisht. Homogeneity index: An objective tool for assessment of conformal radiation treatments. *Journal of medical physics/Association of Medical Physicists of India*, 37(4):207, 2012.

[50] Faiz M Khan and John P Gibbons. *Khan's the Physics of Radiation Therapy*. Lippincott Williams & Wilkins, 2014.

[51] Stine Korreman, Joakim Medin, and Flemming Kjaer-Kristoffersen. Dosimetric verification of rapidarc treatment delivery. *Acta oncologica*, 48(2):185–191, 2009.

[52] Gabriele Kragl, Sacha af Wetterstedt, Barbara Knäusl, Mårten Lind, Patrick McCavana, Tommy Knöös, Brendan McClean, and Dietmar Georg. Dosimetric characteristics of 6 and 10 MV unflattened photon beams. *Radiotherapy and Oncology*, 93(1):141–146, 2009.

[53] Gabriele Kragl, Franziska Baier, Steffen Lutz, David Albrich, Mårten Dalaryd, Bernhard Kroupa, Tilo Wiezorek, Tommy Knöös, and Dietmar Georg. Flattening filter free beams in SBRT and IMRT: dosimetric assessment of peripheral doses. *Zeitschrift für Medizinische Physik*, 21(2):91–101, 2011.

[54] Hanno Krieger. *Strahlenphysik, Dosimetrie und Strahlenschutz: Band 2: Strahlungsquellen, Detektoren und klinische Dosimetrie*. Springer-Verlag, 2013.

[55] Stephen F Kry, Oleg N Vassiliev, and Radhe Mohan. Out-of-field photon dose following removal of the flattening filter from a medical accelerator. *Physics in medicine and biology*, 55(8):2155, 2010.

[56] X. Allen Li. *Adaptive radiation therapy*. CRC Press, 2011.

[57] Daniel A Low, William B Harms, Sasa Mutic, and James A Purdy. A technique for the quantitative evaluation of dose distributions. *Medical physics*, 25(5):656–661, 1998.

[58] Marc A MacKenzie and Donald M Robinson. Intensity modulated arc deliveries approximated by a large number of fixed gantry position sliding window dynamic multileaf collimator fields. *Medical physics*, 29(10):2359–2365, 2002.

[59] Thomas R Mackie, Timothy Holmes, Stuart Swerdloff, Paul Reckwerdt, Joseph O Deasy, James Yang, Bhudatt Paliwal, and Timothy Kinsella. Tomotherapy: a new concept for the delivery of dynamic conformal radiotherapy. *Medical physics*, 20(6):1709–1719, 1993.

[60] Conor K McGarry, Barry F O'Connell, Mark WD Grattan, Christina E Agnew, Denise M Irvine, and Alan R Hounsell. Octavius 4D characterization for flattened and flattening filter free rotational deliveries. *Medical physics*, 40(9):091707, 2013.

[61] PF O'Brien, BA Gillies, M Schwartz, C Young, and P Davey. Radiosurgery with unflattened 6 MV photon beams. *Medical physics*, 18(3):519–521, 1991.

[62] Karl Otto. Volumetric modulated arc therapy: IMRT in a single gantry arc. *Medical physics*, 35(1):310–317, 2008.

[63] Jatinder R Palta and Thomas R Mackie. Medical physics monograph. 29:51–75, 2003.

[64] Samuel Peters, Hans Schiefer, and Ludwig Plasswilm. A treatment planning study comparing elekta vmat and fixed field imrt using the varian treatment planning system eclipse. *Radiat Oncol*, 9:153, 2014.

[65] EB Podgorsak et al. *Radiation oncology physics*, volume 657. 2005.

[66] Ervin B Podgorsak. *Radiation Physics for Medical Physicists (Biological and Medical Physics, Biomedical Engineering)*. Springer, 2012.

[67] Brendan M Prendergast, John B Fiveash, Richard A Popple, Grant M Clark, Evan M Thomas, Douglas J Minnich, Rojymon Jacob, Sharon A Spencer, James A Bonner, and Michael C Dobelbower. Flattening filter-free linac improves treatment delivery efficiency in stereotactic body radiation therapy. *Journal of Applied Clinical Medical Physics*, 14(3), 2013.

[68] D Russo, E Cavalera, A Papaleo, A Leone, FP Ricci, G Di Paola, C Capomolla, M Natali, G Pastore, and M Santantonio. Intensity modulated radiation therapy with volumetric modulation (VMAT). In *3rd Workshop-Plasmi, Sorgenti, Biofisica ed Applicazioni*, pages 73–79, 2013.

[69] Ramaswamy Sadagopan, Jose A Bencomo, Rafael Landrove Martin, Gorgen Nilsson, Thomas Matzen, and Peter A Balter. Characterization and clinical evaluation of a novel IMRT quality assurance system. *Journal of Applied Clinical Medical Physics*, 10(2), 2009.

[70] Bill J Salter, Vikren Sarkar, Brian Wang, Himanshu Shukla, Martin Szegedi, and Prema Rassiah-Szegedi. Rotational IMRT delivery using a digital linear accelerator in very high dose rate'burst mode'. *Physics in medicine and biology*, 56(7):1931, 2011.

[71] DM Shepard, MA Earl, XA Li, S Naqvi, and C Yu. Direct aperture optimization: a turnkey solution for step-and-shoot IMRT. *Medical physics*, 29(6):1007–1018, 2002.

[72] Sotirios Stathakis, Carlos Esquivel, Alonso Gutierrez, Courtney R Buckey, and Niko Papanikolaou. Treatment planning and delivery of IMRT using 6 and 18 MV photon beams without flattening filter. *Applied Radiation and Isotopes*, 67(9):1629–1637, 2009.

[73] Jörg Stein, Thomas Bortfeld, Birgit Dörschel, and Wolfgang Schlegel. Dynamic X-ray compensation for conformal radiotherapy by means of multi-leaf collimation. *Radiotherapy and Oncology*, 32(2):163–173, 1994.

[74] Martin B Tacke, Simeon Nill, Peter Häring, and Uwe Oelfke. 6 mv dosimetric characterization of the 160 MLC, the new siemens multileaf collimator. *Medical physics*, 35(5):1634–1642, 2008.

[75] Grace Tang, Matthew A Earl, Shuang Luan, Shahid A Naqvi, and Cedric X Yu. Converting multiple-arc intensity modulated arc therapy into a single arc for efficient delivery. *International Journal of Radiation Oncology, Biology, Physics*, 3(69):S673, 2007.

[76] M Teoh, CH Clark, K Wood, S Whitaker, and A Nisbet. Volumetric modulated arc therapy: a review of current literature and clinical use in practice. *BJ Radiol*, 84(4):967–996, 2011.

[77] Silke Ulrich, Simeon Nill, and Uwe Oelfke. Development of an optimization concept for arc-modulated cone beam therapy. *Physics in medicine and biology*, 52(14):4099, 2007.

[78] Ann Van Esch, Christian Clermont, Magali Devillers, Mauro Iori, and Dominique P Huyskens. On-line quality assurance of rotational radiotherapy treatment delivery by means of a 2D ion chamber array and the octavius phantom. *Medical physics*, 34(10):3825–3837, 2007.

[79] Arie Van't Riet, Ad CA Mak, Marinus A Moerland, Leo H Elders, and Wiebe van der Zee. A conformation number to quantify the degree of conformality in brachytherapy and external beam irradiation: application to the prostate. *International Journal of Radiation Oncology* Biology* Physics*, 37(3):731–736, 1997.

[80] Oleg N Vassiliev, Stephen F Kry, Deborah A Kuban, Mohammad Salehpour, Radhe Mohan, and Uwe Titt. Treatment-planning study of prostate cancer intensity-modulated radiotherapy with a varian clinac operated without a flattening filter. *International Journal of Radiation Oncology* Biology* Physics*, 68(5):1567–1571, 2007.

[81] Oleg N Vassiliev, Uwe Titt, Falk Pönisch, Stephen F Kry, Radhe Mohan, and Michael T Gillin. Dosimetric properties of photon beams from a flattening filter free clinical accelerator. *Physics in medicine and biology*, 51(7):1907, 2006.

[82] Wilko FAR Verbakel, Johan P Cuijpers, Daan Hoffmans, Michael Bieker, Ben J Slotman, and Suresh Senan. Volumetric intensity-modulated arc therapy vs. conventional IMRT in head-and-neck cancer: a comparative planning and dosimetric study. *International Journal of Radiation Oncology* Biology* Physics*, 74(1):252–259, 2009.

[83] Yuenan Wang, Mohammad K Khan, Joseph Y Ting, and Stephen B Easterling. Surface dose investigation of the flattening filter-free photon beams. *International Journal of Radiation Oncology* Biology* Physics*, 83(2):e281–e285, 2012.

[84] Steve Webb. *The physics of three dimensional radiation therapy: Conformal radiotherapy, radiosurgery and treatment planning*. CRC Press, 1993.

[85] Qiuwen Wu, Radhe Mohan, Monica Morris, Andrew Lauve, and Rupert Schmidt-Ullrich. Simultaneous integrated boost intensity-modulated radiotherapy for locally advanced head-and-neck squamous cell carcinomas. i: dosimetric results. *International Journal of Radiation Oncology* Biology* Physics*, 56(2):573–585, 2003.

[86] Cedric X Yu. Intensity-modulated arc therapy with dynamic multileaf collimation: an alternative to tomotherapy. *Physics in medicine and biology*, 40(9):1435, 1995.

[87] CX Yu. Intensity modulated arc therapy: A new method for delivering conformal radiation therapy. *The theory & practice of intensity modulated radiation therapy. Madison, WI: Advanced Medical Publishing*, pages 107–120, 1997.

Selbsttätigkeiterklärung

Erkläung über die eigenständige Abfassung der Arbeit

Hiermit erkläre ich, dass ich die vorliegende Arbeit selbständig und ohne unzulässige Hilfe oder Benutzung anderer als der angegebenen Hilfsmittel angefertigt habe. Ich versichere, dass Dritte von mir weder unmittelbar noch mittelbar geldwerte Leistungen für Arbeiten erhalten haben, die im Zusammenhang mit dem Inhalt der vorgelegten Dissertation stehen, und dass die vorgelegte Arbeit weder im Inland noch im Ausland in gleicher oder ähnlicher Form einer anderen Prüfungsbehörde zum Zweck einer Promotion oder eines anderen Prüfungsverfahrens vorgelegt wurde. Alles aus anderen Quellen und von anderen Personen übernommene Material, das in der Arbeit verwendet wurde oder auf das direkt Bezug genommen wird, wurde als solches kenntlich gemacht. Insbesondere wurden alle Personen genannt, die direkt an der Entstehung der vorliegenden Arbeit beteiligt waren.

11.01.2016	Amal Sheta
Datum	Unterschrift

Curriculum Vitae

Name	Amal Nabil Atef Sheta
Gender	Female
Date of Birth	10 - 04 - 1979
Place of Birth	Mansoura, Eldakahlia
Nationality	Egyptian
Mother tongue language	Arabic
Marital Status	Married and have a Son
E-mail	amal.sheta@gmail.com

Education

1985–1990	primary school.
1990–1993	preparatory school.
1993–1996	secondary school.
1996–2001	Bachelor degree in Biophysics.
2006–2009	**Master degree in Medical Physics**.

Skills

Computer	International Computer Driving Licence**(ICDL)**
Languages	English **(TOEFL)**

Conferences

2013	Deutsch Gesellschaft fr Medizinische physic e.v. **(DGMP)**, Koeln, Deutschland A. Sheta and U. Wolf "IMRT and Rotational IMRT (mARC) Using Flat and Unflat Photon Beam"

ACKNOWLEDGEMENTS

Firstly I would like to express my sincere gratitude to my supervisor Professor. Dr. Ulrich Wolf. I have been amazingly fortunate to have an supervisor who gave me the freedom to explore on my own, and at the same time the guidance to recover when my steps faltered. His continuous support of my Ph.D study and related research, his patience, motivation, immense knowledge and providing me with an excellent atmosphere helped me overcome many crisis situations and finish this dissertation. His guidance helped me in all the time of research and writing of this thesis. I could not have imagined having a better advisor and mentor for my Ph.D study.

My sincere thanks also goes to the director of the radiotherapy department, Professor.Dr. med. Rolf-Dieter Kortmann who provided me an opportunity and gave me access to use the department equipments and research facilities. Without his precious support it would not be possible to conduct this research.

I am most grateful to Mrs. Noreen Murr, Mr. Frank Heinicke, Dr. Stefan Pohlmann, Mr. Jens Taubmann, Mr. Walter Wilke and all the staff in the department of radiation therapy for their help and training me to use the facilities of the department.

I would like to acknowledge Mrs. Petra Scholz, who reviewed my thesis Linguistically.

Last but not the least, I would like to thank my family and my friends for supporting me spiritually throughout writing this thesis and my life in general.